UNIVERSITY OF OTTAWA

Department of Chemical and Biological Engineering

d-Limonene, a Renewable Component for Polymer Synthesis

by

Shanshan Ren

A thesis submitted to the Faculty of Graduate and Postdoctoral Studies in partial fulfillment of the requirements for the degree of

Doctor of Philosophy in

Chemical Engineering

© Shanshan Ren, Ottawa, Canada, 2017

Abstract

d-Limonene (Lim) was used in various polymer formulations to achieve a more sustainable polymerization. Lim is a renewable and essentially non-toxic compound, derived from citrus fruit peels, that may replace some of the many toxic and fossil-based chemicals used in polymer synthesis.

Bulk free-radical polymerizations of *n*-butyl acrylate (BA) with Lim were performed to investigate Lim co-polymerization kinetics and estimate the monomer reactivity ratios, important parameters in the prediction of copolymer composition. Kinetic modeling of the BA/Lim copolymerization was performed with PREDICI simulation software. The model supports the presence of a significant degradative chain transfer reaction due to Lim. This reaction mechanism is due to the presence of allylic hydrogen in Lim. Nonetheless, relatively high molecular weight polymers were produced. It was concluded that Lim behaves more like a chain transfer agent than a co-monomer.

Terpolymerizations of BA, butyl methacrylate (BMA) with Lim were then performed. In order to predict the terpolymer composition, the monomer reactivity ratios for BA/BMA were estimated. By applying the three pairs of co-monomer reactivity ratios to the integrated Mayo-Lewis equation, terpolymer compositions were ably predicted up to high monomer conversion levels.

Lim was then used as a chain transfer agent to prepare core-shell latex-based

pressure sensitive adhesives (PSA) comprising BA and styrene via seeded semi-batch emulsion polymerization. By varying the concentration of Lim and divinylbenzene crosslinker, the core polymer microstructure was modified to yield different molecular weights and degrees of crosslinking. The core latex was then used as a seed to prepare core-shell latexes. By changing the Lim concentration during the shell-stage polymerization, the molecular weight of shell polymer was also modified. The latexes were characterized for their microstructure and were cast as films for PSA performance evaluation. The PSA performance was shown to be highly related to the polymer microstructure. Tack and peel strength showed a decrease with increasing Lim concentration. Shear strength went through a maximum with a core Lim concentration increase from 0 to 5 phm.

Résumé

d-Limonène (Lim) a été utilisé dans diverses formulations de polymères pour obtenir une polymérisation plus durable. Lim est un composé essentiellement renouvelable et non toxique, provenant de pelures d'agrumes, qui peuvent remplacer certains des nombreux produits chimiques toxiques provenant des matières pétrolières utilisés dans la synthèse du polymère.

Les polymérisations radicalaires en vrac de l'acrylate de n-butyle (BA)/Lim ont été réalisées pour étudier la cinétique de copolymérisation et estimer les rapports de réactivité des monomères, paramètres importants dans la prédiction de la composition du copolymère. La modélisation cinétique de la copolymérisation BA/Lim a été réalisée avec le logiciel de simulation Predici. Le modèle prend en charge la présence d'une reaction dégradable de transfert de chaîne significative due à Lim. Ce mécanisme de réaction est due à la présence d'hydrogène allylique dans Lim. Néanmoins, des polymères à haut poids moléculaire ont été produits. Il a été conclu que le Lim se comporte plus comme un agent de transfert de chaîne qu'un co-monomère.

Des terpolymérisations de BA, le méthacrylate de butyle (BMA) avec Lim ont ensuite été réalisées. Afin de prédire la composition de terpolymère, les rapports de réactivité des monomères pour BA/BMA ont été estimés. En appliquant les trois paires de rapports de réactivité de co-monomères à l'équation de Mayo-Lewis intégré, les compositions de terpolymères ont été bien prédites à des niveaux élevés de

conversion des monomères.

Le Lim a ensuite été utilisé comme agent de transfert de chaîne pour préparer des adhésifs noyau-coquille à base de latex sensibles à la pression (PSA) comprenant le BA et le styrène par polymérisation semi-continue en émulsion ensemencée. En faisant varier la concentration de Lim et un agent de réticulation de divinylbenzène, la microstructure du polymère du noyau a été modifiée pour donner le poids et les degrés de réticulation moléculaires différents. Les noyaux du latex ont ensuite été utilisés comme ensemence pour préparer les latex noyau-coquille. En modifiant la concentration du Lim lors de l'étape de coquille de la polymérisation, la masse moléculaire du polymère de coquille a été également modifié. Les latex ont été caractérisés pour leur microstructure et ont été exprimés sous forme de films pour l'évaluation de la performance du PSA. Les performances du PSA ont été montrées très liés à la microstructure du polymère. L'adhérence et la résistance au pelage ont diminué avec l'augmentation de la concentration du Lim. La résistance au cisaillement est passée par un maximum avec une concentration du Lim au noyau augmentée de 0 à 5 phm.

Statement of contributions

I hereby declare that I am the sole author of this thesis. I performed all of the polymerizations, experiments, polymer characterizations and pressure-sensitive adhesive (PSA) performance testing as well as the associated data analysis (except as indicated next). Prof. Eduardo Vivaldo-Lima (Universidad Nacional Autónoma de México) assisted with the modeling work of BA/Lim. Ms. Lisha Zhang and Ms. Laura Hinojosa-Castellanos are acknowledged for their assistance with some of the polymer experiments, i.e., BA/BMA reactivity ratio estimation and bulk terpolymerizations.

The scientific guidance throughout the project and editorial comments of the written work were provided by my thesis supervisor, Dr. Marc A. Dubé, of the Department of Chemical and Biological Engineering at the University of Ottawa.

Shanshan Ren

October 2016

Acknowledgements

I would like to express my gratitude to my supervisor Prof. Marc A. Dubé for the continuous support and guidance throughout my Ph.D study, for his patience, motivation, and encouragement.

I would like to thank Prof. Eduardo Vivaldo-Lima (Universidad Nacional Autónoma de México), for his help and valuable feedback on the modeling work. I am grateful to all the members of the Polymer Reaction Engineering group. Especially, I would like to express my appreciation to Dr. Stéphane Roberge and Dr. Esther Trevino for their mentorship and valuable research discussions. I am also grateful to the Professors, office staff and technicians of the Department of Chemical and Biological Engineering at the University of Ottawa for their kindness and assistance.

For the financial support during this project, I am grateful to the China Scholarship Council, to the Natural Sciences and Engineering Research Council of Canada and to the University of Ottawa.

I want to thank my parents for their love, support and belief in me. Without you, I would not be the person I am today.

Lastly, I would like to thank my best friend and husband Minh Du Banh, for his love, understanding and constant support.

Table of contents

List of Tables

Chapter 7

Appendix

List of Figures

Chapter 1

Chapter 2

Chapter 3

Chapter 5

Chapter 6

Chapter 7

Chapter 8

Appendix A

Abbreviations

AA	Acrylic acid
AIBN	2,2'-Azobis(2-methylpropionitrile)
AN	Acrylonitrile
ATR-FTIR	Attenuated total reflectance Fourier-transform infrared
BA	Butyl acrylate
BMA	Butyl methacrylate
BPO	Benzoyl peroxide
$CDCl_3$	Deuterated chloroform
CLRP	Controlled/living radical polymerization
CMC	Critical micelle concentration
CTA	Chain transfer agent
dn/dc	Refractive index increment
DSC	Differential Scanning Calorimetry
DVB	Divinylbenzene
EHA	2-ethyl hexyl acrylate
GPC	Gel permeation chromatography
^{1}H-NMR	Proton nuclear magnetic resonance
KPS	Potassium persulfate
KMPS	Potassium metabisulfite

Lim	Limonene
MeOH	Methanol
MMA	Methyl methacrylate
M_n	Number-average molecular weight
M_w	Weight-average molecular weight
MWD	Molecular weight distribution
NMP	Nitroxide-mediated polymerization
PDI	Polydispersity index
PSA	Pressure sensitive adhesive
PSD	Particle size distribution
PSTC	Pressure Sensitive Tape Council
PVDF	Poly(vinylidene fluoride)
RAFT	Reversible addition-fragmentation chain transfer
SDS	Sodium dodecyl sulfate
Sty	Styrene
T_g	Glass transition temperature
THF	Tetrahydrofuran
X_n	Number average chain length

Chapter 1. Introduction

In this project, we are interested in sustainable polymer reaction engineering; one way to achieve this is to replace petroleum-based components with renewable alternatives in the synthesis of polymeric materials. We also seek to reduce the use of toxic materials during the synthesis of polymer products. The final goal of this work is to apply a more environmentally-friendly water-based emulsion polymerization technique with a renewable component for the production of adhesives. By employing water rather than organic solvents as the reaction medium, the emissions of volatile organic compounds can be significantly reduced during the synthetic process. These ideas have been identified as paramount in the application of the 12 principles of green chemistry to polymer production technology[1].

d-Limonene (Lim) is a renewable monoterpene that is mainly extracted from orange peels as a by-product of the orange juice processing industry. Lim is obtained in an almost pure form (~95%) at an annual worldwide production of over 70 million kg[2]. Because of its unique fragrance, Lim is widely used as a flavoring agent in the food, cosmetic and medical industries (i.e., chewing gum, perfume, ointment, hand cleanser). Based on its low-toxicity and non-water soluble nature, Lim is increasingly being used as an ecologically friendly substitute for toxic and caustic solvents such as fluorinated and chlorinated organic solvents, methyl ethyl ketone, xylene and toluene for cleaning and separation purposes[2,3]. Additionally, compared to the production

of fossil-based chemicals, the extraction and distillation of Lim releases fewer toxic pollutants, greenhouse gases and presents fewer negative impacts to the atmosphere (i.e., acidification, smog, ozone-depletion, etc.)[4,5]. Based on these advantages, the use of Lim in polymer synthesis is expected to show great potential in the development of a more sustainable polymer industry[6].

1.1 Thesis Objectives

We hypothesize that Lim can be incorporated in latex-based PSA formulations in order to influence the microstructure and performance of PSA films. Thus, the objective of this thesis is to evaluate Lim's behaviour in free-radical polymerization and its impact on polymer properties, as well as to demonstrate an appropriate approach (i.e., concentration, feeding methods, reaction condition) to incorporate Lim into PSA formulations. The first step of our research was to study the polymerization kinetics in the presence of Lim. As a common compound used in adhesive production, n-butyl acrylate (BA) was chosen to be the co-monomer. The copolymerization of BA/Lim was performed to estimate the monomer reactivity ratios and examine Lim's influence on polymerization rate and copolymer properties. A simulation for this system was developed using PREDICI™ by implementing a degradative chain transfer mechanism for Lim and intramolecular chain transfer of BA to an existing copolymerization kinetic model. Terpolymerization of BA, butyl methacrylate (BMA) and Lim was then performed to improve our understanding of Lim's behaviour during

polymerization with acrylate monomers. At the same time, due to the lack of experimental values for the BA/BMA monomer reactivity ratios, the copolymerization of BA/BMA was performed under the same conditions as the BA/Lim system. Finally, our focus reverted to the eco-friendly emulsion polymerization technique to produce latex-based pressure sensitive adhesives (PSAs). The microstructure and adhesive performance of the PSA products were examined.

1.2 Thesis Outline

This thesis consists of eight chapters. It begins with an introductory chapter (Chapter 1) and a theoretical background chapter (Chapter 2). Chapters 3 to 7 include manuscripts published or submitted to refereed journals: Chapter 3 contains a published manuscript on bulk free-radical copolymerization of BA/Lim; Chapter 4 contains a published manuscript on the kinetic model of copolymerization of BA/Lim using PREDICI®; Chapter 5 contains a submitted manuscript on the reactivity ratio estimation of BA/BMA in free-radical copolymerization; Chapter 6 contains a published manuscript on the bulk terpolymerization of BA/BMA/Lim; and Chapter 7 contains a submitted manuscript on adhesive performance modification using Lim as a chain transfer agent. The final chapter provides an overall general discussion and conclusion based on the analysis from each manuscript. Appendix A presents a published manuscript of nitroxide-mediated polymerization of BA/Lim. A schematic diagram of our research methodology is shown in Figure 1.1.

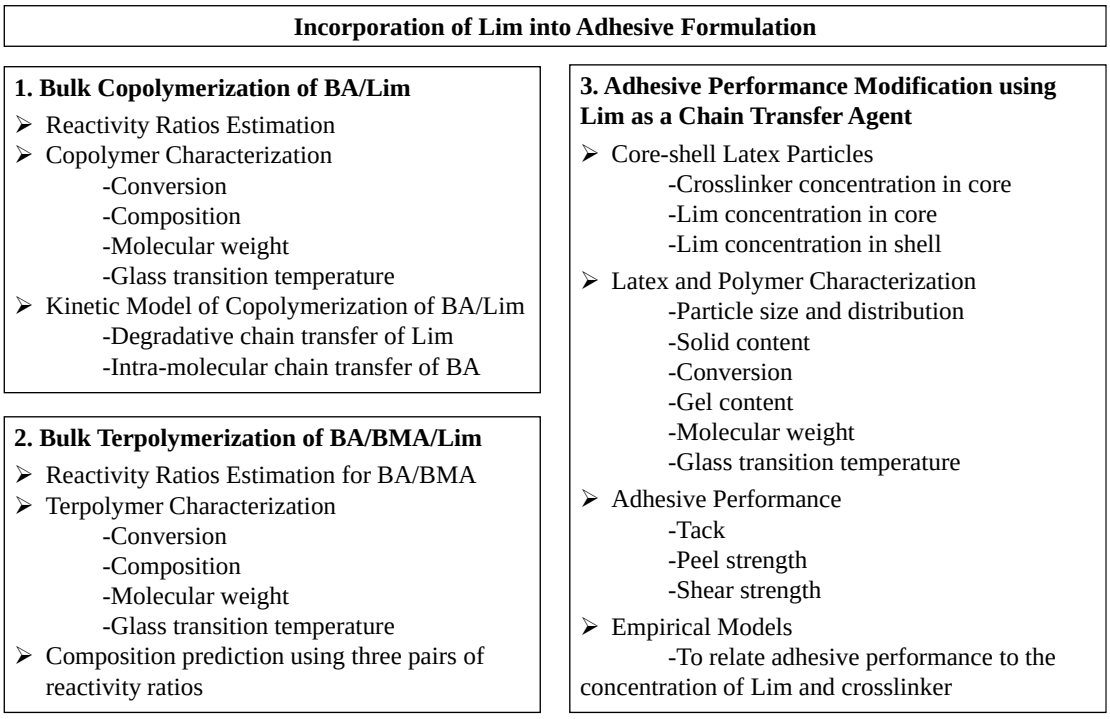

Figure 1.1 Schematic diagram of research methodology.

1.3 References

1. Dubé, M. A.; Salehpour, S. Applying the Principles of Green Chemistry to Polymer Production Technology. *Macromol. React. Eng.* **2014**, *8*, 7–28.

2. Kerton, F. M. Chapter 6:Renewable Solvents and Other "Green" VOCs. In *Chapter 6:Renewable Solvents and Other "Green" VOCs*; 2013; pp. 149–174.

3. Gu, Y.; Jérôme, F. Bio-based solvents: an emerging generation of fluids for the design of eco-efficient processes in catalysis and organic chemistry. *Chem. Soc. Rev.* **2013**, *42*, 9550.

4. Renewable Citrus Products Association *Life Cycle Assessment - Renewable and Sustainable Citrus Oils Final Report*; Environmental Resources Management:

Chicago, 2012.

5. Pourbafrani, M.; McKechnie, J.; MacLean, H. L.; Saville, B. A. Life cycle greenhouse gas impacts of ethanol, biomethane and limonene production from citrus waste. *Environ. Res. Lett.* **2013**, *8*, 015007.

6. Ciriminna, R.; Lomeli-Rodriguez, M.; Carà, P. D.; Lopez-Sanchez, J. A.; Pagliaro, M. Limonene: a versatile chemical of the bioeconomy. *Chem. Commun.* **2014**, *50*, 15288–15296.

Chapter 2. Theoretical Background

2.1 Sustainable Polymer Reaction Engineering

Polymeric materials play an essential role in just about every aspect of our lives. Polymers are made of a long queue of repeating molecular units. Based on the chemical properties, composition, and microstructure of the repeat units (i.e., monomers), polymers can display a broad range of chemical, mechanical, thermal, and electronic properties. These properties dictate their eventual application as rubbers, plastics, fibers, coatings, adhesives, etc. The development of human society is accompanied by increasing needs for large quantities of high performance polymeric materials. However, most polymers are synthesized from petroleum-based starting materials. Due to the consumption of rapidly depleting fossil resources and the associated negative environmental impacts, such as global warming, ozone depletion, smog, and soil acidification, it is difficult for the polymer industry to meet society's need for sustainable development. Sustainability refers to the development of resources that meets the needs of the present without affecting the needs of future generations[1]. However, there are a lot of critical challenges towards achieving more sustainable polymer production. The development of non-toxic, renewable feedstocks; more efficient catalyst and polymerization techniques; and the establishment of crucial relationships between chemical structure, morphology and product performance stand out as important goals.

The Dubé research group has presented a roadmap towards more sustainable polymer reaction engineering using the 12 principles of green chemistry [2]. Some of these were applied in this thesis:

a) Use renewable feedstock: Limonene (Lim) is a renewable chemical compound. As a byproduct from the juicing industry, the production of Lim does not compete with crops for human food or animal feed, and its use as a replacement for fossil-based feedstocks can help us reduce greenhouse gas emissions.

b) Avoid chemical derivatives: no additional modification of Lim is required in this project.

c) Use safer solvents and reaction conditions: Lim is incorporated in a latex-based adhesive formula via emulsion polymerization, where water is used as the reaction medium.

2.2 Terpenes

Terpenes are one of the largest classes of renewable chemical compounds produced in nature[3]. Plants, such as citrus fruits or conifers, produce terpenes through photosynthesis; the utilization of terpene-based products is therefore considered as carbon neutral. Limonene, α-pinene, and β-pinene are the three most common members of the terpene family. They are isomers that share the same chemical formula of $C_{10}H_{16}$, and consist of two isoprene units (see Fig. 2.1).

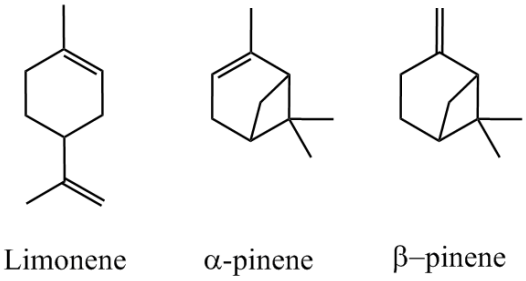

Limonene α-pinene β–pinene

Figure 2.1 Structure of limonene, α-pinene, β-pinene.

The vinyl groups in terpene monomers provide the potential for polymerization. The polymerization of terpenes has been studied since the 1950s[4]. Terpene homopolymers were synthesized in both radical and cationic systems[5–10]. The free-radical copolymerization of terpenes and various conventional monomers have been carried out, but frequently the yield is very low and the product exhibits very low terpene content[11–13]. For cationic polymerization, the comonomers of terpenes are evidently restricted to a limited number of monomers (e.g., isobutylene, styrene), which are adaptable for cationic systems[14–16]. Nowadays, the commercial application of poly(terpene) is more common as resins and as tackifiers in adhesive applications. The homo- or copolymers of terpenes are used as tackifiers or modifiers because of their low molecular weight[17].

2.2.1 Free-radical Polymerization of Lim

Lim has two optical isomers, which are labelled as *d*- and *l*- (alternative labels R- and S-; and + and - are also used, see Figure 2.2). The two enantiomers have the same chemical properties but different odour, and both of them are produced from

natural sources. (+) or *d*-Limonene has a citrus aroma, and is abundant in citrus fruit peels. (-) or *l*-Limonene has a turpentine-like odour, and is usually found in pine needles and cones[18].

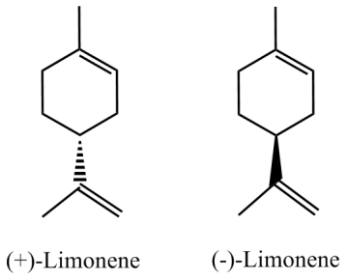

Figure 2.2 Enantiomers of limonene.

Lim possesses two non-conjugated electron-rich double bonds but these are reported to have different reactivity during polymerization due to steric effects and energy differences between the carbon radicals[19,20]. In free-radical polymerization, it is difficult to homopolymerize Lim due to the degradative chain transfer reaction caused by the more reactive allylic hydrogen[21] (see Figure 2.3). However, a recent study showed that poly(Lim) (Glass transition Temperature, T_g = 116^{o}C) was successfully synthesized using benzoyl peroxide as an initiator at 85 ℃ in xylene[22]. According to the proposed mechanism, only the exocyclic double bond of Lim reacted.

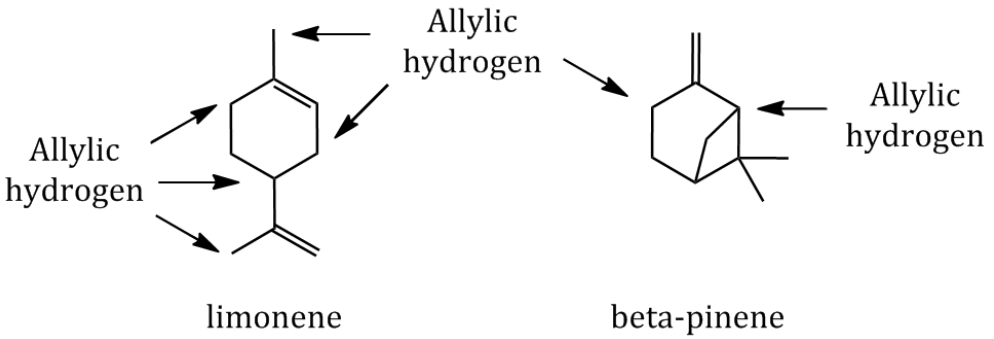

Figure 2.3 Allylic hydrogen of terpene monomers.

The free-radical copolymerization of Lim with various conventional monomers, such as acrylonitrile (AN)[12], methyl methacrylate (MMA)[23], styrene (Sty)[24], butyl methacrylate (BMA)[25] and vinyl acetate (VA)[26], has been studied by Sharma et al. In these systems, only the external double bonds were reacted; the reactivity ratios of Lim with these conventional monomers were reported to have values close to zero (see Table 2.1). The low reactivity ratios exhibited by these systems suggests that the Lim radical has a preference for addition of the co-monomer rather than reacting with Lim monomer. In most studies, conversions beyond 30 wt.% were not reported. Aside from deliberately stopping the polymerization, these low conversions could be explained by the degradative chain transfer mechanism leading to termination of the propagating chain after only a few repeat units[21].

Table 2.1 Free-radical polymerization of Lim with conventional monomers13,30-33.

Monomer 1	Monomer 2	Initiator	(℃)	Solvents	Reactivity ratios
AN	Lim	BPO	70	DMF	$r_1 = 0.0228$, $r_2 = 0.0062$
MMA		BPO	80	xylene	$r_1 = 0.07$, $r_2 = 0.012$
Sty		AIBN	80	xylene	$r_1 = 0.0625$, $r_2 = 0.014$
BMA		BPO	80	xylene	$r_1 = 0.125$, $r_2 = 0.026$
VA		AIBN	65	dioxane	$r_1 = 0.05$, $r_2 = 0.011$

The copolymerization of Lim with maleic anhydride (MAnh) initiated by AIBN showed evidence that the internal double bond of Lim could also react to higher conversion, and yielded copolymer containing 30 to 50% Lim from a 50:50 Lim:MAnh feed[19,20]. The variability in composition was influenced significantly by the solvent (or lack thereof) in the polymerization.

2.2.2 Living Radical Polymerization of Lim

In 2010, Kamigaito and co-workers synthesized AAB sequence-regulated copolymer of Lim and maleimide derivatives in fluoroalcohol via reversible addition-fragmentation chain transfer (RAFT) polymerization[27–29]. The copolymer exhibited high molecular weight and high T_g (220-250^{o}C). The formed AAB alternating sequence was due to the unsaturated and bulky ring of Lim along with the

hydrogen-bonding interaction of fluorinated solvent with carbonyl groups of maleimide derivatives.

2.3 Reactivity ratio estimation

In the early stages of copolymerization (e.g., <5% conversion), the copolymer composition is often different from the monomer feed composition, as monomers show a different inclination to react during copolymerization[30]. A polymer chain propagating model known as the terminal model (or Mayo-Lewis model), assumes the terminal unit of the growing chain is the only factor determining chain composition. In a copolymerization system, the relationship between copolymer composition and feed composition is described by the Mayo-Lewis equation[31]:

$$\frac{d[M_1]}{d[M_2]} = \frac{[M_1](r_1[M_1]+[M_2])}{[M_2]([M_1]+r_2[M_2])}, \qquad \text{(Eq. 2.1)}$$

which can be simplified to,

$$\frac{F_1}{F_2} = \frac{f_1(r_1 f_1 + f_2)}{f_2(r_2 f_2 + f_1)} \qquad \text{(Eq. 2.2)}$$

where F_1 and F_2 are the instantaneous composition of copolymer at corresponding feed compositions, f_1 and f_2; $r_1 = \frac{k_{11}}{k_{12}}, r_2 = \frac{k_{22}}{k_{21}}$, ($k_{ij}$ is the propagation rate constant of a growing radical chain ending in monomer i adding a monomer j unit) are known as the reactivity ratios which represent the tendency of a growing species adding the same monomer compared to the addition of the other monomer. By knowing the reactivity ratios, not only the copolymer composition but also the copolymer microstructure can be predicted. One should recall, that the properties of

the polymer product will be directly influenced by the copolymer composition and microstructure.

Reactivity ratios are typically estimated by substituting feed and instantaneous copolymer composition values from a set of experiments into the Mayo-Lewis equation. In this project, a non-linear error-in-variables model program (RREVM) developed specifically for the estimation of reactivity ratios was used[32]. In order to estimate reactivity ratios of maximum precision, the reactivity ratio estimation runs should follow a statistical design which includes a set of screening runs of equidistant points along the feed composition axis and several replicate runs at two feed composition recommended by Tidwell and Mortimer, $f_1^{'} = \frac{2}{2 + r_1}$, $f_1^{''} = \frac{r_2}{r_2 + 2}$ [33]. It should be noted that the Mayo-Lewis equation being in differential form, requires that all experiments be run at low conversion (<5%) to minimize errors caused by composition drift[34].

2.4 Emulsion polymerization

Emulsion polymerization is a technique which uses water rather than solvent as the reaction media. In its simplest form, emulsion polymerization involves the stabilization of water-insoluble monomer(s) using a surfactant, adding a water-soluble initiator as a free-radical source and resulting in a suspension of polymer particles in water stabilized by surfactant. The heat generated during the reaction can be easily removed by the continuous water phase. Another advantage is that high molecular

weights and high polymerization rates can be simultaneously achieved in emulsion polymerization while the reaction medium keeps the viscosity reasonably low, regardless of polymer molecular weight[35]. In addition, the resulting latex can form a polymeric film via the evaporation of the water. These polymer films can be directly used as product (e.g., coatings, adhesives) without further processing[36].

A typical conventional emulsion polymerization formulation includes monomer(s), water, water-soluble initiator, surfactant, buffers and other agents such as cross-linkers and chain-transfer agent (CTA); their roles are listed in Table 2.2.

Table 2.2 Typical emulsion polymerization formulation.

Ingredient	**Typical amount (wt.%)**	**Role**
monomer	30-50	constituent of polymer
water	40-60	dispersion medium, heat sink
initiator	0.1-0.5	source of free radicals
surfactant	2-8	stabilize droplets, latex particles
buffer	0.2-1	regulate pH, stability
cross-linker	1-5	generate polymer networks
CTA	0-1	control molecular weight and distribution

A conventional emulsion polymerization begins with the combination of water, monomer, surfactant and buffer[37]. The surfactant is added to a level which exceeds a critical micelle concentration (CMC), beyond which micelles (aggregates of surfactant) are formed. The interior of the micelles is hydrophobic and will contain monomer. A large portion of the monomer will also be dispersed as large monomer droplets (d = ~1-10 μm, number density is about 10^{12} - 10^{14} dm^{-3}). The

monomer-swollen micelles (d = ~5-10 nm, number density is about 10^{19} – 10^{21} dm^{-3}) are the pre-cursors to the polymer particles[38]. Upon the addition of the water-soluble initiator, the slightly water-soluble monomer will react in the water phase and once the radical chains become hydrophobic, they will enter the micelles. This will nucleate a particle by causing polymerization within the monomer-swollen micelle. Normally, the entry into the micelle by another radical will terminate the polymerization. Subsequently, yet another radical may enter the particle to re-initiate polymerization and so on.

According to the Harkins-Smith-Ewart model[39–44], there are three stages in the emulsion polymerization. Stage 1 occurs between 0 to 15% conversion. The polymerization is started when the oligomeric radical chains diffuse into the monomer-swollen micelles to initiate polymer particles. Thus, this stage is dominated by the nucleation of polymer particles until all of the micelles are consumed. During this stage, the polymerization rate, particle number and size increase. At the disappearance of micelles, stage 2 (15-40% conversion) begins during which the number of polymer particles remains constant and particle size increases. The particles are continuously supplied with monomer from the monomer droplets. A thermodynamic equilibrium exists to keep the polymer/monomer concentration in the particles constant, and thus the polymerization rate also remains constant in stage 2. It is worth noting that the polymerization takes place inside the micelles rather than the monomer droplets. The large number of micelles makes the total micellar surface area

much greater than that of the monomer droplets and thus, the possibility that the initiator molecules enter into a micelle is much greater. The droplets play the role of "monomer reservoir", that is, to slowly deliver the monomer to the particles until the droplets are depleted. It is the exhaustion of monomer droplets that marks the beginning of the final stage (40-100% conversion). During the final stage, essentially all of the monomer resides within the micelles, and the monomer concentration and polymerization rate decrease as conversion increases to completion.

Besides many advantages cited above, another attractive advantage of emulsion polymerization is the latex particle properties can be specifically designed with respect to various parameters[45]. Thus, emulsion-based products with tailored mechanical properties can be obtained by the copolymerization of different types of monomer, control of the crosslinking degree or the preparation of gradient core-shell morphology latex particles.

2.5 Pressure-Sensitive Adhesives (PSAs)

PSAs are required to not only exhibit proper viscosity to flow over and wet the surface of a substrate but also to exhibit sufficient elasticity and to resist to deformation and flow. PSA performance is controlled by the intrinsic viscoelasticity of the polymer[46], which is determined and affected by various factors, such as T_g, molecular weight and distribution, inherent microstructure and the degree of crosslinking of the copolymer.

The most frequently used measurements to gauge PSA performance are tack, peel strength (adhesion) and shear strength (cohesion). Tack, also called initial tack or quick adhesion, is the immediate holding power of the adhesive upon contact with the surface of another material and the force needed to separate the joint afterward. PSA with a high tack can adhere to the surface quickly. Peel strength is the force needed to peel off the adhesive from a specified surface at a defined rate under a standard angle (90° or 180°). Shear strength is the internal or cohesive strength of the PSA; it is an indicator of the softness of adhesives. Typically, it is measured in terms of the time required to pull a standard strip of PSA from a test panel under a defined load. Peel and tack are important adhesive properties of PSA, and shear reflect the cohesive property of the PSA. These three properties are interrelated, for example, a high-shear adhesive which is less likely to split under pressures and has low tendency to flow normally results in low tack. PSA performance is based on the balance of these three strengths.

The measurement of these strengths depends not only on the intrinsic property of the PSA but also on the surface of the substrate, the test method and conditions; we adopt the standards proposed by the Pressure Sensitive Tape Council in the characterization of PSA samples.

2.5.1 Theory of adhesion

Adhesion is defined as the process of attraction between dissimilar surfaces that cling to each other, whereas cohesion is the molecular attraction that takes place

between similar surfaces[47]. Many theories have been proposed to explain the mechanism of adhesion:

Absorption theory[48]: Adhesion is the intimate contact established via the intermolecular forces (i.e., Van der Waals forces) between the adhesive and the adherend. The formation of continuous contact is related to the wetting ability of the adhesive and surface tension. The wetting process is favored when the adhesive has a lower surface tension compared to the substrate surface, exhibiting a contact angle less than 90^{o}.

Mechanical interlocking theory[49]: All surfaces present a certain roughness; the valleys or pores on surfaces permit the adhesive penetrate the surface resulting in a physical interlock between the adhesive and substrate.

Electrical theory[50]: An electron double layer exists at the interface of the substrate and adhesive, similar to two plates of a capacitor. Adhesion results from the attraction between the opposite charges from each side.

Diffusion theory[51]: Adhesion is due to the diffusion and penetration of adhesive polymer chains into the surface of the substrate. This process can explain the adhesion between adhesive and polymeric material, and is related to the flexibility of the polymer chains and the compatibility (or solubility) between the adhesive and adherend.

The mechanism of adhesion is not fully understood. Practically, it may involve aspects of all the above theories simultaneously. The absorption theory is the most

prevalent model and exhibits wide applicability. It explains that adhesion is established by the contact of adhesive and substrate, which is the initial step for interlocking, diffusion and the formation of electron double layers that may further improve adhesion[52].

2.5.2 Glass transition temperature (T_g) of PSA

PSAs typically contain two components: an elastomer and a tackifier. elastomers with a suitable T_g (ideally from -20ºC to -5ºC) are the intrinsic and basic part of PSAs. T_g is one of the most important factors in determining PSA properties such as tack, peel strength and shear strength[53]. For emulsion-based PSAs, the most frequently used monomers for elastomers are acrylates, i.e., *n*-butyl acrylate (T_g = -54 ℃), for which its homopolymer is "soft" and can provide the PSA with suitable viscosity, flowing and wetting characteristics, but cannot offer sufficient shear strength. Therefore, “hard” monomers (normally with a T_g above 30ºC) such as styrene (Sty, T_g = 100ºC) or methyl methacrylate (MMA, T_g = 105ºC) are copolymerized with acrylate monomers to increase the T_g of elastomer and decrease tack strength to a proper level.

To reach the proper range of T_g, an empirical Flory-Fox equation can be used to estimate the copolymer T_g[54]:

$$\frac{1}{T_g} = \frac{W_A}{T_{gA}} + \frac{W_B}{T_{gB}} \qquad \text{(Eq. 2.3)}$$

where $W_{A/B}$ refers to the weight fraction of monomer A/B in the copolymer; $T_{gA/B}$ (K)

represents the T_g of homopolymer A/B in Kelvin.

Besides the tackifying monomer (soft) and hardening monomer (hard), a third class of functional monomer is also added to provide functional groups for crosslinking, better water-solubility and improving the adhesion to a polar substrate[55,56]. Typically, the functional monomers are unsaturated carboxylic acids (e.g., acrylic acid and methacrylic acid, itaconic acid, fumaric acid, crotonic acid) and hydroxyalkyl acrylates (e.g., 2-hydroxyethyl acrylate).

Tackifiers are optionally added to improve tack and peel strength in PSA, which will have a negative effect on shear strength. Usually, tackifiers are low molecular weight resins with a higher T_g than the elastomer, and are required to exhibit reasonable solubility in the elastomer. Other additives such as rheology modifiers, wetting agents, plasticizers, UV stabilizers and fillers may also be used depending on the end purpose of the PSA[57].

2.5.3 Gel content and crosslinker

It is often necessary to add a crosslinking agent during the polymerization of acrylic PSAs, as non-crosslinking or only physical crosslinks (by hydrogen bonds and van der Waals forces) cannot provide enough thermal stability and are considered to be unworkable as PSAs. The introduction of crosslinking can inhibit decomposition while the copolymer may still be soft at certain temperatures. Generally, higher crosslinked networks reduce the polymer deformability resulting in higher T_g, and less flexibility and solubility[58]. The degree of crosslinking shows a significant influence

on PSA viscoelasticity: highly crosslinked PSA exhibits high shear strength, and slightly crosslinked PSA shows tacky behaviour[59–63]. Therefore, ensuring an appropriate level of crosslinking is a critical factor to produce a PSA with well-balanced adhesive and cohesive strength. Gel content measurement provides information on the degree of crosslinking. It is defined as the ratio of the weight of insoluble polymer to the original weight of the sample.

2.5.4 Molecular weight and chain transfer agent (CTA)

The sol phase molecular weight has a significant impact on PSA performance. Typically, with an increase in molecular weight, the tack and peel strength decrease while the shear strength increases[64]. An increased shear strength is related to better entanglement of high molecular weight polymer chains[65,66]. At the same time, the deformability and flow ability would decrease, resulting in a decrease in tack and peel strength.

To reach an optimal balance of the cohesive strength and flow ability, CTAs are commonly used to control the molecular weight and distribution. According to Chauvet et al.[67], both of the molecular weight and gel content decrease with an increase in CTA concentration for a given crosslinker concentration. It was reported by Kajtna et al.[66] that, with an increase in CTA concentration, the sol phase fraction increases and this could lead to an increase in sol molecular weight, contrary to what we would normally expect; however, when the sol phase fraction is greater than 50 wt%, the molecular weight tends to decrease as would be expected. Qie et al. [68] also

studied the combined effect of CTA and crosslinker on latex microstructure. At given crosslinker concentrations, it was found that by increasing CTA concentration, the sol phase molecular weight decreased and then increased due to the formation of branched polymers. These observed trends describe complex changes in the microstructure with CTA and crosslinker concentrations. Molecular weight is also affected by the comonomer composition and reaction conditions, such as temperature and initiator concentration.

2.6 References

1. Burton, I. Report on Reports: Our Common Future. *Environ. Sci. Policy Sustain. Dev.* **1987**, *29*, 25–29.

2. Dubé, M. A.; Salehpour, S. Applying the Principles of Green Chemistry to Polymer Production Technology. *Macromol. React. Eng.* **2014**, *8*, 7–28.

3. Schwab, W.; Fuchs, C.; Huang, F.-C. Transformation of terpenes into fine chemicals. *Eur. J. Lipid Sci. Technol.* **2013**, *115*, 3–8.

4. Roberts, W. J.; Day, A. R. A Study of the Polymerization of α- and β-Pinene with Friedel—Crafts Type Catalysts. *J. Am. Chem. Soc.* **1950**, *72*, 1226–1230.

5. Modena, M.; Bates, R. B.; Marvel, C. S. Some low molecular weight polymers of d-limonene and related terpenes obtained by Ziegler-type catalysts. *J. Polym. Sci. A* **1965**, *3*, 949–960.

6. Keszler, B.; Kennedy, J. P. Synthesis of high molecular weight poly (β-pinene). In

Macromolecules: Synthesis, Order and Advanced Properties; Advances in Polymer Science; Springer Berlin Heidelberg, 1992; pp. 1–9.

7. Lu, J.; Kamigaito, M.; Sawamoto, M.; Higashimura, T.; Deng, Y.-X. Living Cationic Isomerization Polymerization of β-Pinene. 2. Synthesis of Block and Random Copolymers with Styrene or p-Methylstyrene. *Macromolecules* **1997**, *30*, 27–31.

8. Guiné, R. P. F.; Castro, J. A. A. M. Polymerization of β-pinene with ethylaluminum dichloride (C2H5AlCl2). *J. Appl. Polym. Sci.* **2001**, *82*, 2558–2565.

9. Satoh, K.; Sugiyama, H.; Kamigaito, M. Biomass-derived heat-resistant alicyclic hydrocarbon polymers: poly(terpenes) and their hydrogenated derivatives. *Green Chem.* **2006**, *8*, 878–882.

10. Kukhta, N. A.; Vasilenko, I. V.; Kostjuk, S. V. Room temperature cationic polymerization of β-pinene using modified AlCl3 catalyst: toward sustainable plastics from renewable biomass resources. *Green Chem.* **2011**, *13*, 2362–2364.

11. Ramos, A. M.; Lobo, L. S.; Bordado, J. M. Polymers from pine gum components: Radical and coordination homo and copolymerization of pinenes. *Macromol. Symp.* **1998**, *127*, 43–50.

12. Sharma, S.; Srivastava, A. K. Radical Copolymerization of Limonene with Acrylonitrile: Kinetics and Mechanism. *Polym.-Plast. Technol. Eng.* **2003**, *42*, 485–502.

13. Li, A.-L.; Wang, X.-Y.; Liang, H.; Lu, J. Controlled radical copolymerization of

β-pinene and n-butyl acrylate. *React. Funct. Polym.* **2007**, *67*, 481–488.

14. Lu, J.; Liang, H.; Zhang, R.; Li, B. Synthesis of poly(β-pinene)-b-polytetrahydrofuran from β-pinene-based macroinitiator. *Polymer* **2001**, *42*, 4549–4553.

15. Lu, J.; Liang, H.; Li, A.; Cheng, Q. Synthesis of block and graft copolymers of β-pinene and styrene by transformation of living cationic polymerization to atom transfer radical polymerization. *Eur. Polym. J.* **2004**, *40*, 397–402.

16. Li, A.-L.; Zhang, W.; Liang, H.; Lu, J. Living cationic random copolymerization of β-pinene and isobutylene with 1-phenylethyl chloride/TiCl4/Ti(OiPr)4/nBu4NCl. *Polymer* **2004**, *45*, 6533–6537.

17. Fink, J. K. Chapter 12 - Terpene Resins. In *Reactive Polymers Fundamentals and Applications (Second Edition)*; Plastics Design Library; William Andrew Publishing: Oxford, 2013; pp. 303–315.

18. Breitmaier, E. Hemi- and Monoterpenes. In *Terpenes*; Wiley-VCH Verlag GmbH & Co. KGaA, 2006; pp. 10–23.

19. Doiuchi, T.; Yamaguchi, H.; Minoura, Y. Cyclocopolymerization of d-limonene with maleic anhydride. *Eur. Polym. J.* **1981**, *17*, 961–968.

20. Maślińska-Solich, J.; Kupka, T.; Kluczka, M.; Solich, A. Optically active polymers, 2. Copolymerization of limonene with maleic anhydride. *Macromol. Chem. Phys.* **1994**, *195*, 1843–1850.

21. Dowbenko, R. Allyl Monomers and Polymers. In *Kirk-Othmer Encyclopedia of*

Chemical Technology; John Wiley & Sons, Inc., 2000.

22. Singh, A.; Kamal, M. Synthesis and characterization of polylimonene: Polymer of an optically active terpene. *J. Appl. Polym. Sci.* **2012**, *125*, 1456–1459.

23. Sharma, S.; Srivastava, A. K. Alternating Copolymers of Limonene with Methyl Methacrylate: Kinetics and Mechanism. *J. Macromol. Sci. Part A* **2003**, *40*, 593–603.

24. Sharma, S.; Srivastava, A. K. Synthesis and characterization of copolymers of limonene with styrene initiated by azobisisobutyronitrile. *Eur. Polym. J.* **2004**, *40*, 2235–2240.

25. Sharma, S.; Srivastava, A. K. Free radical copolymerization of limonene with butyl methacrylate: Synthesis and characterization. *Indian J. Chem. Technol.* **2005**, *12*, 62–67.

26. Sharma, S.; Srivastava, A. K. Azobisisobutyronitrile-initiated free-radical copolymerization of limonene with vinyl acetate: Synthesis and characterization. *J. Appl. Polym. Sci.* **2007**, *106*, 2689–2695.

27. Satoh, K.; Matsuda, M.; Nagai, K.; Kamigaito, M. AAB-Sequence Living Radical Chain Copolymerization of Naturally Occurring Limonene with Maleimide: An End-to-End Sequence-Regulated Copolymer. *J. Am. Chem. Soc.* **2010**, *132*, 10003–10005.

28. Matsuda, M.; Satoh, K.; Kamigaito, M. 1:2-sequence-regulated radical copolymerization of naturally occurring terpenes with maleimide derivatives in fluorinated alcohol. *J. Polym. Sci. Part Polym. Chem.* **2013**, *51*, 1774–1785.

29. Matsuda, M.; Satoh, K.; Kamigaito, M. Periodically Functionalized and Grafted Copolymers via 1:2-Sequence-Regulated Radical Copolymerization of Naturally Occurring Functional Limonene and Maleimide Derivatives. *Macromolecules* **2013**, *46*, 5473–5482.

30. Odian, G. Chain Copolymerization. In *Principles of Polymerization*; John Wiley & Sons, Inc., 2004; pp. 464–543.

31. Mayo, F. R.; Lewis, F. M. Copolymerization. I. A Basis for Comparing the Behavior of Monomers in Copolymerization; The Copolymerization of Styrene and Methyl Methacrylate. *J. Am. Chem. Soc.* **1944**, *66*, 1594–1601.

32. Dubé, M.; Sanayei, R. A.; Penlidis, A.; O'Driscoll, K. F.; Reilly, P. M. A microcomputer program for estimation of copolymerization reactivity ratios. *J. Polym. Sci. Part Polym. Chem.* **1991**, *29*, 703–708.

33. Tidwell, P. W.; Mortimer, G. A. An improved method of calculating copolymerization reactivity ratios. *J. Polym. Sci. A* **1965**, *3*, 369–387.

34. Dubé, M. A.; Saldívar-Guerra, E.; Zapata-González, I. Copolymerization. In *Handbook of Polymer Synthesis, Characterization, and Processing*; Saldívar-Guerra, E.; Vivaldo-Lima, E., Eds.; John Wiley & Sons, Inc., 2013; pp. 105–125.

35. Odian, G. Emulsion Polymerization. In *Principles of Polymerization*; John Wiley & Sons, Inc., 2004; pp. 350–371.

36. Chern, C.-S. Introduction. In *Principles and Applications of Emulsion Polymerization*; John Wiley & Sons, Inc., 2008; pp. 1–22.

37. Anderson, C. D.; Daniels, E. S. *Emulsion Polymerisation and Latex Applications*; iSmithers Rapra Publishing, 2003.

38. Chern, C. S. Emulsion polymerization mechanisms and kinetics. *Prog. Polym. Sci.* **2006**, *31*, 443–486.

39. Harkins, W. D. A General Theory of the Reaction Loci in Emulsion Polymerization. *J. Chem. Phys.* **1945**, *13*, 381–382.

40. Harkins, W. D. A General Theory of the Reaction Loci in Emulsion Polymerization. II. *J. Chem. Phys.* **1946**, *14*, 47–48.

41. Harkins, W. D. A General Theory of the Mechanism of Emulsion Polymerization1. *J. Am. Chem. Soc.* **1947**, *69*, 1428–1444.

42. Smith, W. V. The Kinetics of Styrene Emulsion Polymerization1a. *J. Am. Chem. Soc.* **1948**, *70*, 3695–3702.

43. Smith, W. V.; Ewart, R. H. Kinetics of Emulsion Polymerization. *J. Chem. Phys.* **1948**, *16*, 592–599.

44. Smith, W. V. Chain Initiation in Styrene Emulsion Polymerization. *J. Am. Chem. Soc.* **1949**, *71*, 4077–4082.

45. Tauer, K. Latex Particles. In *Colloids and Colloid Assemblies*; Caruso, F., Ed.; Wiley-VCH Verlag GmbH & Co. KGaA, 2003; pp. 1–51.

46. Chang, E. P. Viscoelastic Properties of Pressure-Sensitive Adhesives. *J. Adhes.* **1997**, *60*, 233–248.

47. Marshall, S. J.; Bayne, S. C.; Baier, R.; Tomsia, A. P.; Marshall, G. W. A review of

adhesion science. *Dent. Mater. Off. Publ. Acad. Dent. Mater.* **2010**, *26*, e11–16.

48. Theory Gives Direction to Adhesion Work. *Chem. Eng. News Arch.* **1963**, *41*, 67–88.

49. McBain, J. W.; Hopkins, D. G. On Adhesives and Adhesive Action. *J. Phys. Chem.* **1924**, *29*, 188–204.

50. Derjaguin, B. V.; Smilga, V. P. Electronic Theory of Adhesion. *J. Appl. Phys.* **1967**, *38*, 4609–4616.

51. Voyutskii, S. S.; Vakula, V. L. The role of diffusion phenomena in polymer-to-polymer adhesion. *J. Appl. Polym. Sci.* **1963**, *7*, 475–491.

52. Pizzi, A.; Mittal, K. L. *Handbook of Adhesive Technology, Revised and Expanded*; CRC Press, 2003.

53. Czech, Z.; Milker, R. Development trends in pressure-sensitive adhesive systems. *Mater. Sci. 0137-1339* **2005**, *23*, 1015–1022.

54. Gao, J.; Penlidis, A. A Comprehensive Simulator/Database Package for Reviewing Free-Radical Copolymerizations. *J. Macromol. Sci. Part C* **1998**, *38*, 651–780.

55. Czech, Z. Synthesis and cross-linking of acrylic PSA systems. *J. Adhes. Sci. Technol.* **2007**, *21*, 625–635.

56. Czech, Z.; Pełech, R.; Butwin, A. Biodegradable acrylic pressure-sensitive adhesives. *Czas. Tech. Chem.* **2008**, *R. 105, z. 2-Ch*, 293–301.

57. Jovanović, R.; Dubé, M. A. Emulsion‐Based Pressure‐Sensitive Adhesives: A Review. *J. Macromol. Sci. Part C* **2004**, *44*, 1–51.

58. Stutz, H.; Illers, K.-H.; Mertes, J. A generalized theory for the glass transition temperature of crosslinked and uncrosslinked polymers. *J. Polym. Sci. Part B Polym. Phys.* **1990**, *28*, 1483–1498.

59. Czech, Z. Crosslinking of pressure sensitive adhesive based on water-borne acrylate. *Polym. Int.* **2003**, *52*, 347–357.

60. Czech, Z. Crosslinkable propyleneimine pressure-sensitive adhesive acrylates and their pot life. *Polym. Adv. Technol.* **2004**, *15*, 539–543.

61. Czech, Z. Multifunctional propyleneimines-new generation of crosslinkers for solvent-based pressure-sensitive adhesives. *Int. J. Adhes. Adhes.* **2004**, *24*, 503–511.

62. Czech, Z.; Wojciechowicz, M. The crosslinking reaction of acrylic PSA using chelate metal acetylacetonates. *Eur. Polym. J.* **2006**, *42*, 2153–2160.

63. Czech, Z. New generation of crosslinking agents based on multifunctional methylaziridines. *Int. J. Adhes. Adhes.* **2007**, *27*, 49–58.

64. Snyder, B. S.; Bors, D. A. High cohesive strength pressure-sensitive adhesives incorporating acetoacetate 1994.

65. Gonzâez, I.; Leiza, J. R.; Asua, J. M. Exploring the Limits of Branching and Gel Content in the Emulsion Polymerization of n-BA. *Macromolecules* **2006**, *39*, 5015–5020.

66. Kajtna, J.; Golob, J.; Krajnc, M. The effect of polymer molecular weight and crosslinking reactions on the adhesion properties of microsphere water-based acrylic pressure-sensitive adhesives. *Int. J. Adhes. Adhes.* **2009**, *29*, 186–194.

67. Chauvet, J.; Asua, J. M.; Leiza, J. R. Independent control of sol molar mass and gel content in acrylate polymer/latexes. *Polymer* **2005**, *46*, 9555–9561.

68. Qie, L.; Dubé, M. A. Manipulation of chain transfer agent and cross-linker concentration to modify latex micro-structure for pressure-sensitive adhesives. *Eur. Polym. J.* **2010**, *46*, 1225–1236.

Chapter 3. Copolymerization of Limonene with *n*-Butyl Acrylate

Published in Macromol. React. Eng. (2015) 9: 339–349.

Copolymerization of Limonene with *n*-Butyl Acrylate

Shanshan Ren[1], Esther Trevino[2] and Marc A. Dubé[1,*]

[1] Department of Chemical and Biological Engineering, Centre for Catalysis Research and Innovation, University of Ottawa

[2] Centro de Investigación en Química Aplicada, Saltillo, México

Abstract

The bulk free radical copolymerization of *d*-limonene (Lim) with *n*-butyl acrylate (BA) was carried out at 80°C using benzoyl peroxide as initiator. Low conversion experiments were run to estimate the copolymer reactivity ratios as r_{BA} = 6.07 and r_{Lim} = 0.0067. High conversion experiments were then conducted to validate the reactivity ratios for prediction of cumulative copolymer composition. The presence of allylic hydrogen in Lim caused a notable degradative chain transfer reaction which greatly impeded polymerization. Increasing Lim fractions in the copolymer resulted in a decrease in final conversion and molecular weight, and an increase in glass transition temperature.

Keywords: *d*-limonene; *n*-butyl acrylate; copolymerization; degradative chain transfer; reactivity ratios.

3.1 Introduction

In the face of depleting fossil resources and increasing concerns for the environment, the development of polymeric products from non-toxic, renewable resources is well underway[1]. During the last decade, considerable effort has been devoted to the synthesis of "green" polymers derived from renewable resources, such as wood, essential oils, and plant starches[2,3]. As one of the largest classes of renewable chemical compounds produced in nature, terpenes exhibit great potential for polymerization as they contain isoprene (C_5H_8) as the basic building block in their structure[4]. Terpenes are familiar as main constituents of essential oils in many plants and trees. Plants, such as citrus fruit or conifers, produce terpenes through photosynthesis; the utilization of terpene-based products is therefore considered as carbon-neutral and thereby an interesting option as a chemical feedstock. Terpenes have a strong, particular odour and this has motivated their wide use as flavoring agents in the food, cosmetic and medical industries (e.g., in chewing gums, perfumes, ointments and aromatherapy)[5,6].

Limonene (Lim) is a member of the diverse terpene family and is a major component (>95%) of orange oil; it is mainly extracted from orange peels as a by-product of the juicing process. The production of Lim shows no competition with crops for human food or animal feed and can contribute to the reduction in the emission of greenhouse gases and toxic pollutants compared to its fossil-based counterparts[7]. The ability to achieve a product in an almost pure form, as well as its

abundant production (over 70 million kg/year)[8], makes Lim an ideal renewable compound that could replace many toxic chemicals. Lim is increasingly being used as a renewable reaction medium[9,10] or eco-friendly solvent for cleaning and separation purposes[8,11]. Lim ($C_{10}H_{16}$) is an unsaturated cyclic hydrocarbon which possesses two non-conjugated double bonds: an endocyclic double bond and an exocyclic double bond, both of which provide potential for polymerization (see Figure 3.1(a)). However, because of the ring strain energy and steric impediments, the endocyclic double bond of Lim shows a much lower reactivity than the exocyclic vinyl group during polymerization[12–14]. The polymerization of Lim has been studied since the 1950s[15]. Early attempts at Lim solution polymerization using Lewis acids and Ziegler-Natta catalysts yielded low molecular weight products (M_w = ~1000, less than 10 repeat units)[15,16]. Cationic polymerization efforts yielded a much lower Lim conversion (7%) than styrene (92%) under the same conditions[12]. In the cationic copolymerization of Lim with indene, a non-polar olefin, Lim exhibited low reactivity and acted as a chain-transfer agent by presenting low co-monomer incorporation and decreased molecular weights. More recent efforts using coordination catalysts to copolymerize Lim with ethylene yielded similar results[13]. Lim was also used as both a renewable solvent and chain transfer agent to modify polymer molecular weight[9,10,17,18]. However, a variety of polymerization methods, including free-radical, cationic and coordination polymerization, have shown no evidence for high molecular weight poly(Lim) synthesis. This is mainly due

to the competition between propagation and the chain-transfer reaction resulting from Lim's structure (Figure 3.1). Nonetheless, commercial Lim oligomers are produced for use as tackifiers or modifiers in rubber and adhesive formulations[19].

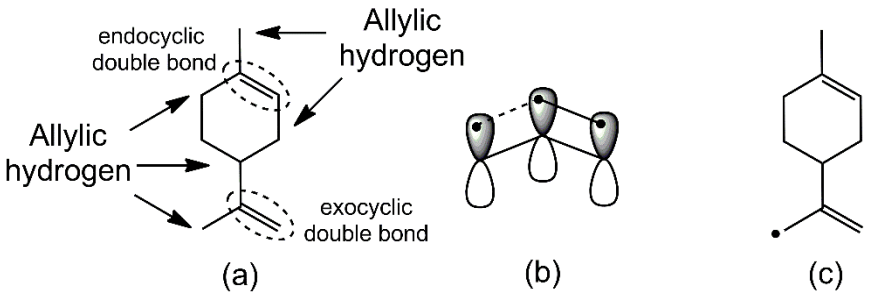

Figure 3.1 (a) Lim and its allylic hydrogen; (b) π orbital of allyl system; and (c) example of Lim allylic radical.

It is well-known that free-radical polymerization presents the advantages of being less sensitive to impurities, requiring moderate reaction temperatures, and having applicability to a broad range of monomers, compared to other methods[20]. Not surprisingly, therefore, free-radical *co*polymerization may provide an effective way to incorporate Lim into polymer products. Doiuchi and coworkers synthesized alternating Lim/maleic anhydride copolymer (1:2 mol:mol) via inter-intramolecular cyclopolymerization[21]. The propagation mechanism was later reinvestigated as the exocyclic double bonds of Lim reacted first and yielded a 1:1 (mol:mol) alternating copolymer. Evidence that the endocyclic double bonds could react further at higher conversion and form branched or crosslinked copolymers with additional maleic anhydride units was shown[22]. Subsequently, the free-radical solution

copolymerization of Lim with a range of vinyl co-monomers, such as acrylonitrile[23], methyl methacrylate[24], styrene[25], butyl methacrylate[14], N-vinyl pyrrolidone and vinyl acetate[26], were studied. In all cases, the polymerization rates were greatly reduced due to the presence of Lim. More recently, the bulk copolymerization of Lim with BMA and 2-ethyl hexyl acrylate was investigated[27].

To our knowledge, the copolymerization of Lim with *n*-butyl acrylate (BA) has not been studied. The low BA homopolymer glass transition temperature (T_g) of -54 ^oC, among other properties, enables its use in coatings and adhesives. Aside from the environmental benefits for its use, the addition of Lim is expected to achieve a variety of physical properties by balancing the T_g and stiffness of the polymer chains in BA-containing coatings and adhesives. In this study, co-monomer reactivity ratios for the bulk free-radical copolymerization of Lim with BA were estimated using low conversion designed experiments. High conversion experiments were then conducted to examine composition drift, molecular weight development and T_g. The effects of degradative chain transfer on the copolymerization mechanism due to Lim are also discussed.

3.2 Experimental

3.2.1 Materials

n-Butyl acrylate (BA) (≥ 99%), benzoyl peroxide (BPO), and 1,1-Di-(tert-butylperoxy)-3,3,5-trimethylcyclohexane (Luperox 231) were purchased

from Sigma Aldrich. BA was passed through an inhibitor removal column (Sigma Aldrich) to remove the monomethyl ether hydroquinone inhibitor before use. BPO was recrystallized twice with acetone and deionized water, dried under vacuum at room temperature, and then stored in a refrigerator at 4^{o}C before use. Luperox 231 was used as received without further purification. Lim was obtained from Fisher Scientific (96%), and was distilled under vacuum at 65-70^{o}C before use.

3.2.2 Reactivity ratio experiments

Bulk free radical polymerizations of BA/Lim were carried out in glass ampoules (10 mm diameter and 200 mm in length). About 5 g of monomer (BA and Lim) plus initiator (0.5 wt% BPO) were pipetted into each ampoule. Each glass ampoule was degassed using a freeze-pump-thaw procedure (typically, three cycles), flame-sealed and the frozen ampoule was placed in an ice water bath while preparing all other ampoules. All the ampoules were then placed in a constant temperature oil bath at 80 ℃. The copolymerizations were stopped at pre-determined time intervals to achieve low conversions (<6%). The ampoules were then removed from the oil bath and immediately immersed in an ice bath to stop the reaction. The polymeric products were precipitated in excess methanol (~100 mL) to remove unreacted monomers. The excess liquid was decanted and the polymer samples were dried in a ventilated oven at 40 ℃ until a constant weight was achieved. To avoid the loss of low molecular weight compounds (i.e., oligomers), the reaction products from low BA feed runs (i.e., f_{BA} (BA molar fraction in feed) = 0.1-0.3), were directly poured into an aluminum dish

and dried to constant weight in a vacuum oven.

Reactivity ratios are typically estimated by substituting feed and instantaneous copolymer composition values from a set of experiments into the Mayo-Lewis equation[28]:

$$\frac{F_{BA}}{F_{Lim}} = \frac{f_{BA}(r_{BA}f_{BA} + f_{Lim})}{f_{Lim}(r_{Lim}f_{Lim} + f_{BA})} \qquad \text{(Eq. 3.1)}$$

where F_{BA} and F_{Lim} are the instantaneous copolymer composition at corresponding feed compositions, f_{BA} and f_{Lim}, respectively. In this study, a non-linear error-in-variables model program (RREVM) developed specifically for the estimation of reactivity ratios was used[29,30]. A preliminary set of experiments, nine equidistant points along the feed composition axis, was performed to low conversion (<6 wt%). The results of these experiments were used to obtain initial estimates of the reactivity ratios using the RREVM software. Four replicate runs at each of the feed compositions, $f'_{BA} = \frac{2}{2 + r_{BA}}, f''_{BA} = \frac{r_{Lim}}{r_{Lim} + 2}$, recommended by Tidwell and Mortimer[31] and using the initial reactivity ratio estimates were then performed to obtain the final reactivity ratios.

3.2.3 High conversion experiments

Experiments geared toward achieving elevated monomer conversions were conducted at various comonomer feed compositions at initiator concentrations of 1 wt% BPO at 80℃. The procedure was essentially the same as for the reactivity ratio

experiments except that ampoules were periodically withdrawn at pre-determined times to achieve a range of monomer conversions. It is noted that during sample work-up, higher conversion samples exhibiting high viscosity were first dissolved in 10-15 mL toluene for 1-2 h and subsequently precipitated in excess methanol (~100 mL). After decanting the supernatant, the samples were then dried in a ventilated oven at 40 ℃ until a constant weight was achieved.

3.2.4 Characterization

Monomer conversions were determined by gravimetry based on the mass of dried polymer. The cumulative composition of isolated copolymers was measured using ^{1}H nuclear magnetic resonance spectroscopy (^{1}H-NMR, 400MHz, Bruker Avance). Polymer samples were dissolved in deuterated chloroform and scanned 32 times at room temperature.

Gel permeation chromatography (GPC) was used to determine the number-average (M_n) and weight-average (M_w) molecular weights and the molecular weight distribution (MWD). An Agilent GPC system was used and consisted of two columns (MZ-Gel SD plus 10^5 Angstroms 300 x 8.00 mm, particle size 5 μm, MZ-Gel SD plus 10^4 Angstroms 300 x 8.00 mm, particle size 5 μm), a multi-angle laser light scattering detector (DAWN HELEOS II, λ=633 nm, Wyatt Technology), a differential refractive index detector (Optilab T-rEX, Wyatt Technology) and a differential viscometer (ViscoStar ll, Wyatt Technology). Tetrahydrofuran (THF) was used as the mobile phase at a 1 mL/min flow rate. Samples diluted in THF were filtered through a

0.45 μm syringe filter prior to injection into the GPC. The refractive index increment (dn/dc) of BA/Lim copolymer (BA mol% = 0.90) was measured (in THF at 25 ℃) as 0.140 mL/g with the Wyatt Optilab T-rEX refractometer (λ = 633 nm). This value was applied to all copolymer samples (F_{BA} = 0.96 to 0.72) for molecular weight calculation.

Differential Scanning Calorimetry (DSC, TA Instruments) was used to determine the copolymer T_g. Polymer samples were put in a closed sample pan and underwent the following heating procedure in air: heating from -95 to 150°C at 10°C /min, isothermal for 3 min at 150°C, cooling from 150 to -95 ℃, isothermal for 3 min at -95 ℃ and then reheating from -95 to 150 ℃ to eliminate the thermal history of the sample. T_g was determined as the inflection point on the heat flow curve using the second heating cycle.

3.3 Results and Discussion

3.3.1 Homopolymerization of Lim

Homopolymerization of Lim was carried out at 80 ℃ using BPO as initiator. As expected, only nearly undetectable amounts of oligomers were obtained, which reflects the difficulty in Lim homopolymerization via free-radical methods. As a non-polar allylic olefin, Lim is difficult to convert to high molecular weight homopolymers and to achieve high conversions. This is explained by the high reactivity of allylic hydrogens, which tend to reduce molecular weight by a

degradative chain transfer mechanism[32,33]. The allylic hydrogen is attached to the allylic carbon next to the double bonds (see Figure 3.1(a)). The high reactivity of allylic hydrogen results from resonance among the unpaired electrons of allylic radicals and π-bonds (Figure 3.1(b))[34,35]. During free-radical polymerization, the propagating polymer radical has a higher probability of reacting with an allylic hydrogen, thus leading to chain transfer to Lim; a new allylic radical is then formed while the polymer chain is terminated (Figure 3.1(c)). This process competes remarkably well with normal chain propagation, and because of the allylic radical stability[20], propagation with monomers is highly likely to stop after only a few monomer units, if any, are added.

3.3.2 Copolymer composition measurement

As noted earlier, the copolymer compositions were measured using ^{1}H-NMR spectroscopy. A typical NMR spectrum along with peak assignments for BA/Lim copolymer is shown in Figure 3.2. The molecular structures for BA and Lim (Lim) bound in the copolymer as well as the structure of Lim incorporated via chain transfer and as the end unit of the polymer chain (Lim') are also shown in Figure 3.2.

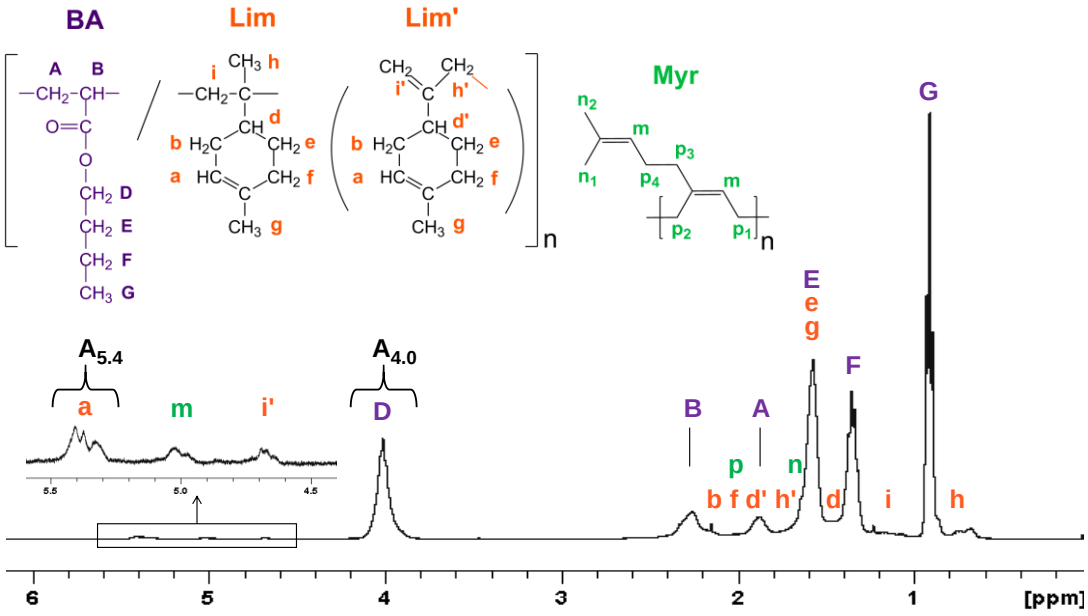

Figure 3.2 ^{1}H-NMR spectrum of BA/Lim copolymer (sample 3 from Table 3.1).

The peaks of the –OCH_2 group for BA are located at ~4.0 ppm; the peaks for the Lim endocyclic and exocyclic double bonds are located at 5.4 ppm and 4.7 ppm, respectively. As the endocyclic double bond of Lim is very stable[12,13,24], it is a reasonable assumption that only the exocyclic double bonds participated in the polymerization, whereas the endocyclic double bonds remained in the polymer chain. Thus, the following equation was used to calculate copolymer composition:

$$BA\% = \frac{\frac{A_{4.0}}{2}}{\frac{A_{4.0}}{2} + A_{5.4}} \qquad \text{(Eq. 3.2)}$$

where $A_{4.0}$ refers to the peak area at δ = 3.8 - 4.2 which corresponds to the -OCH_2- protons of BA (“D” in Figure 3.2), and $A_{5.4}$ refers to the endocyclic double bond of Lim (“a” in Figure 3.2).

Table 3.1 Bulk BA/Lim copolymerization results for reactivity ratio estimation (80°C, [BPO] = 0.5 wt%).

Sample	f_{BA} (mol%)	F_{BA} (mol%)	Time (min)	Conversion (wt%)
1	0.101	0.611	410	4.7
2	0.202	0.728	180	2.6
3	0.299	0.781	120	2.9
4	0.399	0.841	90	3.6
5	0.500	0.872	70	4.0
6	0.600	0.901	60	4.8
7	0.699	0.929	45	5.0
8	0.794	0.952	30	4.7
9	0.896	0.977	15	4.2
TM1-1	0.447	0.857	80	3.6
TM1-2	0.446	0.848	80	3.6
TM1-3	0.450	0.852	80	3.7
TM1-4	0.447	0.853	80	3.6
TM2-1	0.004	0.251	980	1.5
TM2-2	0.004	0.249	980	1.6
TM2-3	0.004	0.254	980	1.2
TM2-4	0.004	0.264	980	1.2

In the copolymer ^{1}H-NMR spectrum, the peak intensity ratio of exocyclic/endocyclic double bonds is far less than 2:1, which is the initial peak ratio of Lim monomer, indicating that the exocyclic double bonds of Lim are mostly reacted through an addition reaction as polymerization proceeds. On the other hand, a small amount of unreacted exocyclic double bonds of Lim (~4.7 ppm) was also observed. This indicates that besides the Lim unit that incorporated through normal chain propagation, another type of Lim unit (Lim' in Figure 3.2), which contains both endocyclic and exocyclic alkene groups, was formed during the copolymerization due

to degradative chain transfer induced by an allylic hydrogen. Lim contains more than one allylic hydrogen (see Figure 3.1 (a)), and these can all become reactive sites for degradative chain transfer. Even though the highly substituted tertiary allylic radical usually presents the highest stability, in the case of Lim, the formation of a primary allylic radical would be more likely due to reduced steric hindrance and is believed to be the dominant species generated during the chain transfer reaction[27]. Since these allylic radicals are not prone to propagate, they either terminate with each other or more likely (because of Lim's bulkiness), with propagating chain radicals to yield polymer chains ending with a Lim' unit. A suggested BA/Lim copolymerization mechanism is shown in Figure 3.3.

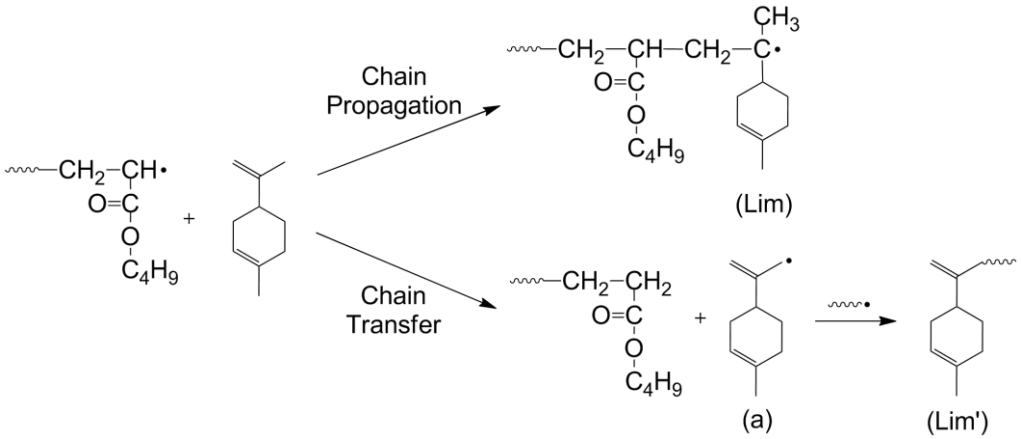

Figure 3.3 Mechanism of propagation and chain transfer in BA/Lim copolymerization.

The copolymer microstructure was further confirmed with a ^{1}H-NMR 2D COSY spectrum of BA/Lim copolymer (F_{BA} = 0.69), which clearly showed the interactions among protons (see Figure 3.4). As seen in Figure 3.4, for BA, the

-OCH_2- (D) was coupled to the -CH_2- (E), -CH_2- (E) was coupled to the -CH_2- (F), and -CH_2- (F) was coupled to the -CH_3 (G). In addition, interactions of the exocyclic and endocyclic double bond protons of Lim were clearly observed: the endocyclic double bond proton =CH- (a) was coupled with the nearby protons of -CH_2- (b) and -CH_3 (g); the exocyclic bond proton =CH_2 (i') was coupled with the nearby methyl protons of -CH_3 (h').

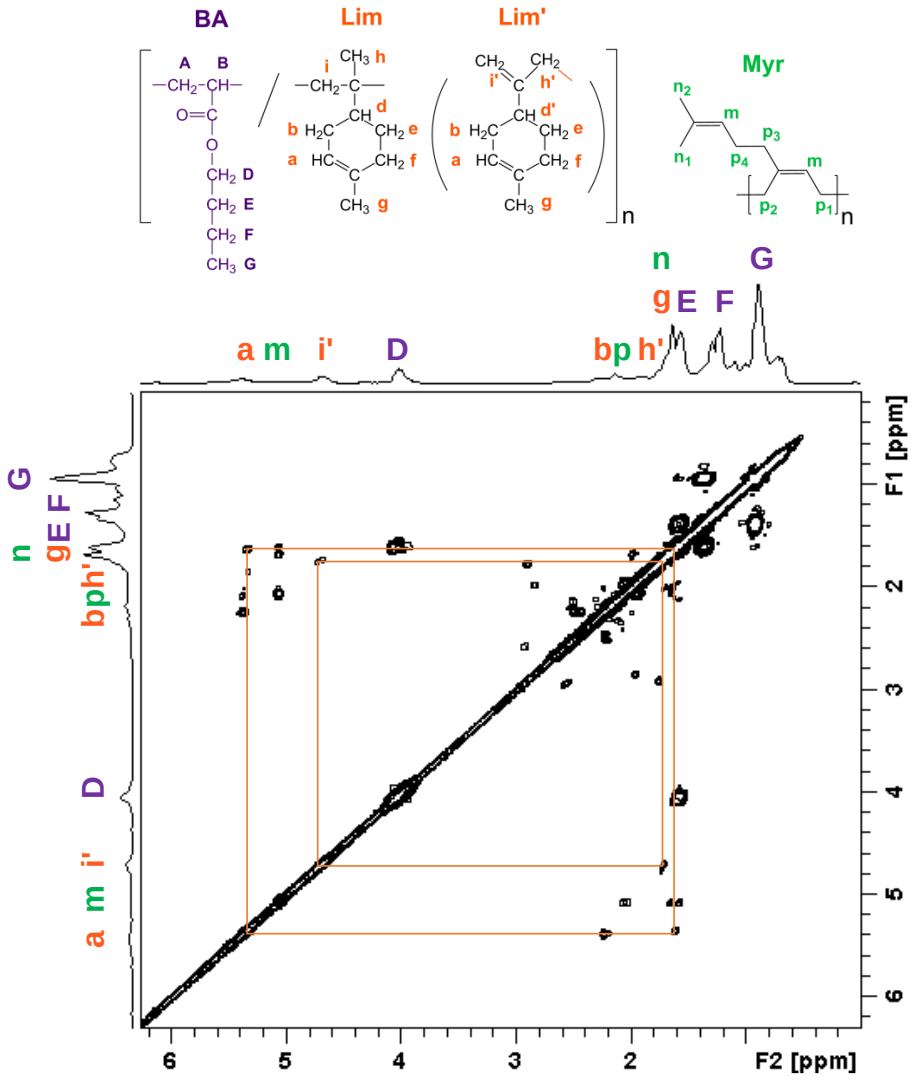

Figure 3.4 ^{1}H-NMR 2D COSY spectrum of BA/Lim copolymer in $CDCl_3$, (F_{BA} = 0.69).

It is worth noting that the NMR peak at ~5.0 ppm is attributable to myrcene units incorporated into the polymer. Myrcene is the main impurity found in Lim at typical levels of ~4-5% (see Figure 3.5). The purification of Lim is often done via distillation and because of their similar boiling points, Lim and myrcene are not readily separated. Myrcene also has a much higher tendency to homopolymerize than Lim, and the three double bonds of myrcene are all prone to reaction. In all of the studies noted earlier, the myrcene peak was not identified. The double bond of poly(myrcene) is clearly observed in our NMR spectrum (see peak "m" in Figure 3.2). The interaction of myrcene protons was also observed in the 2D COSY spectrum (see Figure 3.4). The small peak decreased with reaction time and finally disappeared at higher conversions. One should keep in mind that because of its conjugated nature, myrcene will lead to branching reactions. The level of myrcene in our samples was measured to be 2 wt% of the Lim content. This amount was deemed to have a negligible effect on our results due to the significant incorporation of Lim in the copolymers. The presence of trace amounts of isomers is a common problem when bio-sourced feedstocks are used. For practical commercial production, further purification of Lim would not be cost effective and thus, the inclusion of myrcene is appropriate in this study.

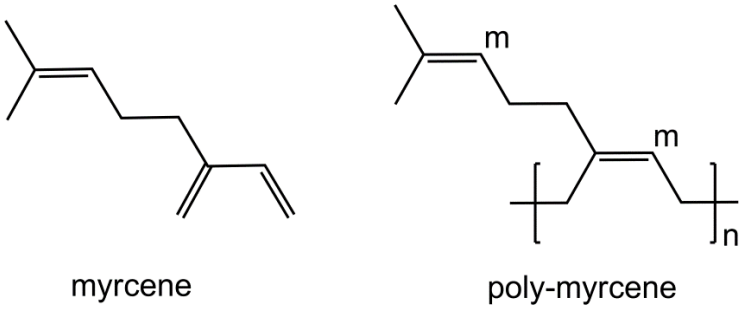

Figure 3.5 Structure of myrcene and poly(myrcene).

3.3.3 Reactivity ratio estimation

The bulk copolymerization of BA/Lim was conducted using BPO at 80℃ under various feed compositions. Monomer feed composition, copolymer composition and conversion data from these experiments are shown in Table 3.1. The polymerizations yielded transparent, viscous polymers. The copolymer compositions and corresponding feed compositions were input to the Mayo-Lewis equation (Equation (1)) via the RREVM computer program for the estimation of reactivity ratios[29]. A measurement error of 5% for the polymer composition data in Table 3.1 was used. The final reactivity ratios were calculated to be r_{BA} = 6.07 and r_{Lim} = 0.0067 and are shown along with 95% joint confidence regions in Figure 3.6. The Mayo-Lewis model and corresponding data are shown in Figure 3.7. As expected, with increasing Lim content in the feed, more Lim units were incorporated into the copolymer. However, for various feed ratios, the final Lim fractions in the copolymer were all substantially less than the Lim feed content. This is reflected in the estimated co-monomer reactivity ratios, which indicate that both BA- and Lim-ended radical

chains preferentially react with BA monomer rather than Lim; thus, the obtained BA/Lim copolymers were rich in BA, and Lim units were distributed infrequently among poly-BA segments.

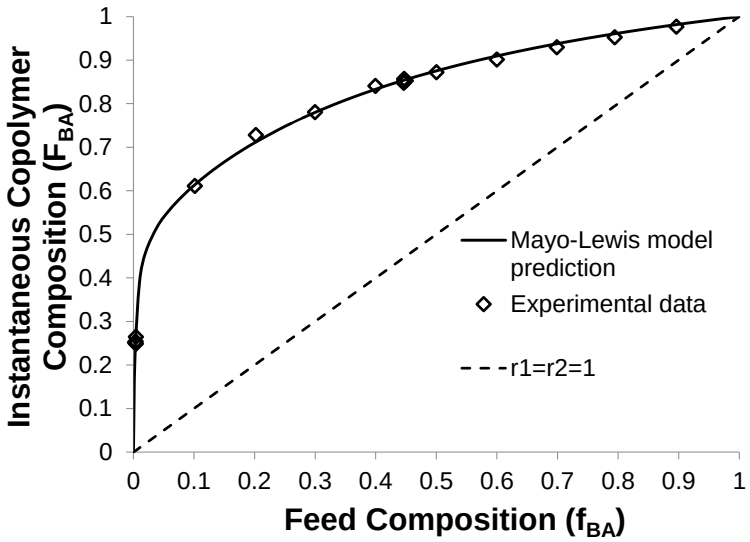

Figure 3.6 Mayo-Lewis plot and experimental data of copolymer composition (F_{BA}) vs. feed composition (f_{BA}).

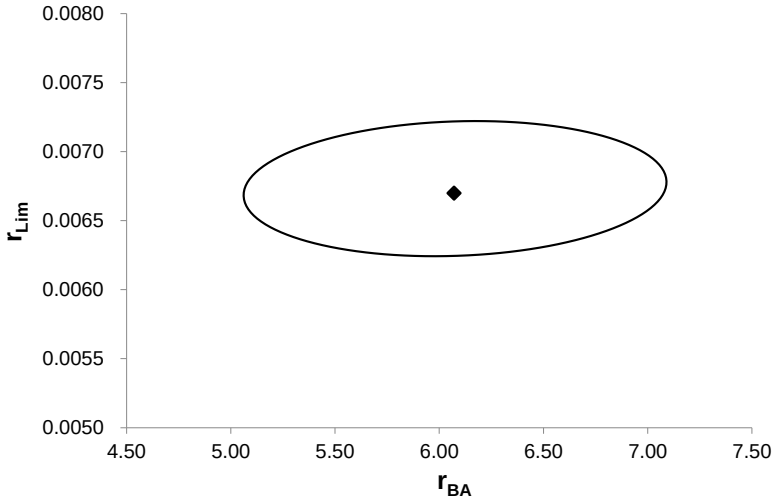

Figure 3.7 Reactivity ratios and 95% joint confidence region for BA/Lim copolymerization.

3.3.4 High conversion polymerization of BA and Lim

High conversion BA/Lim copolymerizations were performed at feed compositions ranging from f_{BA} = 0.1 to 0.9. All runs were conducted at 80ºC using initial initiator concentrations of $[BPO]_0$ = 0.036 mol L^{-1} (1 wt%). Selected conversion vs. time results are plotted in Figure 3.8. The effect of the feed composition is obvious as both the polymerization rate and final conversion were remarkably lower with increasing Lim content in the feed. For example, the copolymerization presented final conversions of 85, 51 and 28% for feed compositions of f_{BA} = 0.9, 0.7 and 0.5, respectively. Given that BPO has a half-life of about 277 min at 80 ℃ (k_d = 4.17 x 10^{-5} s^{-1})[36,37], the concentration of initiator decreased to 8% of its original value after the 17 h polymerizations. Additional experiments were performed at three feed compositions (f_{BA} = 0.6, 0.7, 0.8) using 2 wt.% Luperox 231, a thermal initiator with a half-life of ~10h at 80ºC. Although the initiator concentration was much higher, these copolymerizations resulted in the same conversion range as for BPO runs (see open symbols in Figure 3.8). This implies that the observed limits to conversion and polymerization rate were not due to dead-end polymerization, but rather that the presence of Lim played a role. The decreasing limiting conversions for each run coincide with the decrease in BA monomer concentration in the feed mixture and reflects the fact that Lim is incapable of undergoing any homopolymerization when the amount of BA is low.

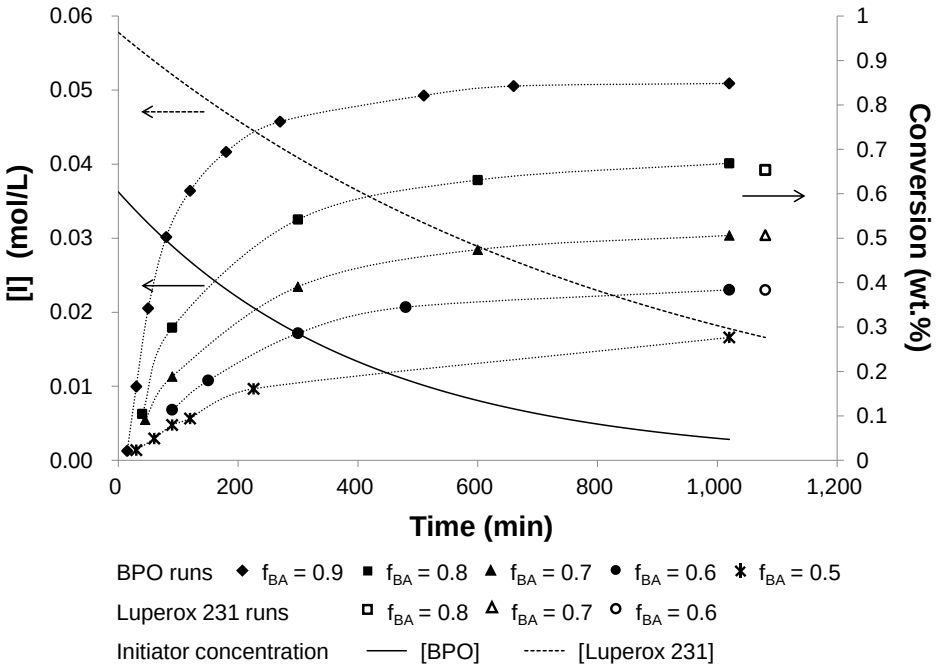

Figure 3.8 Conversion and initiator concentration [I] vs. time for BA/Lim copolymerizations at various feed compositions at 80°C in bulk using [BPO] (1 wt.%) and [Luperox 231] (2 wt.%).

Composition versus conversion results for the nine feed composition runs (f_{BA} = 0.1 to 0.9) and model predictions for the integrated Mayo-Lewis equation are plotted in Figure 3.9. The model predictions were achieved using the reactivity ratios estimated in this work. It is clear that the copolymerization data for each feed composition are fitted well by the integrated Mayo-Lewis model, which serves to further validate the reactivity ratio estimates. The model predictions in Figure 3.9 show a consistent decrease in BA content in the copolymer with increasing conversion. In addition, composition drift becomes more significant with increasing Lim content in the feed and as conversion increases.

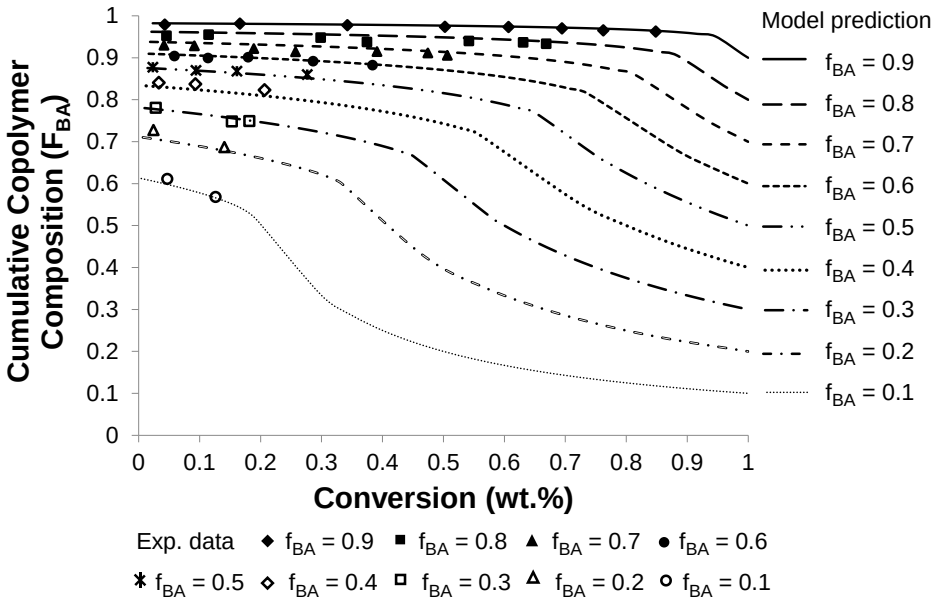

Figure 3.9 Cumulative copolymer composition vs. conversion for BA/Lim bulk copolymerization at various f_{BA}. 80°C, BPO = 1 wt%. Lines are integrated Mayo-Lewis model predictions.

Cumulative molecular weight averages are shown in Table 3.2 and Figure 3.10. The copolymer molecular weight decreased remarkably with increasing Lim fraction in the feed composition. In fact, the molecular weights for the high Lim feed runs (i.e., f_{BA} = 0.3 – 0.1) were too low to be accurately measured with the GPC columns used. The results of this study, taken as a whole, point to significant degradative chain transfer due to the Lim in the copolymerization. For the runs carried out at low Lim feed composition (e.g., f_{BA} = 0.9), both the weight-average molecular weight and the polydispersity index (PDI) increased with conversion. The initial PDI of 1.6 is consistent with the case where termination by combination is favored, as would be expected for BA homopolymerization[38,39]. As conversion increased, termination

became diffusion-controlled and along with branching reactions due to the high BA concentrations, led to a broader molecular weight distribution and higher PDI. However, the weight-average molecular weight profile became relatively flat when the Lim feed composition was increased (e.g., f_{BA} = 0.7 and 0.5). For these runs, more frequent degradative chain transfer reactions occurred and the growing polymer chain was more likely to terminate with a Lim allylic radical rather than another growing polymer chain. Therefore, the polymers exhibited shorter chain lengths and relatively narrower molecular weight distributions (M_w/M_n = ~1.6-1.9) compared to runs at higher BA concentrations. From the discussion above, it is believed that Lim not only acts as a co-monomer but also plays an active role in degradative chain transfer in the copolymerization with BA.

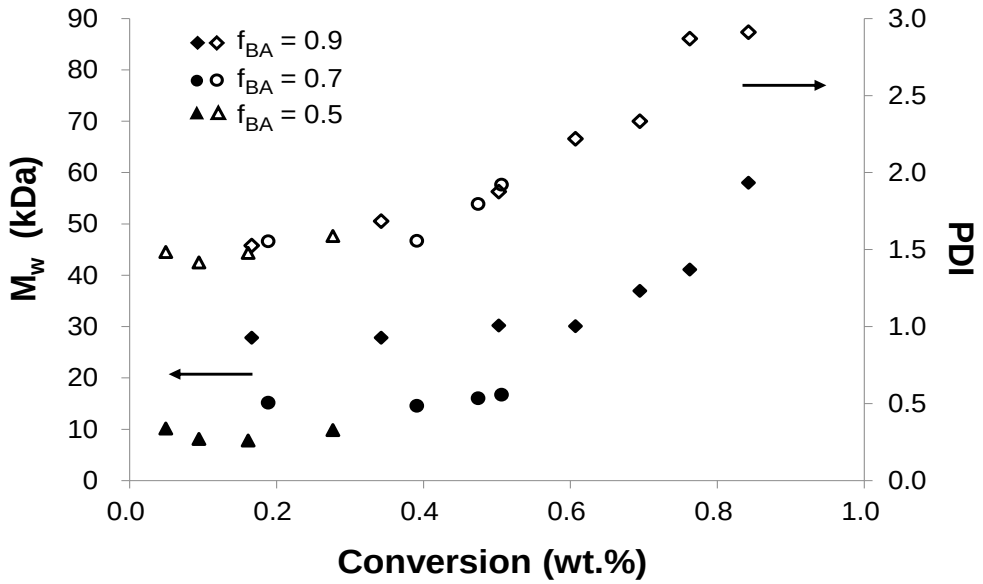

Figure 3.10 Cumulative weight-average (closed symbols, Mw) and polydispersity index (open symbols, PDI) vs. overall conversion.

Table 3.2 Results for final samples of BA/Lim bulk copolymerizations performed at 80°C, [BPO] = 1.0 wt%, 17h reaction time.

Sample	**f_{BA} (mol%)**	**Conv. (wt%)**	**F_{BA} (mol%)**	**F_{lim} (mol%)**	**T_g (°C)**	**M_w (kDa)**	**M_n (kDa)**	**M_w/M_n**
1	0.90	84.3	0.965	0.035	-43.5	58.0	19.9	2.9
2	0.80	66.9	0.933	0.067	-36.9	26.8	11.8	2.3
3	0.70	50.6	0.906	0.094	-27.1	16.7	8.7	1.9
4	0.60	38.4	0.882	0.118	-15.6	12.4	7.2	1.7
5	0.50	27.7	0.860	0.140	-6.7	9.8	6.2	1.6
6	0.40	20.7	0.833	0.167	4.8	7.8	4.8	1.6
7	0.30	18.2	0.749	0.251	-22.4	/	/	/
8	0.20	14.1	0.687	0.313	-27.1	/	/	/
9	0.10	12.6	0.568	0.432	-30.5	/	/	/

Figure 3.11 shows the DSC curves of selected samples. For all the DSC curves, only one T_g was detected. As there was no glass transition observed near -54°C (the T_g for poly-BA), the formation of a copolymer is confirmed. The copolymer T_g was much higher than that for BA homopolymer despite the incorporation of only low amounts of Lim in the copolymer. It should be noted that literature results for Lim homopolymer T_g are scattered because most of the results employ material that is well below the threshold for molecular weight effects on T_g (i.e., below molecular weights of 20,000 Daltons). Nonetheless, because Lim is a fairly rigid molecule, its T_g is certainly high; on a low molecular weight poly(Lim) resin, a T_g of 78°C was measured. Thus, Lim has a significant effect on copolymer T_g.

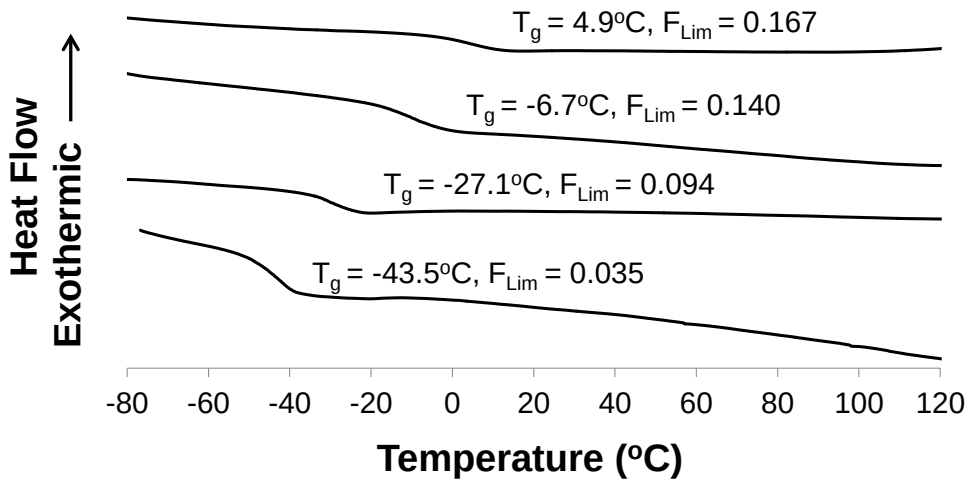

Figure 3.11 DSC curves of poly(n-BA) and BA/Lim copolymers of various composition.

3.4 Conclusion

The bulk free radical copolymerization of BA and Lim was conducted at 80°C. The reactivity ratios, estimated as r_{BA} = 6.07, r_{Lim} = 0.0067, indicate that addition of BA units into the copolymer chain is highly favoured. Nonetheless, inclusion of Lim in the copolymer is indeed possible via two routes; the first being normal propagation and the other by incorporation as the end-unit of the polymer chain due to a degradative chain transfer mechanism. This degradative chain transfer mechanism leads to fairly low incorporation of Lim into the copolymers with significant effects on both molecular weight and T_g. Certainly Lim plays a significant role as a chain transfer agent.

Our ultimate goal is to incorporate Lim into copolymers for use as adhesives

and coatings. The effects on T_g were favourable for the production of such products. On the other hand, the less favourable effects on molecular weight could certainly be compensated using cross-linkers, alternate reaction conditions and possibly terpolymerization.

Another focus of the current study was to incorporate higher amounts of renewable monomers into polymer products. Now that experimentally validated reactivity ratios have been estimated, the use of semi-batch processes to encourage the incorporation of Lim is possible.

3.5 Acknowledgements

Financial support for this work through the Natural Sciences and Engineering Research Council (NSERC) of Canada, Canada Foundation for Innovation (CFI) and Intellectual Ventures is gratefully acknowledged.

3.6 References

1. Dubé, M. A.; Salehpour, S. Applying the Principles of Green Chemistry to Polymer Production Technology. Macromol. React. Eng. 2014, 8, 7–28.

2. Gandini, A. Polymers from Renewable Resources: A Challenge for the Future of Macromolecular Materials. Macromolecules 2008, 41, 9491–9504.

3. Yao, K.; Tang, C. Controlled Polymerization of Next-Generation Renewable Monomers and Beyond. Macromolecules 2013, 46, 1689–1712.

4. Silvestre, A. J. D.; Gandini, A. Chapter 2 - Terpenes: Major Sources, Properties and Applications. In Monomers, Polymers and Composites from Renewable Resources; Elsevier: Amsterdam, 2008; pp. 17–38.

5. Bauer, K.; Garbe, D.; Surburg, H. Common Fragrance and Flavor Materials: Preparation, Properties and Uses; John Wiley & Sons, 2008.

6. Breitmaier, E. Terpenes: Importance, General Structure, and Biosynthesis. In Terpenes; Wiley-VCH Verlag GmbH & Co. KGaA, 2006; pp. 1–9.

7. Pourbafrani, M.; McKechnie, J.; MacLean, H. L.; Saville, B. A. Life cycle greenhouse gas impacts of ethanol, biomethane and limonene production from citrus waste. Environ. Res. Lett. 2013, 8, 015007.

8. Kerton, F. M.; Marriott, R. Alternative Solvents for Green Chemistry; Royal Society of Chemistry, 2013.

9. Mathers, R. T.; Damodaran, K. Renewable chain transfer agents for metallocene polymerizations: The effects of chiral monoterpenes on the polyolefin molecular weight and isotacticity. J. Polym. Sci. Part Polym. Chem. 2007, 45, 3150–3165.

10. Mathers, R. T.; McMahon, K. C.; Damodaran, K.; Retarides, C. J.; Kelley, D. J. Ring-Opening Metathesis Polymerizations in d-Limonene: A Renewable Polymerization Solvent and Chain Transfer Agent for the Synthesis of Alkene Macromonomers. Macromolecules 2006, 39, 8982–8986.

11. Gu, Y.; Jérôme, F. Bio-based solvents: an emerging generation of fluids for the design of eco-efficient processes in catalysis and organic chemistry. Chem. Soc. Rev.

2013, 42, 9550.

12. Brum, F. J. B.; Laux, F. N.; Forte, M. M. C. Synthesis of hydrocarbon polymers by cationic polymerization and their thermal properties. Des. Monomers Polym. 2013, 16, 291–301.

13. Nakayama, Y.; Sogo, Y.; Cai, Z.; Shiono, T. Copolymerization of ethylene with 1,1-disubstituted olefins catalyzed by ansa-(fluorenyl)(cyclododecylamido) dimethyltitanium complexes. J. Polym. Sci. Part Polym. Chem. 2013, 51, 1223–1229.

14. Sharma, S.; Srivastava, A. K. Free radical copolymerization of limonene with butyl methacrylate: Synthesis and characterization. Indian J. Chem. Technol. 2005, 12, 62–67.

15. Roberts, W. J.; Day, A. R. A Study of the Polymerization of α- and β-Pinene with Friedel—Crafts Type Catalysts. J. Am. Chem. Soc. 1950, 72, 1226–1230.

16. Modena, M.; Bates, R. B.; Marvel, C. S. Some low molecular weight polymers of d-limonene and related terpenes obtained by Ziegler-type catalysts. J. Polym. Sci. A 1965, 3, 949–960.

17. Mathers, R. T.; Damodaran, K.; Rendos, M. G.; Lavrich, M. S. Functional Hyperbranched Polymers Using Ring-Opening Metathesis Polymerization of Dicyclopentadiene with Monoterpenes. Macromolecules 2009, 42, 1512–1518.

18. Delancey, J. M.; Cavazza, M. D.; Rendos, M. G.; Ulisse, C. J.; Palumbo, S. G.; Mathers, R. T. Controlling crosslinking in thermosets via chain transfer with monoterpenes. J. Polym. Sci. Part Polym. Chem. 2011, 49, 3719–3727.

19. Benedek, I.; Feldstein, M. M. Technology of pressure-sensitive adhesives and products; Handbook of pressure-sensitive adhesives and products; CRC Press: Boca Raton, FL, 2008.

20. Odian, G. Radical Chain Polymerization. In Principles of Polymerization; John Wiley & Sons, Inc., 2004; pp. 198–349.

21. Doiuchi, T.; Yamaguchi, H.; Minoura, Y. Cyclocopolymerization of d-limonene with maleic anhydride. Eur. Polym. J. 1981, 17, 961–968.

22. Maślińska-Solich, J.; Kupka, T.; Kluczka, M.; Solich, A. Optically active polymers, 2. Copolymerization of limonene with maleic anhydride. Macromol. Chem. Phys. 1994, 195, 1843–1850.

23. Sharma, S.; Srivastava, A. K. Radical Copolymerization of Limonene with Acrylonitrile: Kinetics and Mechanism. Polym.-Plast. Technol. Eng. 2003, 42, 485–502.

24. Sharma, S.; Srivastava, A. K. Alternating Copolymers of Limonene with Methyl Methacrylate: Kinetics and Mechanism. J. Macromol. Sci. Part A 2003, 40, 593–603.

25. Sharma, S.; Srivastava, A. K. Synthesis and characterization of copolymers of limonene with styrene initiated by azobisisobutyronitrile. Eur. Polym. J. 2004, 40, 2235–2240.

26. Sharma, S.; Srivastava, A. K. Azobisisobutyronitrile-initiated free-radical copolymerization of limonene with vinyl acetate: Synthesis and characterization. J. Appl. Polym. Sci. 2007, 106, 2689–2695.

27. Zhang, Y.; Dubé, M. A. Copolymerization of n-Butyl Methacrylate and D-Limonene. Macromol. React. Eng. 2014, 8, 805–812.

28. Mayo, F. R.; Lewis, F. M. Copolymerization. I. A Basis for Comparing the Behavior of Monomers in Copolymerization; The Copolymerization of Styrene and Methyl Methacrylate. J. Am. Chem. Soc. 1944, 66, 1594–1601.

29. Dubé, M.; Sanayei, R. A.; Penlidis, A.; O'Driscoll, K. F.; Reilly, P. M. A microcomputer program for estimation of copolymerization reactivity ratios. J. Polym. Sci. Part Polym. Chem. 1991, 29, 703–708.

30. Polic, A. L.; Duever, T. A.; Penlidis, A. Case studies and literature review on the estimation of copolymerization reactivity ratios. J. Polym. Sci. Part Polym. Chem. 1998, 36, 813–822.

31. Tidwell, P. W.; Mortimer, G. A. An improved method of calculating copolymerization reactivity ratios. J. Polym. Sci. A 1965, 3, 369–387.

32. Bartlett, P. D.; Altschul, R. The Polymerization of Allyl Compounds. II. Preliminary Kinetic Study of the Peroxide-Induced Polymerization of Allyl Acetate. J. Am. Chem. Soc. 1945, 67, 816–822.

33. Dowbenko, R. Allyl Monomers and Polymers. In Kirk-Othmer Encyclopedia of Chemical Technology; John Wiley & Sons, Inc., 2000.

34. Gobbi, A.; Frenking, G. Resonance Stabilization in Allyl Cation, Radical, and Anion. J. Am. Chem. Soc. 1994, 116, 9275–9286.

35. Litt, M.; Eirich, F. R. Polymerization of allyl acetate. J. Polym. Sci. 1960, 45,

379–396.

36. Barnett, B.; Vaughan, W. E. The Decomposition of Benzoyl Peroxide. II. The Rates of Decomposition in Various Solvents. J. Phys. Colloid Chem. 1947, 51, 942–955.

37. Soulé, Ezequiel R.; Borrajo, J.; Williams, R. J. J. Presence of Two Maxima in the Isothermal Free-Radical Polymerization Rate of Isobornyl Methacrylate Retarded by Oxygen. Macromolecules 2004, 37, 1551–1557.

38. Moad, G.; Solomon, D. H. 5 - Termination. In The Chemistry of Radical Polymerization (Second Edition); Elsevier Science Ltd: Amsterdam, 2005; pp. 233–278.

39. Elizalde, O.; Arzamendi, G.; Leiza, J. R.; Asua, J. M. Seeded Semibatch Emulsion Copolymerization of n-Butyl Acrylate and Methyl Methacrylate. Ind. Eng. Chem. Res. 2004, 43, 7401–7409.

40. Robin, S.; Guerret, O.; Couturier, J.-L.; Pirri, R.; Gnanou, Y. Synthesis and Characterization of Poly(styrene-b-n-butyl acrylate-b-styrene) Triblock Copolymers Using a Dialkoxyamine as Initiator. Macromolecules 2002, 35, 3844–3848.

41. Lorimer, J. W.; Jones, D. E. G. Refractive index increments of polymers in solution: 2. Refractive index increments and light-scattering in polydisperse systems of low molecular weight. Polymer 1972, 13, 52–56.

42. Margerison, D.; Bain, D. R.; Kiely, B. Variation of refractive index increment with molecular weight. Polymer 1973, 14, 133–136.

43. Candau, F.; Fran ̧ois, J.; Benoit, H. Effect of molecular weight on the refractive index increment of polystyrenes in solution. Polymer 1974, 15, 626–630.

Chapter 4. Modeling of the Copolymerization Kinetics of *n*-Butyl Acrylate and *d*-Limonene using PREDICI

Published in Processes 2016, 4(1), 1.

Modeling of the Copolymerization Kinetics of *n*-Butyl acrylate and *d*-Limonene using PREDICI

Shanshan Ren [1], Eduardo Vivaldo-Lima[2], Marc A. Dubé[1,*]

[1] Department of Chemical and Biological Engineering, Centre for Catalysis Research and Innovation, University of Ottawa.

[2] Facultad de Química, Departamento de Ingeniería Química, Universidad Nacional Autónoma de México, México.

Abstract

Kinetic modeling of the bulk copolymerization of *d*-limonene (Lim) and *n*-butyl acrylate (BA) at 80°C was performed using PREDICI. Model predictions of conversion, copolymer composition and average molecular weights are compared to experimental data at five different feed compositions (BA mol fraction = 0.5 to 0.9). The model illustrates the significant effects of degradative chain transfer due to the allylic structure of Lim as well as the intramolecular chain transfer mechanism due to BA.

Keywords: modeling; polymerization kinetics; *n*-butyl acrylate; *d*-limonene

4.1 Introduction

Due to environmental constraints and the need to reduce human dependence on fossil resources, the use of renewable chemical compounds and the incorporation of a naturally-occurring carbon framework into polymer chains has attracted great interest[1,2]. As one of the largest class of renewable feedstocks, terpenes present great potential to replace fossil-based chemical compounds because of their low toxicity, abundant production, and significantly low contribution to the carbon cycle[3–5]. *d*-Limonene (Lim) is a cyclic monoterpene which consists of one isoprene (C_5H_8) unit and is obtained as a by-product from the orange juice industry. For all practical purposes, the free-radical homopolymerization of Lim is not possible. However, the free-radical copolymerization of Lim with various monomers, such as *n*-butyl acrylate (BA)[6], butyl methacrylate (BMA)[7], 2-ethyl hexyl acrylate (EHA)[8], etc., has been reported. In our previous studies[6,9], it was shown that degradative chain transfer due to the presence of Lim competed remarkably with chain propagation. The suppression of both rate of polymerization and molecular weight development were observed. In order to get better insight on the mechanism and the corresponding kinetic parameters related to Lim, a comprehensive model of free-radical copolymerization of BA/Lim was developed using the PREDICI simulation package. The model is an extension of previous efforts for the BMA/Lim and EHA/Lim systems[10]. The current effort includes further refinement of the Lim rate parameters and addition of an intramolecular chain transfer (i.e., back-biting) mechanism for BA.

BA is a common monomer that is widely used in coating and adhesive formulations due to its excellent resistance to water, solvent and sunlight, as well as the transparency and low-temperature flexibility of its polymer. The mechanism and kinetic parameters of BA have been well-studied for various homo- and copolymerization systems. Recently, it has been reported that the polymerization rate of BA measured by the pulsed-laser polymerization method is much slower than expected for chain-end propagation, and this is due to the intramolecular chain-transfer of BA (also referred to as backbiting) yields tertiary radicals which present much slower propagation rates than the typical secondary radicals resulting from chain-end propagation[11–13]. The backbiting mechanism was considered in this work, and the corresponding parameters were mainly taken from Hutchinson and Rantow's work[11,14–17]. Other basic kinetic parameters used in this work were obtained from the WATPOLY database from the University of Waterloo[18–20], which contains parameters for a wide range of monomers, initiators, solvents, CTAs, etc., and can provide good predictions on polymerization rate, composition and molecular weight in bulk/solution/emulsion systems under a broad range of reaction conditions.

4.2 Experimental Section

The polymerization conditions and experimental data used herein are from a previous experimental study of the BA/Lim system[6]. Several bulk

copolymerizations for five separate BA/Lim feed concentrations were conducted at 80^{o}C using benzoyl peroxide (BPO) as the initiator. Polymerizations were performed in glass ampoules in an oil bath. Oxygen was removed using several freeze-pump-thaw cycles. Monomer conversion was determined by gravimetry; copolymer composition was measured by ^{1}H-NMR spectroscopy; and average molecular weights and distribution were obtained by gel permeation chromatography (GPC) equipped with a multi-angle light scattering detector, a differential refractive index detector and a differential viscometer. The initial monomer and initiator concentrations are shown in Table 4.1.

Table 4.1 Experimental conditions for BA/Lim bulk polymerization at 80^{o}C.

Monomer Feed (BA molar fraction)	[BA] (mol L^{-1})	[Lim] (mol L^{-1})	[BPO] (mol L^{-1})
f_{BA} = 0.9	6.13	0.68	0.036
f_{BA} = 0.8	5.38	1.35	0.036
f_{BA} = 0.7	4.65	2.00	0.036
f_{BA} = 0.6	3.91	2.67	0.036
f_{BA} = 0.5	3.26	3.26	0.036

4.3 Model development

The polymerization mechanism was implemented in PREDICI and was based on conventional free-radical bulk copolymerization kinetics. Equations describing intramolecular chain transfer (BA) and degradative chain transfer (Lim) were added to the mechanism. Parameter values were taken initially from the literature (including

from our previous modeling work on BMA/Lim[10]). The only parameters adjusted were the homopropagation rate constants for BA and Lim. The model equations and initial and final parameter values are shown in Table 4.2. In Table 4.2, unreferenced initial parameters were initial guesses for the parameters.

Table 4.2 Polymerization mechanism and kinetic rate constants used for the PREDICI simulation of the bulk free-radical copolymerization of BA/Lim at 80°C[a].

Description	Step in PREDICI	Variables	Initial value (L mol^{-1} s^{-1} unless otherwise stated)
Initiation			
Initiator decomposition	$I \rightarrow 2fR^{\bullet}$	k_d, f	$k_d = 2.52 \times 10^{-5}$ s^{-1}[21], f=0.6
First propagation to Lim	$R^{\bullet}+M_1 \rightarrow Lim^{\bullet}$	k_{i1}	1.3[10], adjusted value = 0.325
First propagation to BA	$R^{\bullet}+BA \rightarrow BA^{\bullet}$	k_{i2}	4.97×10^4[17,22]
Propagation			
Self-propagation of Lim	$PLim(s)^{\bullet}+Lim \rightarrow PLim(s+1)^{\bullet}$	k_{p11}	1.3[10], adjusted value = 0.325
Cross-propagation	$PLim(s)^{\bullet}+BA \rightarrow PBA(s+1)^{\bullet}$	k_{p12}	19.9, adjusted value = 48.5
Self-propagation of BA	$PBA(s)^{\bullet}+BA \rightarrow PBA(s+1)^{\bullet}$	k_{p22}	4.97×10^4[17,22] adjusted value = 2.49×10^5
Cross-propagation	$PBA(s)^{\bullet}+Lim \rightarrow PLim(s+1)^{\bullet}$	k_{p21}	8.2×10^3, adjusted value = 4.10×10^4
Chain transfer			
Chain transfer to BA	$PLim(s)^{\bullet}+BA \rightarrow P(s)+BA^{\bullet}$	k_{fm12}	1.44×10^{-2}
Chain transfer to BA	$PBA(s)^{\bullet}+BA \rightarrow P(s)+BA^{\bullet}$	k_{fm22}	3.68×10^{-1}[21]
Degradative chain transfer	$PLim(s)^{\bullet}+Lim \rightarrow P(s)+ALim^{\bullet}$	k_{fm11}	4.65×10^{-1}

Degradative chain transfer	$PBA(s)^{\bullet}+Lim \rightarrow P(s)+ALim^{\bullet}$	k_{fm21}	2.93×10^{2}
Re-initiation of $ALim^{\bullet}$	$ALim^{\bullet}+Lim \rightarrow Lim^{\bullet}$	k_{ra1}	1.67×10^{-10}[10]
Re-initiation of $ALim^{\bullet}$	$ALim^{\bullet}+BA \rightarrow BA^{\bullet}$	k_{ra2}	1.67×10^{-8}[10]
Termination			
By combination	$PLim(s)^{\bullet}+PLim(r)^{\bullet} \rightarrow P(s+r)$	k_{tc11}	1.79×10^{8}
	$PLim(s)^{\bullet}+PBA(r)^{\bullet} \rightarrow P(s+r)$	k_{tc12}	1.79×10^{8}
	$PBA(s)^{\bullet}+PBA(r)^{\bullet} \rightarrow P(s+r)$	k_{tc22}	1.79×10^{8}[14,17]
	$ALim^{\bullet}+ALim^{\bullet} \rightarrow AA$	k_{tcaa}	9.95×10^{7}
	$PLim(s)^{\bullet}+ALim^{\bullet} \rightarrow P(s)$	k_{tc1a}	1.79×10^{8}
	$PBA(s)^{\bullet}+ALim^{\bullet} \rightarrow P(s)$	k_{tc2a}	1.79×10^{8}
By disproportionation	$PLim(s)^{\bullet}+PLim(r)^{\bullet} \rightarrow P(s)+P(r)$	k_{td11}	1.99×10^{7}
	$PLim(s)^{\bullet}+PBA(r)^{\bullet} \rightarrow P(s)+P(r)$	k_{td12}	1.99×10^{7}
	$PBA(s)^{\bullet}+PBA(r)^{\bullet} \rightarrow P(s)+P(r)$	k_{td22}	9.95×10^{7}[14,17]
Intramolecular chain transfer of BA			
Backbiting of BA	$PBA(s)^{\bullet} \rightarrow QBA(s)^{\bullet}$	k_{bb}	5.76×10^{3}[16,21]
Short-chain branching	$QBA(s)^{\bullet}+Lim \rightarrow PLim(s+1)^{\bullet}$	k_{p21}^{tert}	8.23
Short-chain branching	$QBA(s)^{\bullet}+BA \rightarrow PBA(s+1)^{\bullet}$	k_{p22}^{tert}	49.9[16,21]
Degradative chain transfer	$QBA(s)^{\bullet}+Lim \rightarrow P(s)+ALim^{\bullet}$	k_{fm2a}^{tert}	1.83
Termination of BA tertiary radicals			
By combination ($QBA^{\bullet}$)	$QBA(s)^{\bullet}+QBA(r)^{\bullet} \rightarrow P(s+r)$	$k_{tc22}^{tert\text{-}tert}$	1.99×10^{7}[14,17]
	$QBA(s)^{\bullet}+PBA(r)^{\bullet} \rightarrow P(s+r)$	$k_{tc22}^{tert\text{-}sec}$	5.97×10^{7}[14,17]
	$QBA(s)^{\bullet}+PLim(r)^{\bullet} \rightarrow P(s+r)$	$k_{tc21}^{tert\text{-}sec}$	5.97×10^{7}
	$QBA(s)^{\bullet}+ALim^{\bullet} \rightarrow P(s)$	$k_{tc2a}^{tert\text{-}a}$	9.95×10^{7}
By disproportionation ($QBA^{\bullet}$)	$QBA(s)^{\bullet}+QBA(r)^{\bullet} \rightarrow P(s)+P(r)$	$k_{td22}^{tert\text{-}tert}$	1.79×10^{8}[14,17]
	$QBA(s)^{\bullet}+PBA(r)^{\bullet} \rightarrow P(s)+P(r)$	$k_{td22}^{tert\text{-}sec}$	1.39×10^{8}[14,17]
	$QBA(s)^{\bullet}+PLim(r)^{\bullet} \rightarrow P(s)+P(r)$	$k_{td21}^{tert\text{-}sec}$	1.39×10^{8}

$QBA(s)^{\bullet}+ALim^{\bullet}\rightarrow P(s)+A$	$k_{td2a}^{\text{tert-a}}$	9.95×10^{7}

[a] $R^{\bullet}$ = initiator radical; BA and Lim = monomer units; $BA^{\bullet}$ and $Lim^{\bullet}$ = primary radicals; $RBA(s)^{\bullet}$ and $RLim(r)^{\bullet}$= polymer radicals of sizes s and r and ending in BA and Lim, respectively; $ALim^{\bullet}$ = allylic radicals resulting from degradative chain transfer of Lim; $QBA^{\bullet}$ = mid-chain tertiary radical from intramolecular chain transfer of BA; P(s) and P(r) = dead polymers.

4.3.1 Initiation

The initiation reaction involves two steps:

$$I \xrightarrow{k_d} 2f\,R^{\bullet} \qquad \text{(Eq. 4.1)}$$

$$R^{\bullet} + M_i \xrightarrow{k_{pii}} R_i(1)^{\bullet} \qquad \text{(Eq. 4.2)}$$

Firstly, the homolysis of BPO initiator (I) yields a pair of primary radicals ($R^{\bullet}$). The decomposition rate of BPO is expressed by an Arrhenius relation, the pre-exponential factor and activation energy values were taken from the WATPOLY simulator database developed by Gao and Penlidis[18–21]:

$$k_d\ (s^{-1}) = 1.07\times10^{14}\exp(-1.515\times10^{4}/T) \qquad \text{(Eq. 4.3)}$$

The primary radicals generated by the homolysis step then react with monomer and produce a chain-initiating radical, $R_i(1)^{\bullet}$. However, not all initiator radicals can react with monomer, they may recombine, or abstract a proton from Lim. These factors were considered in the simulation by introducing an initiator efficiency factor (f). The value of f was set at 0.6, meaning 60% of the primary radicals produced by homolysis could initiate the polymerization[10].

4.3.2 Propagation

Using the terminal model, a total of four homo- and cross-propagation reactions were considered:

$$R_i(1)^{\bullet} + M_j \xrightarrow{k_{pij}} R_j(s+1)^{\bullet} \qquad \text{(Eq. 4.4)}$$

where k_{pij} is the rate constant of monomer j (M_j) adding to a propagating chain radical ending in monomer i. Note that in this work, 1 refers to Lim and 2 refers to BA. The initially guessed propagation rate constant of BA was:

$$k_{p22}\ (L\ mol^{-1}\ s^{-1}) = 2.21\times10^{7}\exp(-2153/T) \qquad \text{(Eq. 4.5)}$$

The parameter values were taken from a comprehensive study of BA propagation rate constants using the pulsed-laser polymerization method[22] . The initially guessed homopolymerization rate constant for Lim (k_{p11}) was taken from our previous modeling study of BMA/Lim copolymerization[10]. The cross-propagation rate constants, k_{p12} and k_{p21} were calculated from the reactivity ratios. Using terminal model kinetics, the reactivity ratios are defined as $r_i = \frac{k_{pii}}{k_{pij}}$. The values of r_1 = 0.0067 and r_2 = 6.07 were determined previously using low conversion bulk experiments at 80°C[6]. As noted above, the homopropagation rate constants for BA and Lim were the only parameters adjusted in this work. Of course, because of the reactivity ratios, this also resulted in an adjustment to the cross-propagation rate constants.

4.3.3 Chain transfer to BA and the degradative chain transfer of Lim

In bulk polymerization, the influence of chain transfer to monomer on molecular weight cannot be ignored due to the high concentration of monomer. The chain transfer to BA is expressed as:

$$R_i(s)^{\bullet} + M_2 \xrightarrow{k_{fmij}} P(s) + R_2(1)^{\bullet} \qquad \text{(Eq. 4.6)}$$

The initially guessed rate constant for chain transfer to BA was taken from the WATPOLY database[21,23]:

$$k_{fm22}\ (L\ mol^{-1}\ s^{-1}) = 1.56 \times 10^4 \exp(-3762/T) \qquad \text{(Eq. 4.7)}$$

As demonstrated in our previous study[6], the highly reactive allylic hydrogen of Lim can easily be abstracted by the growing polymer radical, and yield an inactive chain along with an allylic radical (see Figure 4.1). Since the allylic radical is very stable, it is highly unlikely to initiate additional propagation; this mechanism is referred to as degradative chain transfer, and is the dominant chain transfer reaction in the BA/Lim system:

$$R_i(s)^{\bullet} + Lim \xrightarrow{k_{fmi1}} P(s) + A_{Lim}{}^{\bullet} \qquad \text{(Eq. 4.8)}$$

$$ALim^{\bullet} + M_i \xrightarrow{k_{r1i}} R_i(1) \qquad \text{(Eq. 4.9)}$$

Here the symbol $ALim^{\bullet}$ was used to distinguish the allylic radical from the propagating Lim radical ($RLim^{\bullet}$). To obtain an estimate of the chain transfer constant to Lim (C_s), the Mayo equation was used:

$$\frac{1}{\overline{X}_n} = \frac{1}{\overline{X}_{n0}} + C_s \frac{[S]}{[M]} \qquad \text{(Eq. 4.10)}$$

where C_s is defined as the ratio of the chain transfer to Lim rate constant to the BA

propagation rate constant, that is, $C_s = \frac{k_{fm21}}{k_{p22}}$, $\overline{X}_n$ is the number-average degree of polymerization, $\overline{X}_{n0}$ is the number-average degree of polymerization in the absence of solvent/chain transfer agent, [S] and [M] are the molar concentrations of solvent/chain transfer agent and/or monomer, respectively. By plotting $\frac{1}{\overline{X}_n}$ vs. $\frac{[S]}{[M]}$, C_s was calculated from the slope as 4.9×10^{-3}. An assumption that Lim acts more like a solvent or chain transfer agent rather than a propagating monomer was used to simplify the equation. The corresponding Mayo plot is given in Figure 4.2.

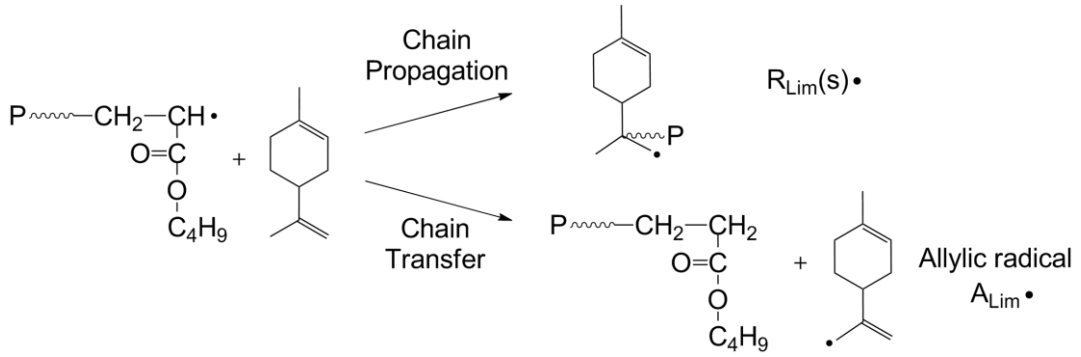

Figure 4.1 Ideal reaction schematic of chain propagation and degradative chain transfer of Lim.

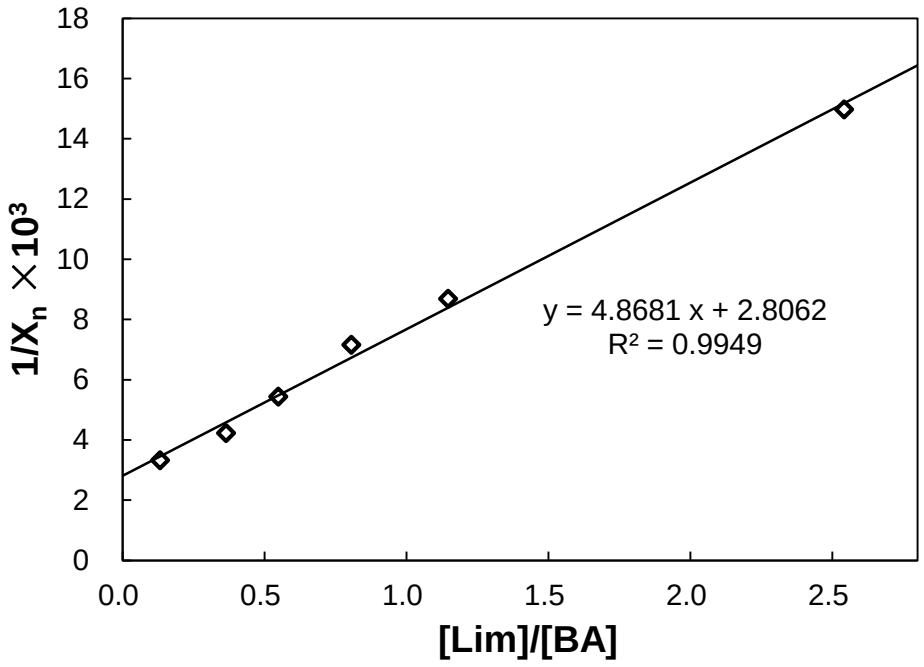

Figure 4.2 Mayo plot for the estimation of chain transfer constant to Lim (C_s).

To simplify the model, it is reasonable to assume the propagating radicals present the same chain transfer reactivity (H-atom abstraction) to a particular monomer as their propensity of adding to that monomer during propagation[11]. Accordingly, k_{fm21} and k_{fm12} were calculated as:

$$\frac{k_{fm21}}{k_{fm11}} = \frac{k_{p21}}{k_{p11}} \quad \text{and} \quad \frac{k_{fm12}}{k_{fm22}} = \frac{k_{p12}}{k_{p22}} \qquad \text{(Eq. 4.11)}$$

The value of the re-initiation rate constant for the allylic radical was assumed to be very small as the radical is stable and would not be expected to re-initiate a new propagating chain. Values of 1.67×10^{-10} L mol^{-1} s^{-1} and 1.67×10^{-8} L mol^{-1} s^{-1} were used for k_{r11} and k_{r12}, respectively, according to a previous study[10].

4.3.4 Termination

The termination reaction occurs by both combination and disproportionation of polymer radicals (Figure 4.3):

$$R_i(s)^{\bullet} + R_j(r)^{\bullet} \xrightarrow{k_{tcij}} P(s+r) \qquad \text{(Eq. 4.12)}$$

$$R_i(s)^{\bullet} + R_j(r)^{\bullet} \xrightarrow{k_{tdij}} P(s) + P(r) \qquad \text{(Eq. 4.13)}$$

The overall termination rate constant of BA, $k_{t22} = k_{tc22} + k_{td22}$, was fitted to an Arrhenius expression as[17,24]:

$$k_{t22}\ (\text{L mol}^{-1}\ \text{s}^{-1}) = 1.34 \times 10^{9} \exp(-674/T) \qquad \text{(Eq. 4.14)}$$

The termination rate constants of Lim-related species, i.e., k_{tc11}, k_{td11}, k_{tcaa}, k_{tc1a} and k_{tc2a}, and cross termination, i.e., k_{tc12} and k_{td12}, were set to the same level as for BA radicals. Due to the lack of any known values for these parameters in the literature and because BA feed concentrations were at 50% or higher, this was considered a best option for an initial guess. The ratio of termination by combination to overall termination rate ($\frac{k_{tc}}{k_t}$), is taken as 0.9 for both the BA and Lim radicals as recommend by Peck and Hutchinson for the termination for secondary-secondary radicals[14].

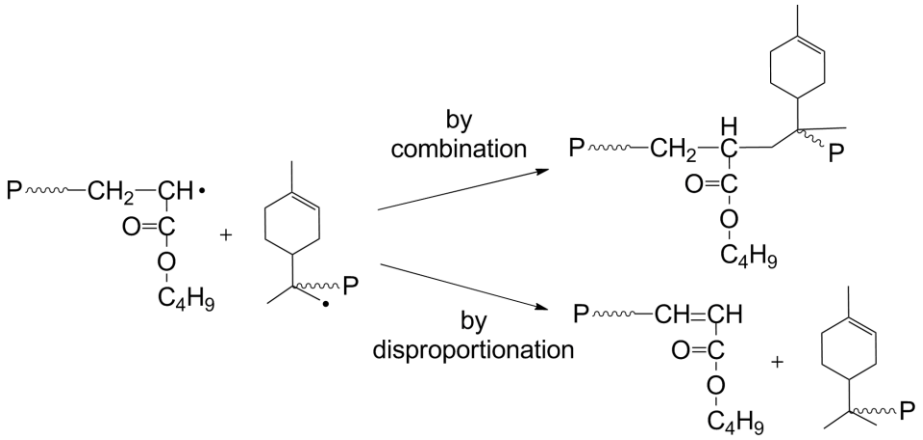

Figure 4.3 Ideal reaction schematic of termination reaction of BA/Lim copolymerization.

4.3.5 Backbiting of BA

There is evidence that intramolecular chain transfer to polymer is significant during the chain propagation reaction of BA[14,25,26]. The mid-chain tertiary radicals resulting from a backbiting mechanism are quite stable and present slower propagation rates compared to the secondary radicals resulting from regular chain-end propagation. The propagation of tertiary radicals creates short-chain branches in the polymer. The backbiting and short-chain branching mechanisms were included in this model:

$$R_2(s)^{\bullet} \xrightarrow{k_{bb}} Q_2(s)^{\bullet} \qquad \text{(Eq. 4.15)}$$

$$Q_2(s)^{\bullet} + M_i \xrightarrow{k_{p2i}^{tert}} R_i(s+1)^{\bullet} \qquad \text{(Eq. 4.16)}$$

The symbol $Q^{\bullet}$ represents the mid-chain tertiary radical. The rate constants for backbiting (k_{bb}) and short branching propagation (k_{p2i}^{tert}) were fitted using[16,21] :

$$k_{bb}\ (\mathrm{L\ mol^{-1}\ s^{-1}}) = 3.87\times10^{6}\exp(-2299/T) \qquad \text{(Eq. 4.17)}$$

$$k_{p22}{}^{tert}\ (L\ mol^{-1}\ s^{-1}) = 59.9\exp(-64.2/T) \qquad \text{(Eq. 4.18)}$$

$$k_{p21}{}^{tert} = \frac{k_{p22}{}^{tert}}{r_2} \qquad \text{(Eq. 4.19)}$$

The mid-chain tertiary radical can terminate with either a tertiary radical or a chain-end secondary radical:

$$Q_2(s)^{\bullet} + Q_2(r)^{\bullet} \xrightarrow{k_{tc}{}^{tert-tert}} P(s+r) \quad Q_2(s)^{\bullet} + Q_2(r)^{\bullet} \xrightarrow{k_{td}{}^{tert-tert}} P(s) + P(r) \qquad \text{(Eq. 4.20)}$$

$$Q_2(s)^{\bullet} + R_i(r)^{\bullet} \xrightarrow{k_{tc}{}^{tert-sec}} P(s+r) \quad Q_2(s)^{\bullet} + R_i(r)^{\bullet} \xrightarrow{k_{td}{}^{tert-sec}} P(s) + P(r) \qquad \text{(Eq. 4.21)}$$

By assuming the termination rate constant for BA is independent of radical type, the overall termination rate constant of tertiary radicals is taken to be the same as k_{t22}[14,17]. Unlike secondary radicals, termination by disproportionation is favored by tertiary radicals. The ratio of termination by combination to overall termination rate was taken as 0.1 for tertiary-tertiary radicals, 0.3 for tertiary-secondary radicals[17,21], and 0.5 for tertiary-allylic radicals.

All the rate constants were assumed as chain-length independent for the purposes of model simplification. Note that diffusion-control effects were not considered in the BA/Lim kinetic model, although it is known that they may have a significant impact on the polymerization at high conversions due to the high viscosity of the media. In the BA/Lim data used in this study, conversion was kept relatively low (due to the degradative chain transfer presented by Lim) and the reaction medium was not viscous enough to induce diffusion-controlled behaviour.

4.4 RESULTS AND DISCUSSION

4.4.1 Backbiting of BA

Figure 4.4 shows conversion vs. time data and Figure 4.5 shows molecular weight vs. time data along with model predictions at f_{BA} = 0.9 with and without considering the backbiting mechanism using the initial rate constants. As the data illustrate, modeling without considering backbiting led to an overestimation of conversion results, while modeling with backbiting showed a considerable underestimation of the results. This reflects the fact that the backbiting mechanism yields tertiary radicals which exhibit a much lower reactivity, and the overall reaction rate is therefore reduced. In Figure 4.5, the model with backbiting provides a more reasonable prediction of the average molecular weights, whereas the model without backbiting yielded a much higher prediction. Each backbiting event results in the creation of a short branch on the main polymer chain, and the molecular weight is decreased accordingly. In order to balance the conversion and molecular weight simulation results, the rate constants of propagation for both species (BA and Lim) were adjusted to new values to present better predictions (see values in Table 4.2). It is important to point out that k_p for BA was estimated using the experimental data at high BA content (f_{BA} = 0.9), whereas k_p for Lim was estimated using the experimental data at low BA content (f_{BA} = 0.5).

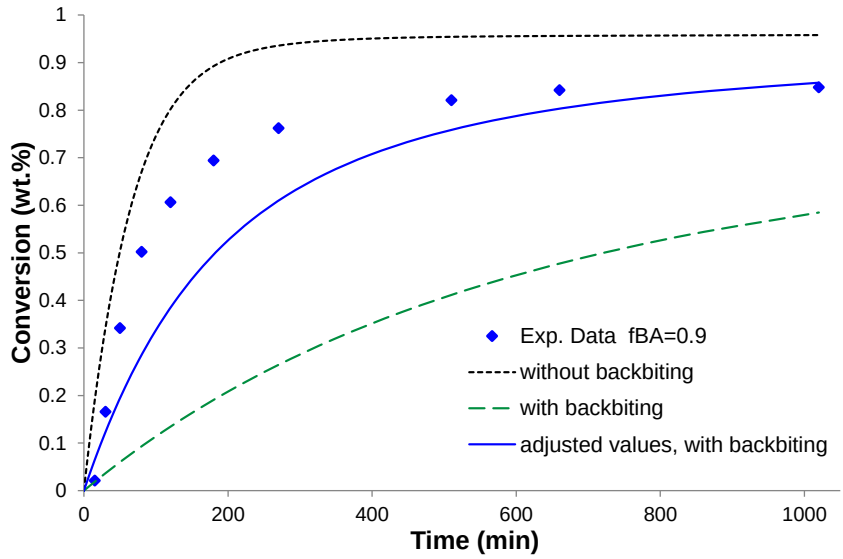

Figure 4.4 Conversion vs. time simulation with and without backbiting, BA/Lim copolymerization at feed composition fBA = 0.9, at 80°C in bulk using BPO (1 wt.%).

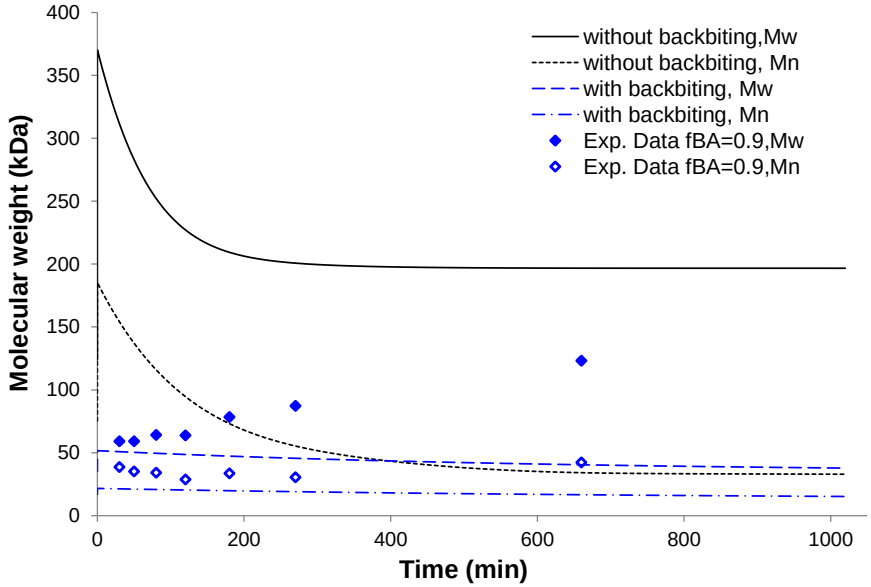

Figure 4.5 Molecular weight vs. time simulation with and without backbiting, BA/Lim copolymerization at feed composition fBA = 0.9, at 80°C in bulk using BPO (1 wt.%).

4.4.2 Conversion vs. time results

The conversion vs. time model predictions at five different initial feed compositions (f_{BA} = 0.5 to 0.9) along with the experimental data are shown in Figure 4.6. The agreement between the model and the experimental data is reasonably good. The model prediction trends in the data are well-predicted by the model; increases in BA feed content resulted in higher reaction rates. However, predictions at higher BA feed fractions were less impressive. One possible explanation could be that the degradative chain transfer reaction of Lim competes with the backbiting mechanism, as the BA chain-end radicals possibly abstracted the hydrogen from the Lim molecule rather than from an acrylate unit on its own chain. In other words, backbiting, which is the main cause for a decrease in the polymerization rate, is less dominant in the presence of Lim.

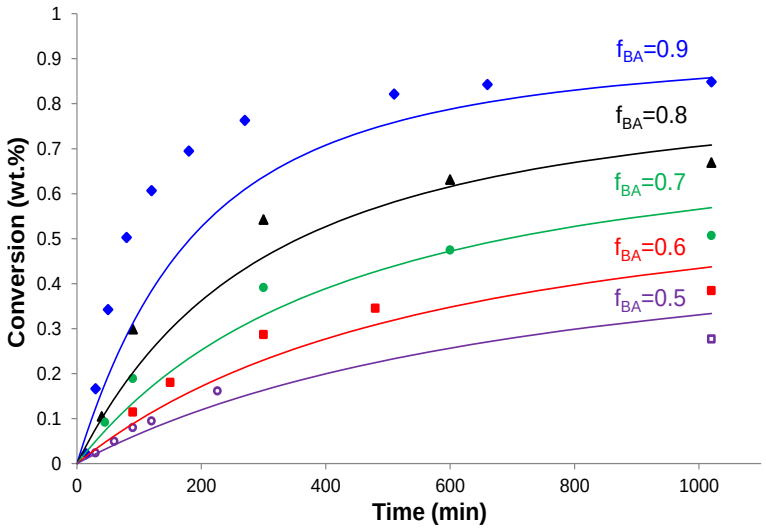

Figure 4.6 Conversion vs. time profiles for BA/Lim bulk copolymerizations at various feed compositions. Solid lines are model predictions.

4.4.3 Copolymer composition vs. Conversion

Composition vs. conversion profiles for different feed compositions are shown in Figure 4.7. As mentioned earlier, the propagation rate constants were calculated using the reactivity ratios previously estimated from low-conversion BA/Lim experiments[6]. The agreement between model profiles and experimental data are in general, very good. The good predictions of the composition vs. conversion data validates the reactivity ratio values estimated.

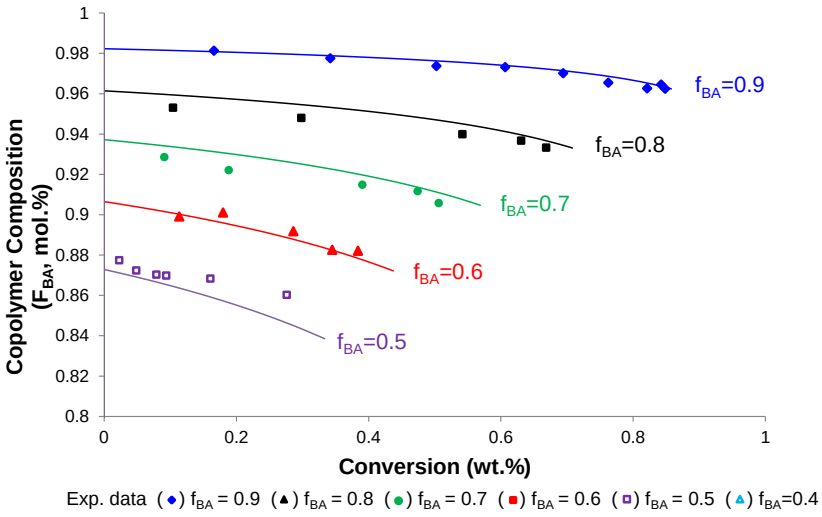

Figure 4.7 Composition vs. conversion profiles for BA/Lim copolymerizations at various feed compositions. Solid lines are model prediction.

4.4.4 Molecular weight of soluble copolymer

Figure 4.8 shows plots of the molecular weight development vs. conversion at four different feed compositions. The number-average molecular weight (M_n) is

relatively well predicted by the model but the weight-average molecular weight (M_w) shows some discrepancy. Nonetheless, good prediction of molecular weight data is often difficult to achieve. One can, however, make important conclusions about the reaction mechanisms despite some model mismatch. The model reveals that the average molecular weight decreases significantly with increasing Lim concentration in the feed. Given the propagation and chain transfer rate constants for Lim fitted to this model (see Table 4.2), it can be concluded that Lim acts more like a chain transfer agent than a co-monomer. One may also note that M_n decreases with increasing conversion, which is consistent with the fact that more short-chain polymers were produced. The production of increasing amounts of short-chain polymers likely resulted from increased degradative chain transfer due to increased Lim concentration as BA was preferentially incorporated into the copolymer during the early stages of the polymerization (see reactivity ratios described earlier, and Figure 4.7).

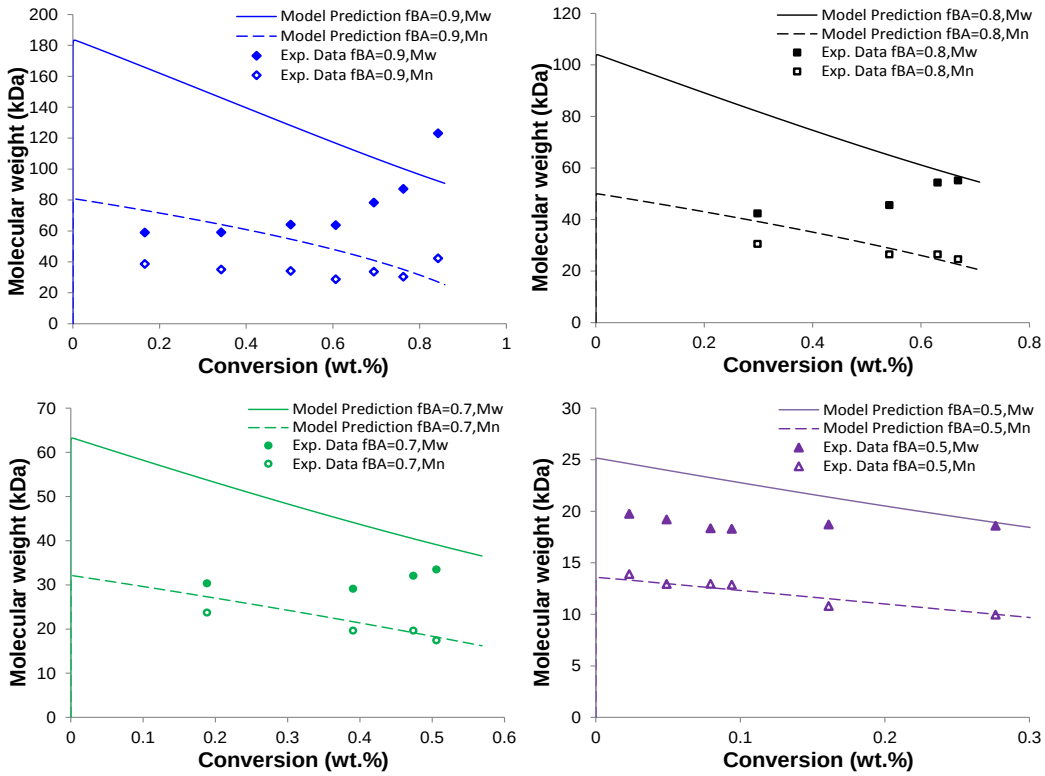

Figure 4.8 Molecular weight vs. conversion profiles for BA/Lim copolymerization at various feed compositions.

One possible explanation for the broadening polydispersity evident from Figure 4.8 could relate to long-chain branching caused by the intermolecular chain transfer of BA (a propagating radical abstracts the hydrogen from an acrylate unit in the middle of another chain)[14], which can result in a significant increase in M_w. In this case, additional studies would be required to pursue these ideas further.

4.5 Conclusions

A kinetic model of the bulk polymerization of BA/Lim has been developed with the addition of important mechanisms for degradative chain transfer to Lim and

backbiting for BA. Rate constants related to BA and Lim species were calculated based on literature values, reactivity ratios and degradative chain transfer constants estimated from previous experimental results. Fitting of the propagation rate constants resulted in moderately good conversion and molecular weight predictions and very good predictions of copolymer composition. The model supports the presence of a significant degradative chain transfer to Lim reaction as well as a backbiting mechanism for BA. Future work including a long-chain branching mechanism may shed further light on this copolymer system. In any event, this work provides greater insight into the use of an important bio-based, renewable monomer.

4.6 Acknowledgements

The authors acknowledge the support of the China Scholarship Commission for the support of Ms. Shanshan Ren. Furthermore, financial support for this project by Intellectual Ventures and the Natural Sciences and Engineering Research Council (NSERC) of Canada is greatly appreciated. E. Vivaldo-Lima acknowledges support from DAGPA-UNAM (PASPA Program) and the University of Ottawa Distinguished Visiting Researcher Program.

4.7 References

1. Belgacem, M. N.; Gandini, A. *Monomers, Polymers and Composites from Renewable Resources*; Elsevier, 2011.

2. Ahmed, J.; Tiwari, B. K.; Imam, S. H.; Rao, M. A. *Starch-Based Polymeric Materials and Nanocomposites: Chemistry, Processing, and Applications*; CRC Press, 2012.

3. Kim, Y. W.; Kim, M. J.; Chung, B. Y.; Bang, D. Y.; Lim, S. K.; Choi, S. M.; Lim, D. S.; Cho, M. C.; Yoon, K.; Kim, H. S.; Kim, K. B.; Kim, Y. S.; Kwack, S. J.; Lee, B.-M. Safety Evaluation And Risk Assessment Of d-Limonene. *J. Toxicol. Environ. Health Part B* **2013**, *16*, 17–38.

4. Ciriminna, R.; Lomeli-Rodriguez, M.; Carà, P. D.; Lopez-Sanchez, J. A.; Pagliaro, M. Limonene: a versatile chemical of the bioeconomy. *Chem. Commun.* **2014**, *50*, 15288–15296.

5. Wilbon, P. A.; Chu, F.; Tang, C. Progress in Renewable Polymers from Natural Terpenes, Terpenoids, and Rosin. *Macromol. Rapid Commun.* **2013**, *34*, 8–37.

6. Ren, S.; Trevino, E.; Dubé, M. A. Copolymerization of Limonene with n-Butyl Acrylate. *Macromol. React. Eng.* **2015**, *9*, 339–349.

7. Zhang, Y.; Dubé, M. A. Copolymerization of n-Butyl Methacrylate and D-Limonene. *Macromol. React. Eng.* **2014**, *8*, 805–812.

8. Zhang, Y.; Dubé, M. A. Copolymerization of 2-Ethylhexyl Acrylate and D-Limonene. *Polym.-Plast. Technol. Eng.* **2015**, *54*, 499–505.

9. Ren, S.; Zhang, L.; Dubé, M. A. Free-radical terpolymerization of n-butyl acrylate/butyl methacrylate/d-limonene. *J. Appl. Polym. Sci.* **2015**, *132*.

10. Zhang, Y.; Dubé, M. A.; Vivaldo-Lima, E. Modeling Degradative Chain Transfer

in d-Limonene/n-Butyl Methacrylate Free-Radical Copolymerization. *J. Renew. Mater.* **2015**, *3*, 318–326.

11. Li, D.; Grady, M. C.; Hutchinson, R. A. High-Temperature Semibatch Free Radical Copolymerization of Butyl Methacrylate and Butyl Acrylate. *Ind. Eng. Chem. Res.* **2005**, *44*, 2506–2517.

12. Beuermann, S.; Paquet, D. A.; McMinn, J. H.; Hutchinson, R. A. Determination of Free-Radical Propagation Rate Coefficients of Butyl, 2-Ethylhexyl, and Dodecyl Acrylates by Pulsed-Laser Polymerization. *Macromolecules* **1996**, *29*, 4206–4215.

13. Lyons, R. A.; Hutovic, J.; Piton, M. C.; Christie, D. I.; Clay, P. A.; Manders, B. G.; Kable, S. H.; Gilbert, R. G. Pulsed-Laser Polymerization Measurements of the Propagation Rate Coefficient for Butyl Acrylate. *Macromolecules* **1996**, *29*, 1918–1927.

14. Peck, A. N. F.; Hutchinson, R. A. Secondary Reactions in the High-Temperature Free Radical Polymerization of Butyl Acrylate. *Macromolecules* **2004**, *37*, 5944–5951.

15. Nikitin, A. N.; Hutchinson, R. A. Effect of Intramolecular Transfer to Polymer on Stationary Free Radical Polymerization of Alkyl Acrylates, 2. *Macromol. Theory Simul.* **2006**, *15*, 128–136.

16. Rantow, F. S.; Soroush, M.; Grady, M. C.; Kalfas, G. A. Spontaneous polymerization and chain microstructure evolution in high-temperature solution polymerization of n-butyl acrylate. *Polymer* **2006**, *47*, 1423–1435.

17. Nikitin, A. N.; Hutchinson, R. A.; Buback, M.; Hesse, P. Determination of Intramolecular Chain Transfer and Midchain Radical Propagation Rate Coefficients for Butyl Acrylate by Pulsed Laser Polymerization. *Macromolecules* **2007**, *40*, 8631–8641.

18. Gao, J.; Penlidis, A. A Comprehensive Simulator/Database Package for Reviewing Free-Radical Homopolymerizations. *J. Macromol. Sci. Part C* **1996**, *36*, 199–404.

19. Gao, J.; Penlidis, A. A Comprehensive Simulator/Database Package for Reviewing Free-Radical Copolymerizations. *J. Macromol. Sci. Part C* **1998**, *38*, 651–780.

20. Gao, J.; Penlidis, A. A comprehensive simulator/database package for bulk/solution free-radical terpolymerizations. *Macromol. Chem. Phys.* **2000**, *201*, 1176–1184.

21. Dorschner, D. Multicomponent Free Radical Polymerization Model Refinements and Extensions with Depropagation. Master's thesis, University of Waterloo: Waterloo, 2010.

22. Asua, J. M.; Beuermann, S.; Buback, M.; Castignolles, P.; Charleux, B.; Gilbert, R. G.; Hutchinson, R. A.; Leiza, J. R.; Nikitin, A. N.; Vairon, J.-P.; van Herk, A. M. Critically Evaluated Rate Coefficients for Free-Radical Polymerization, 5,. *Macromol. Chem. Phys.* **2004**, *205*, 2151–2160.

23. Jung, W. Mathematical Modeling of Free-radical Six-component Bulk and Solution Polymerization. **2008**.

24. Beuermann, S.; Buback, M. Rate coefficients of free-radical polymerization

deduced from pulsed laser experiments. *Prog. Polym. Sci.* **2002**, *27*, 191–254.

25. Plessis, C.; Arzamendi, G.; Leiza, J. R.; Schoonbrood, H. A. S.; Charmot, D.; Asua, J. M. Modeling of Seeded Semibatch Emulsion Polymerization of n-BA. *Ind. Eng. Chem. Res.* **2001**, *40*, 3883–3894.

26. Ahmad, N. M.; Heatley, F.; Lovell, P. A. Chain Transfer to Polymer in Free-Radical Solution Polymerization of n-Butyl Acrylate Studied by NMR Spectroscopy. *Macromolecules* **1998**, *31*, 2822–2827.

Chapter 5. Bulk Free-Radical Copolymerization of *n*-Butyl Acrylate and *n*-Butyl Methacrylate: Reactivity Ratio Estimation

Macromol. React. Eng. 2016. doi:10.1002/mren.201600050.

Bulk Free-Radical Copolymerization of *n*-Butyl Acrylate and *n*-Butyl Methacrylate: Reactivity Ratio Estimation

Shanshan Ren, Laura Hinojosa-Castellanos, Lisha Zhang, and Marc A. Dubé*

Department of Chemical and Biological Engineering, Centre for Catalysis Research and Innovation, University of Ottawa

Abstract

The reactivity ratios for the bulk free-radical copolymerization of *n*-butyl acrylate/*n*-butyl methacrylate were estimated at 80°C. By performing a series of low conversion runs including replicate runs, the reactivity ratios were estimated as r_{BA} = 0.46 and r_{BMA} = 2.01. Runs to high conversions were then conducted at three different feed compositions (f_{BMA} = 0.2, 0.5 and 0.8) to validate the reactivity ratios. The composition data from the high conversion experiments showed good agreement with the estimated reactivity ratios in the integrated form of the Mayo-Lewis model. The molecular weight, gel content and glass transition temperature of BA/BMA copolymers were also determined.

Keywords: copolymerization, reactivity ratios, *n*-butyl acrylate, *n*-butyl methacrylate

5.1 Introduction

Acrylate polymers have been broadly used in industry, especially in coating, adhesive and paint formulations due to their resistance to solvents, water, and UV radiation[1,2]. *n*-Butyl acrylate (BA) and *n*-butyl methacrylate (BMA) are two of the most common components for producing adhesives and coatings. Particular attention has been focused on kinetic studies of BA homopolymerization to understand its unique intra- and inter-molecular chain transfer behaviour[3–6]. This mechanism leads to the formation of highly branched and gel polymers. As is the case for many polymers, copolymerization of BA with, for example, methacrylate monomers, such as methyl methacrylate (MMA) has been studied to control polymer product performance[7–10]. For example, BA/MMA copolymer properties have been manipulated by the addition of MMA to reduce the gel content of the copolymer through a reduction in the formation rate of six-membered transition rings of BA[11]. There are not many studies on BA/BMA kinetics reported in the research literature. The work of Hutchinson et al. for BA/BMA high temperature (i.e., 140^{o}C) solution copolymerizations in xylene is the most notable. They studied the interaction between the depropagation behaviour of BMA and the backbiting and β-scission of BA[12–14].

In copolymerization, the copolymer microstructure (i.e., sequence length distribution, molecular weight and distribution, gel content, etc.) determines the end-use properties of the copolymer. The copolymer microstructure is strongly dependent on the comonomer feed composition and the reactivity ratios, parameters in

the Mayo-Lewis model[15]. However, there are no reported experimentally determined reactivity ratios for bulk BA/BMA copolymerizations in the open literature. There are however some closely related values that have been guessed[9,16], calculated using the Q-e scheme[17] or determined via emulsion polymerization[18]. It should be noted that the estimates determined via emulsion polymerization were not corrected for monomer partitioning and are thus, not directly comparable to bulk copolymerization values[19]. There are also reported values for the BA/tert-BMA system[20]. All of the above noted values are shown in Table 5.1.

Table 5.1 Comparison of reactivity ratios.

	r_{BMA}	r_{BA}	T (^oC)
BA/tert-BMA system[20]	1.564 (tert-BMA)	0.238	78
Guessed values (BA/MMA system)[9,12,16]	1.84	0.32	80
Q-e scheme[17]	2.53	0.29	/
From emulsion polymerization data[18]	2.21	0.27	70

In this study we estimate the reactivity ratios for the bulk copolymerization of BA/BMA at 80^{o}C. The reactivity ratios are estimated using a series of low conversion experiments with the RREVM program[21]. These results were validated using higher conversion experiments. Additional polymer characterization for molecular weight, gel content and glass transition temperature (T_g) was also performed.

5.2 Experimental

5.2.1 Materials

BA (Sigma-Aldrich, 99%), BMA (Sigma-Aldrich, 99%), were purified of monomethyl ether hydroquinone inhibitor using an inhibitor removal column (Sigma Aldrich).Benzoyl peroxide (BPO, Sigma-Aldrich) was recrystallized twice with acetone and deionized water, dried under vacuum at room temperature, and then stored in a refrigerator at 4^{o}C before use. Methanol and tetrahydrofuran used for sample workup and characterization were used without further purification.

5.2.2 Polymerization

The bulk free-radical copolymerization of BA/BMA was carried out in glass ampoules (10 mm diameter and 200 mm in length; ampoule volume 15.7 mL). In each experiment, 5 g monomer/initiator mixture of BA, BMA and BPO (0.1 wt%) were pipetted into each glass ampoule. A freeze-pump-thaw procedure (three cycles) was performed on each ampoule to remove oxygen before flame-sealing. The ampoules were then immersed in an oil bath at 80 ℃, were removed at pre-determined times and quenched in an ice bath. The polymeric products were precipitated in a 10-fold excess of methanol. After decanting the excess liquid, the remaining polymer was dried in a vacuum oven at 25^{o}C to a constant weight.

5.2.3 Characterization

The overall monomer conversion was determined by gravimetry based on the mass of dried polymer. The copolymer composition (F_{BMA} and F_{BA}) was measured

with a ^{1}H-NMR spectrometer (Bruker, 400MHz) using $CDCl_3$ as the solvent at room temperature. Gel content was determined using the membrane partitioning method reported by Tobing and Klein[22]. About 0.03 g sample was placed in a poly(vinylidene fluoride) porous membrane pouch (pore size of 5 μm and pouch diameter of 47 mm) and then sealed with an impulse sealer. The pouch was immersed in tetrahydrofuran (THF) and gently shaken for 6 h. The swollen pouch was then dried in a fume hood until a constant weight was achieved. Gel content was calculated by dividing the weight of the sample after solvent extraction by its original weight. The soluble polymer in the THF solution was then concentrated by evaporation and characterized for molecular weight. The solution was filtered through a 0.45 μm syringe filter, and analyzed for average molecular weights using a GPC system (Agilent Technology) with two columns in series (MZ-Gel SD plus 10^5 Angstroms 300 x 8.00 mm, particle size 5 μm, MZ-Gel SD plus 10^4 Angstroms 300 x 8.00 mm, particle size 5 μm) and THF as eluent (flow rate = 1 mL/min). The detection system consisted of a multi-angle laser light scattering detector (Wyatt Dawn Heleos II, λ = 633 nm), a differential refractive index detector (Wyatt Optilab T-rEX) and a differential viscometer (Wyatt ViscoStar ll). The refractive index increment (dn/dc) used to calculate the molecular weight was estimated based on the dn/dc values for the homopolymers weighted by each copolymer composition. For poly(BA) and poly(BMA), the dn/dc (in THF, 25ºC) values were taken to be 0.064 mL g^{-1} and 0.076 mL g^{-1}, respectively[23]. Data analysis was performed using the software provided.

Differential scanning calorimetry (DSC, TA Instruments, Model Q1000) was used to measure the glass transition temperatures (T_g) of the copolymers. Each sample was analyzed over the temperature range from -80 to 130^{o}C at a heating/cooling rate of 10^{o}C/min. The T_g was defined as the inflection point on the second heat flow curve.

5.2.4 Experimental design

5.2.4.1 Low conversion runs for reactivity ratio estimation

A series of low conversion (<10 wt%) experiments were performed at equidistant feed compositions (f_{BA} = 0.1 to 0.9). Initial estimates of reactivity ratios, r_{BMA} and r_{BA}, were obtained by substituting the feed and instantaneous copolymer compositions into the Mayo-Lewis equation[15]:

$$\frac{F_{BMA}}{F_{BA}} = \frac{f_{BMA}(r_{BMA}f_{BMA} + f_{BA})}{f_{BA}(r_{BA}f_{BA} + f_{BMA})} \qquad \text{(Eq. 5.1)}$$

where F_{BMA} and F_{BA} (mole fractions) are the instantaneous copolymer composition, and f_{BMA} and f_{BA} (mole fractions) are the corresponding feed compositions. In this study, a non-linear error-in-variables model program (RREVM) was used to calculate the reactivity ratio estimates[21,24]. Four replicate low conversion experiments were then performed at each of two recommended feed compositions[25] using the initial reactivity ratio estimates:

$$f'_{BMA} = \frac{2}{2 + r_{BMA}} \qquad \text{(Eq. 5.2)}$$

$$\text{and} \quad f''_{BMA} = \frac{r_{BA}}{r_{BA} + 2} \qquad \text{(Eq. 5.3)}$$

The final reactivity ratios were then obtained by analyzing all the low conversion data using the RREVM software.

5.2.4.2 Full conversion runs for reactivity ratio validation

In order to validate the estimated reactivity ratios and examine the copolymer composition drift with conversion, experiments geared toward achieving full conversion were conducted at three different co-monomer feed compositions, f_{BMA} = 0.2, 0.5, and 0.8. The procedure was essentially the same as for the low conversion runs at initiator concentrations of 0.1 wt% BPO at 80^{o}C.

5.3 Result and Discussion

5.3.1 Reactivity ratio estimation

The copolymer compositions were measured by ^{1}H-NMR spectroscopy. A typical NMR spectra for BA/BMA polymer is shown in Figure 5.1. The following equation was used to calculate copolymer composition:

$$BMA\ mol\% = \frac{2A_{1.0}}{3A_{4.0}} - 1 \qquad \text{(Eq. 5.4)}$$

where $A_{1.0}$ refers to the peak area in the range δ = 0.7 to 1.1, which represents the –CH_3 protons of BA (“G” in Figure 5.1) and the two sets of –CH_3 protons of BMA (“M and I” in Figure 5.1), and $A_{4.0}$ refers to the peak area in the range δ = 3.8 to 4.2 which corresponds to the –OCH_2– protons of BA and BMA (“D and J” in Figure 5.1).

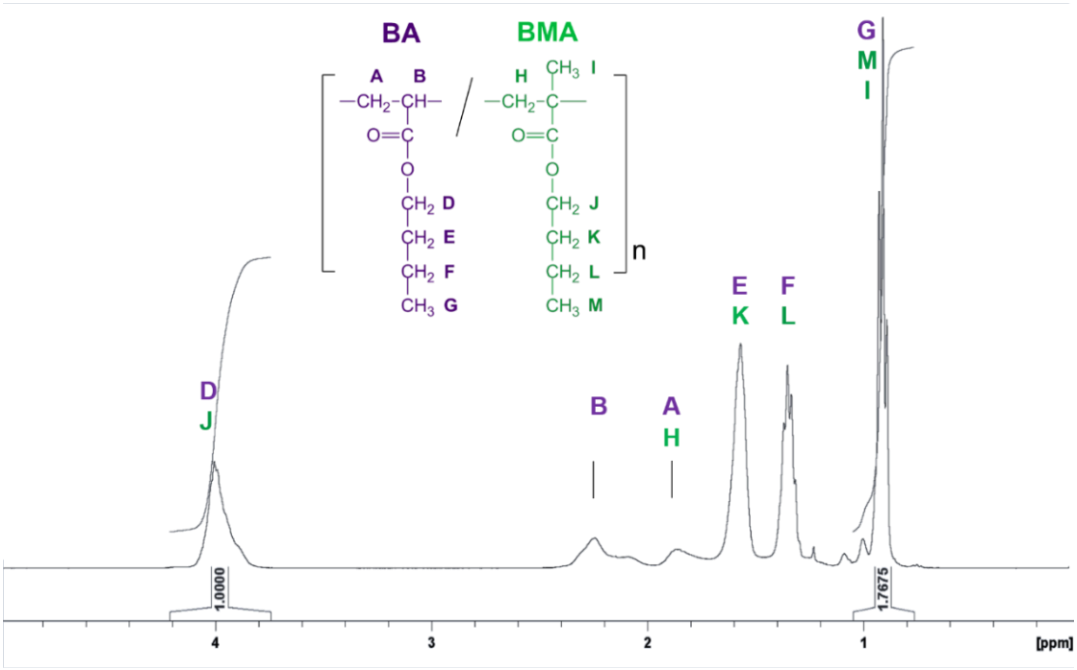

Figure 5.1 1H-NMR spectrum of BA/BMA copolymer (FBMA = 0.178, FBA = 0.822).

Table 5.2 presents the low conversion data for reactivity ratio estimation of BA/BMA copolymerization. Samples 1-9 were the preliminary set of experiments. By inputting the feed compositions and copolymer compositions into the Mayo-Lewis equation (Equation 5.1) using the RREVM computer program[21], an initial estimate of reactivity ratios was calculated as r_{BMA} = 2.1 and r_{BA} = 0.49. Four replicate runs were then performed at two compositions, f_{BMA} = 0.49 and 0.20, calculated using equations 5.2 and 5.3. Final values of r_{BMA} = 2.01 and r_{BA} = 0.46 were calculated using the data from all 17 runs (Table 5.2). A suggested composition measurement error of 5% was used in data processing along with a feed composition error of 1%. The joint confidence region for the reactivity ratio estimation is shown in Figure 5.2.

Comparison of the reactivity ratio values to that shown in Table 5.1 reveals that the r_{BMA} value is not significantly different from the various estimates that have been used in the past. However, the estimate for r_{BA} is significantly different. Differences from those values should not be surprising, given that none of those in Table 5.1 were collected using a designed experiment protocol and/or under the same conditions. The values of the reactivity ratios for the BA/BMA system clearly show that the polymerization of BMA is preferred over BA, which is in good agreement with the observation for the copolymerization of butyl acrylate/methacrylate monomers[9]. Thus, different feed compositions of BMA and BA can greatly affect the compositions of the copolymers and composition drift will likely be a factor. The composition data as well as the Mayo-Lewis model using the predicted reactivity ratios are shown in Figure 5.3; an excellent fit to the data is observed.

Table 5.2 Bulk BA/BMA copolymerization results for reactivity ratio estimation at 80ºC, [BPO] = 0.1 wt%.

Sample	**Feed composition f_{BMA} (mol fraction)**	**Copolymer composition F_{BMA} (mol fraction)**	**Time (min)**	**Conversion (wt.%)**
1	0.100	0.187	25	1.4
2	0.200	0.335	20	2.1
3	0.300	0.459	18	1.5
4	0.410	0.620	18	2.9
5	0.501	0.668	18	3.9
6	0.601	0.762	15	3.8
7	0.700	0.820	15	6.8
8	0.801	0.882	15	6.5
9	0.897	0.968	15	1.0
TM1-1	0.487	0.656	15	5.1
TM1-2	0.487	0.654	15	5.9
TM1-3	0.487	0.651	15	4.0
TM1-4	0.487	0.655	15	5.0
TM2-1	0.196	0.344	22	8.5
TM2-2	0.196	0.348	22	9.0
TM2-3	0.196	0.344	22	5.7
TM2-4	0.196	0.353	22	9.5

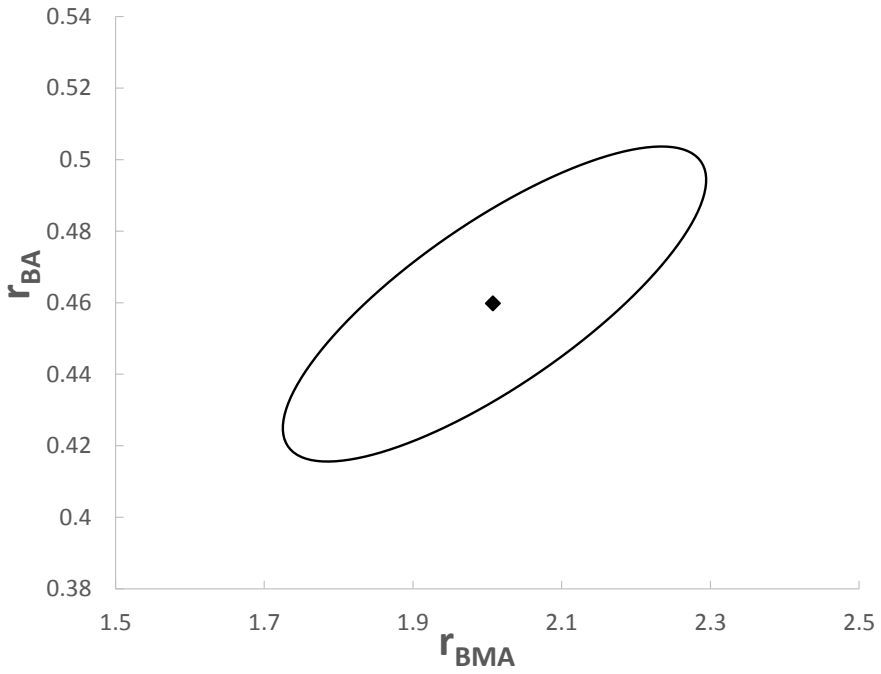

Figure 5.2 Reactivity ratio point estimate and 95% joint confidence region for BA/BMA copolymerization compared to literature values.

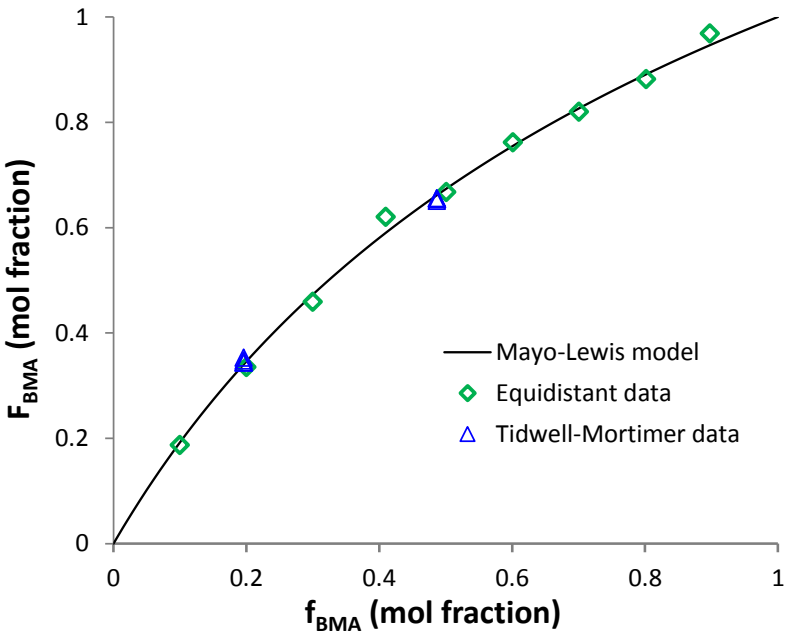

Figure 5.3 Mayo-Lewis plot and experimental data of copolymer composition (F_{BMA}) versus feed composition (f_{BMA}).

5.3.2 Full conversion experiments

Full conversion copolymerizations of BA/BMA were performed at three feed compositions, f_{BMA} = 0.2, 0.5, and 0.8. All of the runs were carried out at 80^{o}C with a BPO concentration of 0.1 wt%. Autoacceleration was observed in the conversion data at roughly 12, 20 and 27 wt% conversion for the experiments at f_{BMA} = 0.2, 0.5, and 0.8, respectively (Figure 5.4). Thus, increasing BA concentration resulted in an earlier autoacceleration. It is known that the bulk polymerization of BA leads to highly branched and high gel content polymers[13,26,27]. With the increase in BA concentration, the intra- and intermolecular chain transfer of BA would be more frequent. At similar molecular weight ranges, resulting branched polymer chains would exhibit less flexibility and induce a faster decrease in translational diffusion and the termination rate, and thus, earlier autoacceleration[28]. In addition, increasing BA feed concentration also led to higher overall polymerization rates (Figure 5.4). This is in agreement with the fact that BA exhibits a higher polymerization rate than BMA in their respective homopolymerizations. Comparing the propagation and termination rate parameters, k_p and k_t, respectively, and the value of $k_p/k_t^{1/2}$, which directly reflects the rate of polymerization, one notes that at 80^{o}C, BA has the larger homopolymerization rate (Table 5.3). This rate effect competes with that of the reactivity ratios.

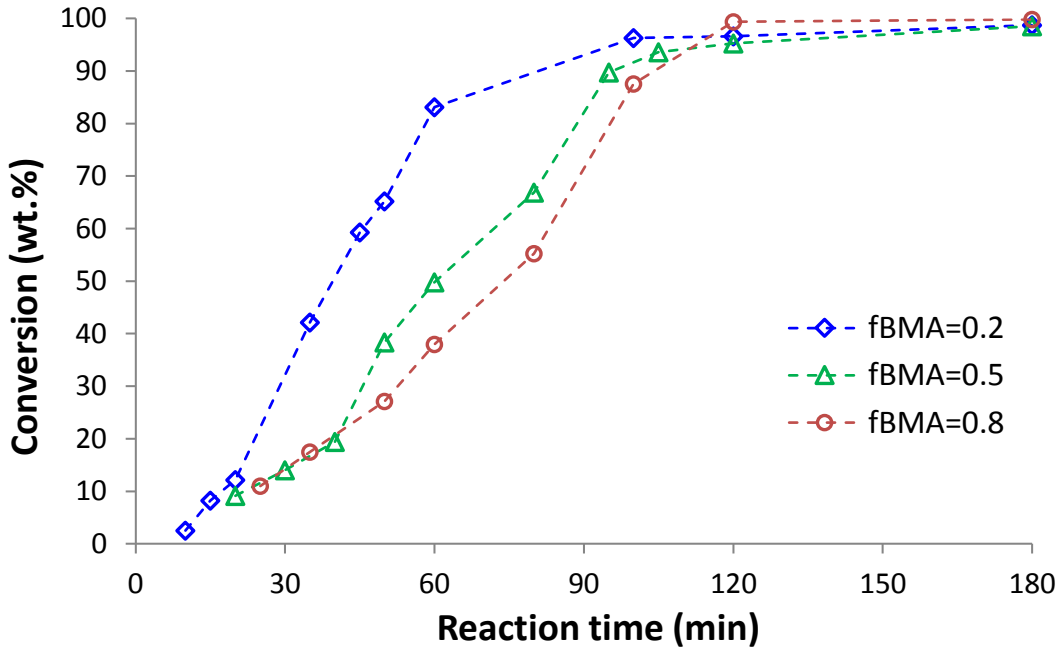

Figure 5.4 Conversion vs. time for bulk BA/BMA copolymerizations at various feed compositions.

Table 5.3 Kinetic parameters for the propagation and termination of BA and BMA homopolymerizations at 80°C.

Monomer	**k_p at 80°C (L mol^{-1} s^{-1})**	**k_t at 80°C (L mol^{-1} s^{-1})**	**$k_p/k_t^{1/2}$ at 80°C (L$^{1/2}$/mol$^{-1/2}$ S$^{-1/2}$)**
BA	4.97×10^{4}	1.99×10^{8}	3.53
BMA	1.22×10^{3}	1.44×10^{7}	0.32

The cumulative copolymer composition vs. conversion results along with the model predictions for BA/BMA copolymerization at three feed compositions (f_{BMA} = 0.2, 0.5, and 0.8) are shown in Figure 5.5. The model predictions were achieved by numerical integration of the differential form of the Mayo-Lewis equation on a

spreadsheet using the estimated reactivity ratios:

$$\frac{d[M_1]}{d[M_1]} = \frac{[M_1](r_{BMA}[M_1]+[M_2])}{[M_2](r_{BA}[M_2]+[M_1])} \quad \text{(Eq. 5.5)}$$

$[M_1]$ and $[M_2]$ are the molar concentrations of the BMA and BA monomers, respectively; $d[M_1]/d[M_2]$ is the molar ratio of BMA and BA units in the copolymer. The good agreement between the composition data and the model further support the validity of the reactivity ratios. A relatively small decrease in BMA content in copolymer was observed with increasing conversion. Composition drift ranged from 9 to 17% depending on feed composition. While significant, most of the drift took place only at elevated conversions. Nevertheless, this is consistent with the relatively close values of the two reactivity ratios for the BA/BMA copolymer system.

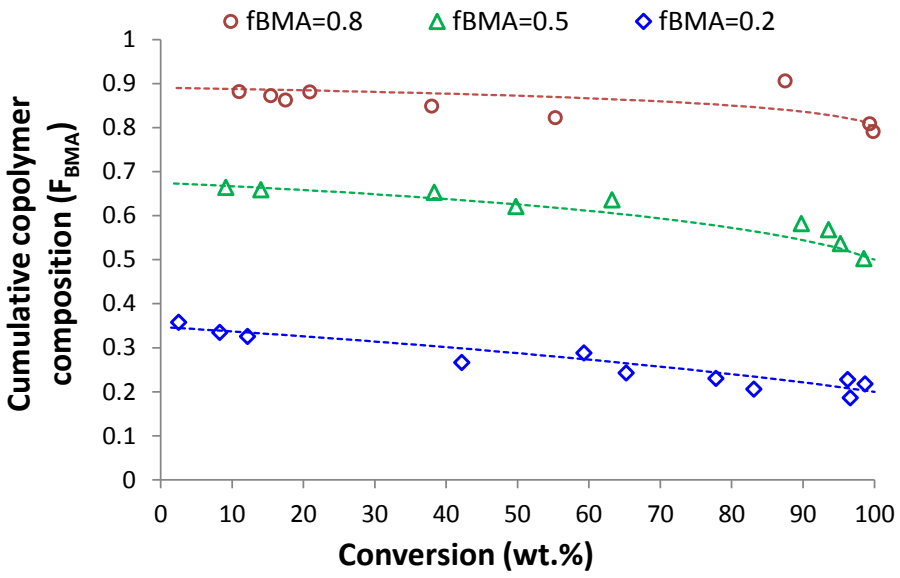

Figure 5.5 Cumulative copolymer composition vs. conversion for BA/BMA bulk copolymerization at various f_{BMA}. Dashed lines are integrated Mayo-Lewis model predictions.

The gel content for the BA/BMA copolymers was negligible for the runs at f_{BMA} = 0.5 and 0.8, but the gel content increased at the end of the polymerization at f_{BMA} = 0.2 (high BA concentration). Because of the higher preference in reactivity of BMA, its presence in the reaction mixture likely interfered with the inter- and intra-molecular chain transfer of BA which would normally lead to the formation of gel. Nonetheless, the molecular weight of the sol polymers was high (M_w > 900 kDa).

The development of the weight-average molecular weight of the sol polymer with respect to conversion is shown in Figure 5.6. The cumulative weight-average molecular weight of BA/BMA copolymers ranged from 960 to 2700 kDa. A relatively flat molecular weight profile with conversion was observed up to higher conversions for the higher BMA feed concentrations (f_{BMA} = 0.8). On the other hand, a significant increase in sol molecular weight was observed for the high BA concentration experiment (f_{BMA} = 0.2). These observations are entirely consistent with the conversion data and autoacceleration behavior[28].

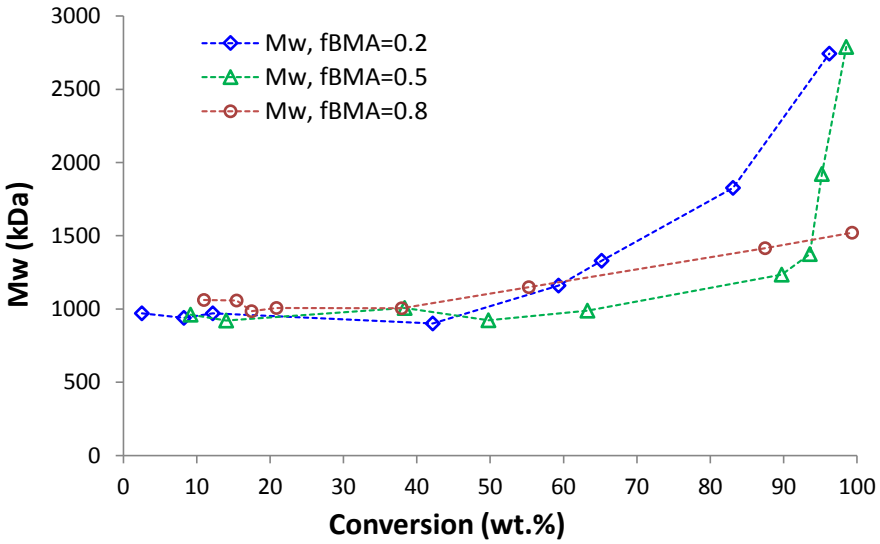

Figure 5.6 Molecular weight vs. conversion results at various BA/BMA monomer feed ratios. (Dashed lines are not model predictions but are provided to make the plot more readable).

The observed trend in polymer T_g is closely related to the copolymer composition (Table 5.4). This was expected, given the homopolymer T_g values for poly(BA) and poly(BMA) of -54°C and 20°C, respectively. For all the selected samples, only one T_g was detected.

Table 5.4 T_g results for selected BA/BMA samples.

Feed composition f_{BMA} (mol fraction)	**Conversion (wt%)**	**Copolymer composition**		**T_g (°C)**
		F_{BMA} (mol fraction)	**F_{BA} (mol fraction)**	
0.2	65	0.24	0.76	-39.9
	99	0.22	0.78	-41.2
0.5	38	0.65	0.35	-11.6
	99	0.50	0.50	-25.4
0.8	38	0.85	0.15	12.5
	100	0.79	0.21	6.0

5.4 Conclusion

Reliable reactivity ratios for bulk free-radical BA/BMA copolymerization at 80^{o}C were estimated as r_{BMA} = 2.01and r_{BA} = 0.46. These estimates indicate that addition of the BMA unit to the copolymer chain is favored during copolymerization. It was found that the BA/BMA ratio greatly affected copolymer T_g, molecular weight development and gel content level of the copolymer. The presence of a small amount of BMA critically reduced the formation of gel polymer by decreasing the inter- and intra-molecular chain transfer of BA.

5.5 Acknowledgements

The authors acknowledge the support of the MITACS Globalink program for Ms. Laura Hinojosa-Castellanos and Ms. Lisha Zhang, the China Scholarship Commission for the support of Ms. Shanshan Ren. Furthermore, financial support for this project by the Natural Sciences and Engineering Research Council (NSERC) of Canada is greatly appreciated.

5.6 References

1. Ebnesajjad, S.; Landrock, A. H. Chapter 5 - Characteristics of Adhesive Materials. In *Adhesives Technology Handbook (Third Edition)*; William Andrew Publishing: Boston, 2015; pp. p. 84–159.

2. Paul B. Foreman Acrylic Adhesives. In *Technology of Pressure-Sensitive Adhesives*

and Products; Handbook of Pressure-Sensitive Adhesives and Products; CRC Press, 2008; p. p. 5_2.

3. Gilbert, B. C.; Smith, J. R. L.; Milne, E. C.; Whitwood, A. C.; Taylor, P. Kinetic and structural EPR studies of radical polymerization. Monomer, dimer, trimer and mid-chain radicals formed via the initiation of polymerization of acrylic acid and related compounds with electrophilic radicals (˙OH, SO4–˙ and Cl2–˙). *J. Chem. Soc. Perkin Trans. 2* **1994**, 1759–1769.

4. Ahmad, N. M.; Heatley, F.; Lovell, P. A. Chain Transfer to Polymer in Free-Radical Solution Polymerization of n-Butyl Acrylate Studied by NMR Spectroscopy. *Macromolecules* **1998**, *31*, 2822–2827.

5. Plessis, C.; Arzamendi, G.; Leiza, J. R.; Schoonbrood, H. A. S.; Charmot, D.; Asua, J. M. Seeded Semibatch Emulsion Polymerization of n-Butyl Acrylate. Kinetics and Structural Properties. *Macromolecules* **2000**, *33*, 5041–5047.

6. González, I.; Leiza, J. R.; Asua, J. M. Exploring the Limits of Branching and Gel Content in the Emulsion Polymerization of n-BA. *Macromolecules* **2006**, *39*, 5015–5020.

7. Dubé, M. A.; Penlidis, A. A systematic approach to the study of multicomponent polymerization kinetics—the butyl acrylate/methyl methacrylate/vinyl acetate example: 1. Bulk copolymerization. *Polymer* **1995**, *36*, 587–598.

8. Roos, S. G.; Müller, A. H. E.; Matyjaszewski, K. Copolymerization of n-Butyl Acrylate with Methyl Methacrylate and PMMA Macromonomers: Comparison of

Reactivity Ratios in Conventional and Atom Transfer Radical Copolymerization. *Macromolecules* **1999**, *32*, 8331–8335.

9. Hakim, M.; Verhoeven, V.; McManus, N. T.; Dubé, M. A.; Penlidis, A. High-temperature solution polymerization of butyl acrylate/methyl methacrylate: Reactivity ratio estimation. *J. Appl. Polym. Sci.* **2000**, *77*, 602–609.

10. Jiang, S.; Sudol, E. D.; Dimonie, V. L.; El-Aasser, M. S. Dispersion copolymerization of methyl methacrylate and n-butyl acrylate. *J. Polym. Sci. Part Polym. Chem.* **2007**, *45*, 2105–2112.

11. Elizalde, O.; Arzamendi, G.; Leiza, J. R.; Asua, J. M. Seeded Semibatch Emulsion Copolymerization of n-Butyl Acrylate and Methyl Methacrylate. *Ind. Eng. Chem. Res.* **2004**, *43*, 7401–7409.

12. Li, D.; Grady, M. C.; Hutchinson, R. A. High-Temperature Semibatch Free Radical Copolymerization of Butyl Methacrylate and Butyl Acrylate. *Ind. Eng. Chem. Res.* **2005**, *44*, 2506–2517.

13. Peck, A. N. F.; Hutchinson, R. A. Secondary Reactions in the High-Temperature Free Radical Polymerization of Butyl Acrylate. *Macromolecules* **2004**, *37*, 5944–5951.

14. Grady, M. C.; Simonsick, W. J.; Hutchinson, R. A. Studies of higher temperature polymerization of n-butyl methacrylate and n-butyl acrylate. *Macromol. Symp.* **2002**, *182*, 149–168.

15. Mayo, F. R.; Lewis, F. M. Copolymerization. I. A Basis for Comparing the

Behavior of Monomers in Copolymerization; The Copolymerization of Styrene and Methyl Methacrylate. *J. Am. Chem. Soc.* **1944**, *66*, 1594–1601.

16. Li, D.; Hutchinson, R. A. Penultimate Propagation Kinetics of Butyl Methacrylate, Butyl Acrylate, and Styrene Terpolymerization. *Macromol. Rapid Commun.* **2007**, *28*, 1213–1218.

17. J. Brandrup; Edmund H. Immergut; E. A. Grulke *Polymer Handbook*; 4th Ed.; John Wiley and Sons: New York, 1999.

18. Šňpárek, J. A contribution to the semicontinuous emulsion polymerization. II. Copolymerization of butyl methacrylate and butyl acrylate. *Angew. Makromol. Chem.* **1972**, *25*, 113–119.

19. Dubé, M. A.; Saldívar-Guerra, E.; Zapata-González, I. Copolymerization. In *Handbook of Polymer Synthesis, Characterization, and Processing*; Saldívar-Guerra, E.; Vivaldo-Lima, E., Eds.; John Wiley & Sons, Inc., 2013; pp. 105–125.

20. Siołek, M.; Matlengiewicz, M. Reactivity Ratios of Butyl Acrylates in Radical Copolymerization with Methacrylates. *Int. J. Polym. Anal. Charact.* **2014**, *19*, 222–233.

21. Dubé, M.; Sanayei, R. A.; Penlidis, A.; O'Driscoll, K. F.; Reilly, P. M. A microcomputer program for estimation of copolymerization reactivity ratios. *J. Polym. Sci. Part Polym. Chem.* **1991**, *29*, 703–708.

22. Tobing, S. D.; Klein, A. Molecular parameters and their relation to the adhesive performance of acrylic pressure-sensitive adhesives. *J. Appl. Polym. Sci.* **2001**, *79*,

2230–2244.

23. Podzimek, S. Light Scattering. In *Light Scattering, Size Exclusion Chromatography and Asymmetric Flow Field Flow Fractionation*; John Wiley & Sons, Inc., 2011; p. p. 71.

24. Polic, A. L.; Duever, T. A.; Penlidis, A. Case studies and literature review on the estimation of copolymerization reactivity ratios. *J. Polym. Sci. Part Polym. Chem.* **1998**, *36*, 813–822.

25. Tidwell, P. W.; Mortimer, G. A. An improved method of calculating copolymerization reactivity ratios. *J. Polym. Sci. A* **1965**, *3*, 369–387.

26. Plessis, C.; Arzamendi, G.; Leiza, J. R.; Schoonbrood, H. A. S.; Charmot, D.; Asua, J. M. Modeling of Seeded Semibatch Emulsion Polymerization of n-BA. *Ind. Eng. Chem. Res.* **2001**, *40*, 3883–3894.

27. McCord, E. F.; Shaw, W. H.; Hutchinson, R. A. Short-Chain Branching Structures in Ethylene Copolymers Prepared by High-Pressure Free-Radical Polymerization: An NMR Analysis. *Macromolecules* **1997**, *30*, 246–256.

28. Odian, G. Radical Chain Polymerization. In *Principles of Polymerization*; John Wiley & Sons, Inc., 2004; pp. 198–349.

Chapter 6. Free-radical Terpolymerization of *n*-Butyl Acrylate/ Butyl Methacrylate/*d*-Limonene

Published in J. Appl. Polym. Sci., 132, 42821.

Free-radical Terpolymerization of *n*-Butyl Acrylate/Butyl Methacrylate/*d*-Limonene

Shanshan Ren, Lisha Zhang, Marc A. Dubé

Department of Chemical and Biological Engineering, Centre for Catalysis Research and Innovation, University of Ottawa

Abstract

d-Limonene (Lim) is a renewable monoterpene derived from citrus fruit peels. It is being investigated for use as part of a more sustainable polymer formulation. The bulk free-radical terpolymerization of *n*-butyl acrylate (BA)/butyl methacrylate (BMA)/Lim was carried out at 80°C using benzoyl peroxide as initiator. The terpolymerization was studied at various initial BA/BMA/Lim molar ratios and the products were characterized for conversion, terpolymer composition, molecular weight and glass transition temperature.

Lim was observed to undergo a significant degradative chain transfer reaction which greatly influenced the polymerization kinetics. The rate of polymerization, final conversion and polymer molecular weight were all significantly reduced due to the presence of Lim. Nonetheless, relatively high weight-average molecular weight polymers (20,000 – 120,000 Daltons) were produced. The terpolymer composition was well predicted using reactivity ratios estimated for each of the three copolymer

sub-systems.

Keywords: Biopolymers and renewable polymers; radical polymerization; properties and characterization; kinetics; copolymers

6.1 Introduction

Multicomponent polymerization is a common strategy used for tuning the properties of various polymer products, especially for coatings and adhesives. By manipulating the monomer feed composition, the addition of other components (e.g., chain transfer agent, cross-linker), and controlling the reaction conditions, specific physical and mechanical properties can be achieved.

Driven by the need to reduce our dependence on fossil fuels and to mitigate environmental effects, increased effort is being directed to the use of renewable materials to replace fossil-based monomers in polymerization. Various natural raw materials, such as cellulose, lignin, starch, vegetable oils, lactic acid, itaconic acid, terpenes and rosins, have shown great potential in the development of renewable polymers[1–7]. Depending on microstructural and final application requirements, different approaches, such as physical blending, chemical modification and *in situ* polymerization have been used to achieve the integration of the renewable feedstock into polymers[8–10].

d-Limonene (Lim) is a naturally occurring monoterpene which is mainly extracted from orange peels as a byproduct of the juicing industry. Compared to the extraction and refinement of fossil-based feedstock, the production of Lim (e.g., mechanical separation and distillation) releases much less greenhouse gases and toxic pollutants to the environment. Current annual worldwide production of Lim is over 70 million kg[11]. Because it is essentially non-toxic (based on toxicological studies in both in vitro and in vivo)[12,13] and provides an intense citrus fruit odour, Lim has been widely used in food, fragrances and medicine as well as a safe alternative to many toxic solvents[14–16]. Lim is a cyclic olefin which contains two unconjugated C=C double bonds: an endocyclic double bond and an exocyclic double bond. As a monomer, Lim presents great potential to replace non-polar monomers (such as styrene) because it is renewable and non-toxic. The rigid structure of the Lim molecule results in a polymer glass transition temperature, T_g, of about 116^{o}C[17]. The use of Lim in multi-component polymer formulations therefore could improve hardness and stiffness and increase the application temperature range of the resulting polymer.

Many studies have shown that Lim has a high propensity towards chain transfer reactions as the allylic hydrogens next to the double bonds are very reactive and tend to be easily captured by living radicals[18–22]. During polymerization, molecular weight development is greatly influenced by this chain transfer reaction mechanism. Thus, Lim could be used to modify the molecular weight in

multicomponent systems where lower molecular weight may be required.

In this paper, we present a study of the *n*-butyl acrylate (BA)/butyl methacrylate (BMA)/Lim bulk terpolymerization. A primary goal is to demonstrate the use of copolymer reactivity ratios for each of the three copolymer subsystems (i.e., BA/BMA, BA/Lim, BMA/Lim) to predict the terpolymer composition. Other data, such as conversion, molecular weight, and T_g were collected to provide further kinetic information.

6.2 Experimental

6.2.1 Materials

Lim was obtained from Fisher Scientific (96% purity), and was distilled under vacuum before use. BA (≥99% purity), BMA (≥99% purity) and benzoyl peroxide (BPO) were purchased from Sigma Aldrich. BA and BMA were purified of monomethyl ether hydroquinone inhibitor using an inhibitor removal column (Sigma Aldrich). BPO was recrystallized twice with acetone and deionized water, dried under vacuum at room temperature, and then stored in a refrigerator at 4^{o}C before use. All other solvents used for sample workup and characterization were used as received.

6.2.2 Polymerization

Bulk free radical polymerizations of BA/BMA/Lim were carried out in glass ampoules (10 mm diameter and 200 mm in length; 15.7 mL). About 5 g of monomer

plus initiator (1.0 wt% BPO) were pipetted into each ampoule. Initial molar ratios of BA/BMA/Lim of 80/10/10, 40/50/10, 70/10/20, 40/40/20, 60/10/30, 50/20/30, and 50/10/40 were used. Each ampoule was degassed using a pump-freeze-thaw procedure (typically, three cycles), flame-sealed and subsequently immersed in a constant temperature oil bath at 80 ℃. For each of the seven reaction conditions, a total of five to seven ampoules were prepared and removed from the oil bath at pre-determined times to achieve a range of monomer conversions. The polymeric products were precipitated in a 10-fold excess of methanol and refrigerated (4 ℃) for 4 h. The excess liquid was decanted and the polymer samples were dried in a vacuum oven at 25ºC until a constant weight was achieved. Using ^{1}H-NMR spectroscopy, the decanted liquid was verified for the presence of oligomeric materials and only insignificant amounts were detected.

6.2.3 Characterization

The overall monomer conversion was determined by gravimetry based on the mass of dried polymer. The terpolymer composition (F_{BA}, F_{BMA}, F_{Lim}, mole fractions) was measured with a ^{1}H-NMR spectrometer (Bruker, 400MHz) using $CDCl_3$ as the solvent at room temperature. Molecular weights were obtained using a GPC system (Agilent technology) with two columns in series (MZ-Gel SD plus 10^5 Angstroms 300 x 8.00 mm, particle size 5 μm, MZ-Gel SD plus 10^4 Angstroms 300 x 8.00 mm, particle size 5 μm) and tetrahydrofuran (THF) as eluent. The detection system consisted of a multi-angle laser light scattering detector (Wyatt Dawn Heleos II, λ =

633 nm), a differential refractive index detector (Wyatt Optilab T-rEX) and a differential viscometer (Wyatt ViscoStar ll). Samples diluted in THF were filtered through a 0.45 μm syringe filter prior to injection into the GPC. Data analysis was performed using Wyatt Astra software. The refractive index increment (dn/dc) used to calculate the molecular weight was estimated based on the dn/dc values for the homopolymers weighted by each terpolymer composition. For poly(BA) and poly(BMA), the dn/dc (THF, 25^{o}C) values were taken to be 0.064 mL g^{-1} and 0.076 mL g^{-1}, respectively[23]; for poly(Lim), a dn/dc value of 0.133 mL g^{-1} for poly(Lim) resin (donated by Pinova Inc.) was measured and used. The use of the weighted average of dn/dc values was verified experimentally for two separate terpolymer compositions and the approach was found to be consistent and accurate. Because of the use of a multi-angle light scattering technique, the molecular weights measured are considered absolute values. The glass transition temperatures (T_g) of the terpolymers were determined using differential scanning calorimetry (DSC, TA Instruments, Model Q1000). Polymer samples were put in a closed sample pan and underwent the following heating procedure in air: heating from -95 to 150^{o}C at 10^{o}C /min, isothermal for 3 min at 150^{o}C, cooling from 150 to -95^{o}C, isothermal for 3 min at -95^{o}C and then reheating from -95 to 150^{o}C to eliminate the thermal history of the sample. T_g was determined as the inflection point on the heat flow curve using the second heating cycle.

6.3 RESULTS AND DISCUSSION

6.3.1 Conversion vs. time results

Monomer conversions plotted vs. time for the seven feed compositions are shown in Figure 6.1. Within the group of seven monomer feeds, there were four acrylic (i.e., BA + BMA) /Lim feed ratios and seven separate BA/BMA ratios. By comparing the runs at four different acrylic/Lim levels, it can be seen how polymerization rate and final conversion levels related to both the Lim level and the BA/BMA ratio. As the Lim level increased from 10 to 40 mol%, the polymerization rate was reduced, and the final (limiting) conversion attained was lowered. For example, the polymerization presented final conversions of 85, 65 and 50 wt.% for BA/BMA/Lim feed compositions of 80/10/10, 70/10/20 and 60/10/30, respectively. This is related to the fact that Lim's allylic structure led to significant degradative chain transfer reactions. According to the degradative chain transfer mechanism, free radicals reacting with the allylic hydrogen of Lim, result in highly stable radicals that do not react further, but tend to react with macro-radicals and terminate the polymer chains, thus slowing the polymerization rate (Figure 6.2). The limiting conversions support the inability for Lim to homopolymerize via free radical mechanisms. It is evident that Lim could only be incorporated into the polymer chain while there was acrylic (BA and/or BMA) monomer remaining in the system. Composition results shown later support this as well. Similar behaviour has been previously observed in the BA/Lim system[24].

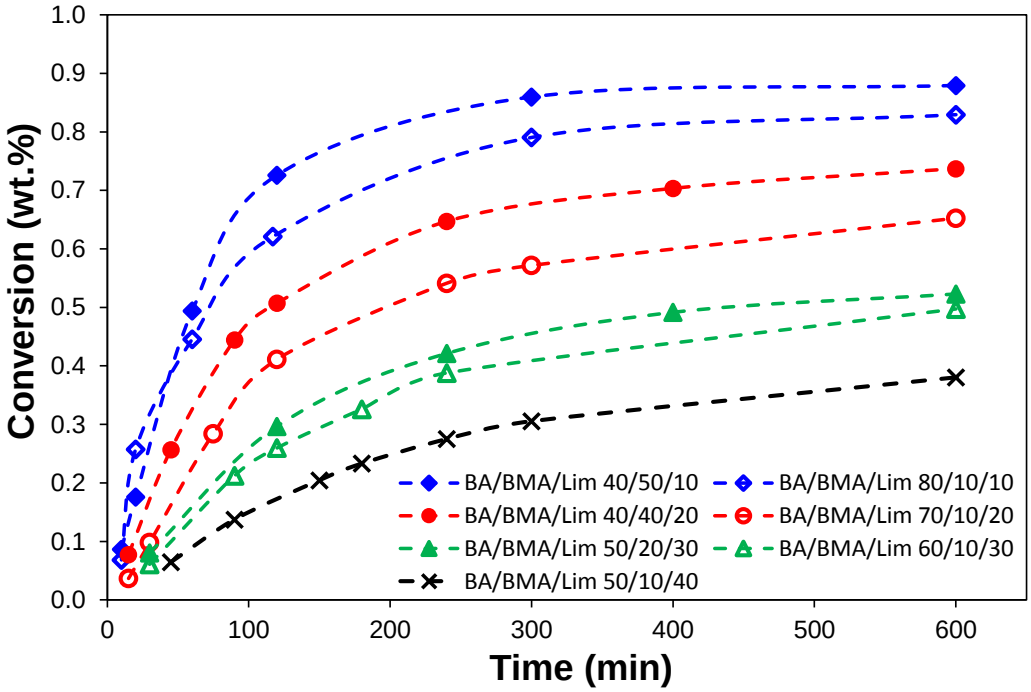

Figure 6.1 Monomer conversion vs. time for various BA/BMA/Lim compositions at T = 80°C and 1 wt.% BPO. The dash lines are not model predictions but are used for clarity.

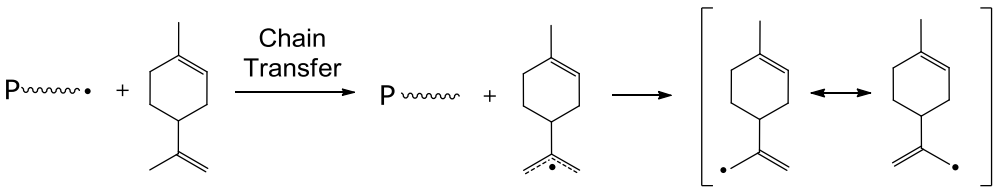

Figure 6.2 Schematic representation of degradative chain transfer of Lim.

6.3.2 Composition vs. conversion results

The prediction of terpolymer composition has been accomplished successfully for other systems using the Mayo-Lewis equation and the corresponding copolymerization reactivity ratios up to high conversion levels for bulk, solution and emulsion polymerization[25,26]. In previous studies, we investigated the

copolymerization of BMA/Lim and BA/Lim[24,27]. For these systems, reactivity ratios were estimated from low conversion polymerizations, and then validated with full conversion runs. Reliable experimental values of the reactivity ratios for BA/BMA were not available in the literature and therefore, using similar techniques as reported for the BA/Lim and BMA/Lim systems, estimates of the reactivity ratios were found to be $r_{BMA} = 2.01$ and $r_{BA} = 0.46$.

The mole fraction of each monomer bound in the terpolymer chains was determined using ^{1}H NMR spectroscopy. A typical NMR spectrum along with peak assignment for BA/BMA/Lim terpolymer is shown in Figure 6.3. Similar to the BA/Lim copolymer NMR results[24], two types of Lim units (Lim and Lim') were detected from the terpolymer NMR spectra: the Lim unit (containing only an internal C=C double bond) which was incorporated through the addition reaction on the external C=C double bond and the Lim' unit (containing both the internal and external C=C double bonds) which was integrated into the polymer chain as an end group through the degradative chain transfer mechanism. The terpolymer composition vs. conversion results and model predictions for each feed composition are plotted in Figure 6.4. Note that the model predictions were obtained by integrating the Mayo-Lewis equation using the three pairs of reactivity ratios estimated from low conversion bulk copolymerization experiments at 80 ℃ (Table 6.1). The composition data for each feed are fitted well by the integrated Mayo-Lewis model, which further validates the reactivity ratio estimated from previous work[24,27]. In all of the

composition vs. conversion plots, a fairly constant composition (low composition drift) was observed. This is related to the widely differing reactivity ratios for the BA/Lim and BMA/Lim system, whereas r_{BA} and r_{BMA} are each above 6, and r_{Lim} values are close to zero. The behaviour of this terpolymer system is remarkably similar in this respect to that of BA/methyl methacrylate/vinyl acetate[25]. Therein, the copolymer reactivity ratios of the acrylic comonomers are high (>5) whereas the corresponding reactivity ratios of the vinyl acetate is well below 0.1 in both cases[28,29]. In our case, the polymerization was dominated by BA and BMA, and the polymer composition exhibited very little drift initially. As the polymerization proceeded, more significant changes in composition were only observed when BA and BMA were nearly depleted. The Mayo-Lewis model predictions indicate significant composition drift beyond the experimental data points. It should be noted, however, once the acrylic monomers were depleted, no further polymerization could occur because of the fact that Lim cannot undergo homopolymerization. In Figure 6.4, all the polymerizations stopped before the predicted composition drift could occur. As a result, narrow composition distributions were achieved for all of the BA/BMA/Lim terpolymers.

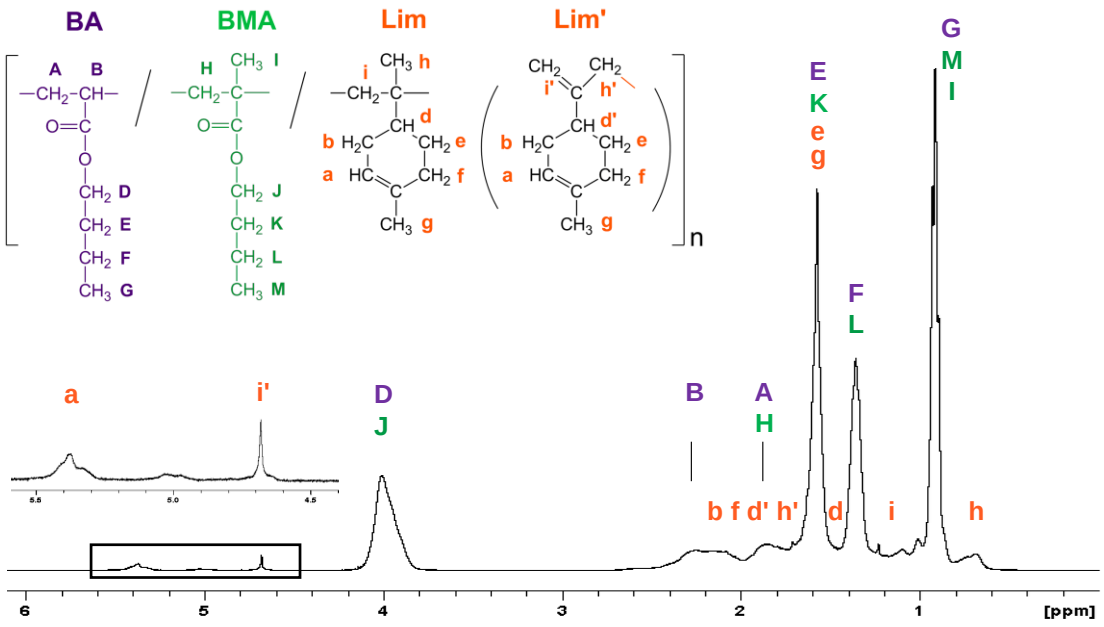

Figure 6.3 ^{1}H-NMR spectrum for BA/BMA/Lim terpolymer (Sample feed composition BA/BMA/Lim:50/10/40, polymer composition BA/BMA/Lim:65/25/10, conversion = 38 wt.%).

The effect of initial feed composition on terpolymer composition is also evident. With a higher BA content in the feed, the initial terpolymer composition was higher in BA (Figure 6.4 a, c, e, and g) compared to the case with a lower BA feed content (Figure 6.4 b and d). The Lim content in the terpolymer is relatively insensitive to the change of BA/BMA ratio because of the similar reactivity ratios for the BA/Lim and BMA/Lim systems.

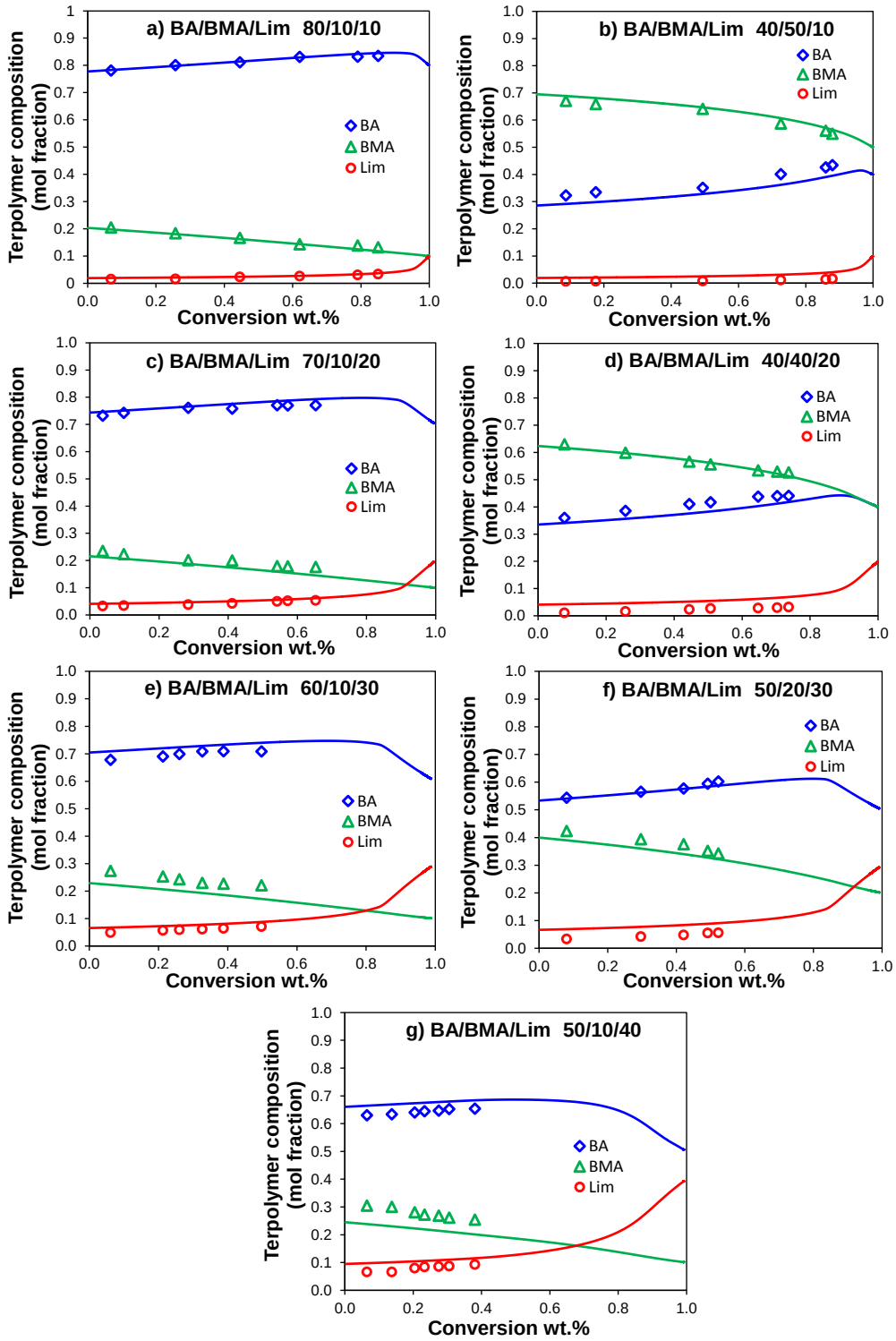

Figure 6.4 Terpolymer composition vs. conversion for various BA/BMA/Lim monomer feed ratios, T = 80°C and 1 wt.% BPO. Solid lines are integrated Mayo-Lewis model predictions using three pairs of reactivity ratios shown in Table 6.1.

Table 6.1 Reactivity ratios for BMA/BA, BMA/Lim and BA/Lim at 80°C.

Monomers	r_1	r_2
BMA/BA[a]	2.01	0.46
BMA/Lim[27]	6.10	0.046
BA/Lim[24]	6.01	0.0067

[a] Reactivity ratios for BMA/BA copolymerization were estimated using a series of low conversion experiments in work to be published elsewhere.

6.3.3 Molecular weight vs. conversion results

The absolute molecular weights of BA/BMA/Lim terpolymers are reported in Figure 6.5 for the BA/BMA/Lim monomer feed ratios of 80/10/10, 70/10/20 and 50/10/40. Figure 6.6 shows the SEC traces of selected terpolymer samples at different feed composition and different polymerization times. In the copolymerization of BA/Lim, it was observed that the molecular weight development was dominated by the degradative chain transfer reaction of Lim[24]. Not surprisingly, this effect was observed in the terpolymerization. The highest molecular weight (M_w = 125.8 kDa, M_n = 42.0 kDa) was observed in the runs carried out at the lowest Lim level (BA/BMA/Lim 80/10/10). For the same feed, it can be seen that the polydispersity index (PDI) increased from an initial value of 1.5 to 3.0 at a conversion of 83 wt.% (see Figure 6.6 a). This is related to the branching reactions due to the high BA concentrations along with the diffusion-controlled behaviour which occurs at high conversions when the reaction medium became viscous. With an increasing Lim fraction in the monomer feed, the terpolymers exhibited lower molecular weight and relatively narrower molecular weight distributions (Compare Figure 6.6 a to c, and b

to d); this implies that more frequent chain transfer events occurred. For example, at the BA/BMA/Lim feed of 70/10/20 and 50/10/40, the final M_n and PDI were 25.7 kDa and 2.0, and 13.9 kDa and 1.6, respectively. The relative small PDI is also related to the fact that Lim cannot undergo homopolymerization, thus the remaining Lim, which acted more like a solvent, diluted the reaction medium, maintained a low viscosity and prevented any gel effect during the final stages of the polymerization.

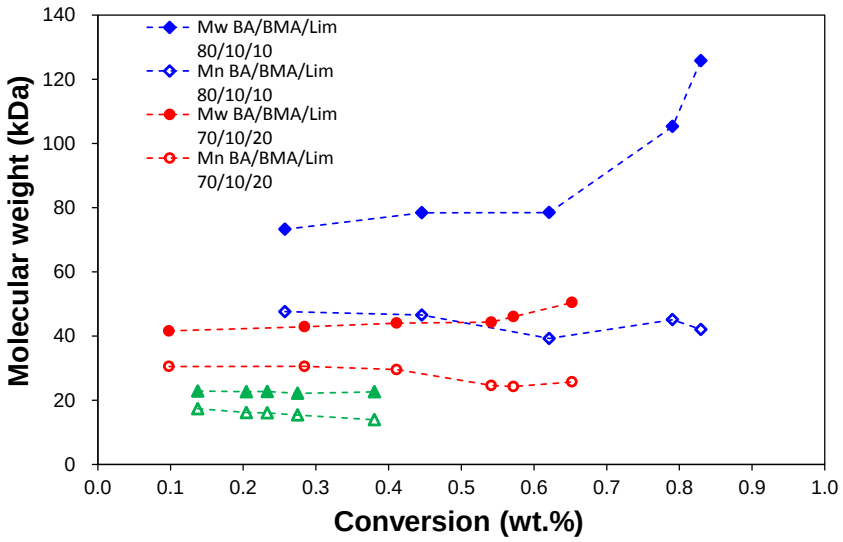

Figure 6.5 Terpolymer molecular weight vs. conversion results at various BA/BMA/Lim monomer feed ratios, T = 80°C, 1 wt.% BPO.

The terpolymer average chain length (X_n) and the average number of Lim units per chain for the highest conversion sample of each feed composition were calculated based on the composition and absolute molecular weight data (see Table 6.2). Generally, the average number of Lim units in each BA/BMA/Lim terpolymer chain ranged from 5 to 11. The presence of greater than one Lim unit per chain

indicates that Lim not only incorporated through the degradative chain transfer mechanism as an end group of a polymer chain, but also by means of chain propagation through the addition reaction at the external C=C double bond. This conclusion further supports the observations from our NMR spectra discussed above.

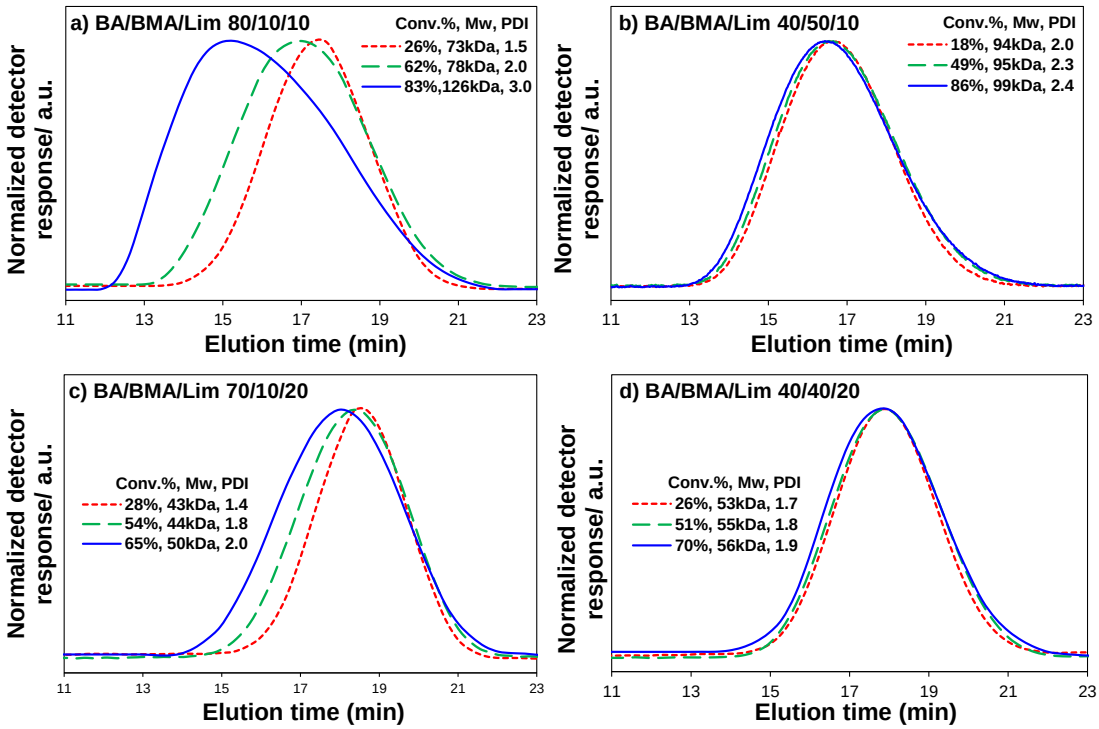

Figure 6.6 GPC chromatograms of selected samples at various feed compositions, T = 80^{o}C, and 1 wt.% BPO.

Table 6.2 Characterization results for BA/BMA/Lim terpolymers performed at various feed composition, 80°C, [BPO] = 1.0 wt.%.

BA/BMA/ Lim feed composition	Conv. (wt.%)	F_{BA} (mol %)	F_{BMA} (mol %)	F_{Lim} (mol %)	M_n (kDa)	X_n	Average number of Lim units per chain	T_g (°C)
80/10/10	85.1	0.835	0.132	0.034	42.0	323	11	-39.6
40/50/10	87.9	0.434	0.550	0.016	45.5	335	5	-16.6
70/10/20	65.2	0.770	0.176	0.053	25.7	196	10	-35.9
40/40/20	73.7	0.441	0.527	0.032	30.9	227	7	-16.1
60/10/30	49.7	0.708	0.221	0.071	18.4	139	10	-31.8
50/20/30	52.3	0.602	0.342	0.056	18.4	138	8	-30.9
50/10/40	38.0	0.653	0.254	0.092	13.9	105	10	-30.2

The effect of varying the BA/BMA monomer feed ratio on molecular weight at a fixed Lim level was also examined. Only slight differences were observed in the M_n values when the BA/BMA ratio was changed, whereas the polydispersity development of the terpolymer was quite different. It is known that polydispersity is directly related to the termination mechanism. At the high BA feed of 80/10/10 (see Figure 6.6 a), the initial PDI of 1.5 indicates a termination by combination mechanism was favored as is the case for BA homopolymerization[30]. In contrast, at the high BMA monomer feed ratio of 40/50/10 (see Figure 6.6 b), the initial PDI of 2.0 was a consequence of greater termination by disproportionation, which is favored by methacrylate monomers[31,32]; the PDI was then increased to 2.4 at 86% conversion. Similar molecular weight and PDI trends were observed in the feeds of 70/10/20 and 40/40/20, see Figures. 6.6 c and 6.6 d. These findings have important implications for future efforts in the modeling of this terpolymer system.

6.3.4 Glass transition temperature vs. composition and molecular weight

The glass transition temperature results for the BA/BMA/Lim terpolymer samples of each feed composition are shown in Table 6.2. The observed T_g trends are related primarily to terpolymer composition. The rigid molecular structure of Lim endows it with a relatively high T_g; a T_g of 116^{o}C has been reported for poly(Lim)[17]. A low molecular weight poly(Lim) resin (donated by Pinova Inc.) was tested and a T_g of 78^{o}C was measured. In general, the terpolymer T_g increases with a decreasing proportion of BA and an increasing proportion of BMA and Lim. Normally, for polymers with M_n above 20,000 Daltons, molecular weight does not affect T_g[33]. However, for the relatively low molecular weight sample (BA/BMA/Lim feed of 50/10/40), the T_g was lower than expected based on polymer composition effects. This reflects the effect of lower molecular weight which provides greater polymer chain mobility leading to a lower T_g[34]. Thus, for the low molecular weight samples, the terpolymer composition is only one factor modifying terpolymer T_g. For instance, the 50/20/30 sample (F_{BA} = 0.602, F_{BMA} = 0.342, F_{Lim} = 0.056) showed a T_g of -30.9^{o}C with a M_n of 18.4 kDa, while a slightly higher T_g of -30.2^{o}C was detected for the 50/10/40 sample (F_{BA} = 0.654, F_{BMA} = 0.254, F_{Lim} = 0.093) at a fairly low M_n of 13.9 kDa. By comparing the compositions of these two samples, one would expect significantly differing T_g values. However, the effect of molecular weight (notably at a molecular weight range below 20 kDa) compensated for the composition effect.

6.4 Conclusion

Lim is an ideal "green" material because it is renewable and essentially non-toxic, and has very low global warming potential. Our investigation of the use of Lim in a polymer formulation is part of a greater movement towards more sustainable polymer production. In this study, the bulk free-radical terpolymerization of BA/BMA/Lim was examined at 80^{o}C. It has been found that Lim has a dominant influence on molecular weight development, polymerization rate, and terpolymer composition. The allylic structure of Lim results in significant chain transfer which competes remarkably with chain propagation. With increasing amounts of Lim, polymers with shorter average chain lengths were produced while the allylic radicals resulted in a reduced rate of polymerization. In terms of terpolymer composition, because of the large difference in the copolymer reactivity ratios, the terpolymer exhibits a fairly constant composition (i.e., very little drift) with conversion for every monomer feed studied.

These findings have led to a better understanding of the kinetic mechanism of the multi-component polymerization when using Lim as a co-monomer. This has provided us with insight into ways to incorporate greater amounts of this renewable component into a polymer matrix. For example, the use of a lower reaction temperature may help reduce the rate of degradative chain transfer due to Lim relative to the propagation reaction. Another option would include the addition of cross-linkers to compensate for mechanical property losses resulting from the reduced

molecular weights. Semi-batch feed policies could also be implemented to encourage the incorporation of the less reactive monomer and eliminate composition drift. Given the comonomers used in this study (i.e., BA and BMA), potential applications in adhesives and coatings are envisaged.

6.5 Acknowledgements

The authors acknowledge the support of the MITACS Globalink program for Ms. Lisha Zhang, the China Scholarship Commission for the support of Ms. Shanshan Ren. Furthermore, financial support for this project by Intellectual Ventures and the Natural Sciences and Engineering Research Council (NSERC) of Canada is greatly appreciated.

6.6 References

1. Liu, Y.; Yao, K.; Chen, X.; Wang, J.; Wang, Z.; Ploehn, H. J.; Wang, C.; Chu, F.; Tang, C. Sustainable thermoplastic elastomers derived from renewable cellulose, rosin and fatty acids. *Polym. Chem.* **2014**, *5*, 3170–3181.

2. Yang, L.; Wang, X.; Cui, Y.; Tian, Y.; Chen, H.; Wang, Z. Modification of renewable resources—lignin—by three chemical methods and its applications to polyurethane foams. *Polym. Adv. Technol.* **2014**, *25*, 1089–1098.

3. Zeng, J.-B.; Jiao, L.; Li, Y.-D.; Srinivasan, M.; Li, T.; Wang, Y.-Z. Bio-based blends of starch and poly(butylene succinate) with improved miscibility, mechanical

properties, and reduced water absorption. *Carbohydr. Polym.* **2011**, *83*, 762–768.

4. Lligadas, G.; Ronda, J. C.; Galià, M.; Cádiz, V. Renewable polymeric materials from vegetable oils: a perspective. *Mater. Today* **2013**, *16*, 337–343.

5. Jamshidian, M.; Tehrany, E. A.; Imran, M.; Jacquot, M.; Desobry, S. Poly-Lactic Acid: Production, Applications, Nanocomposites, and Release Studies. *Compr. Rev. Food Sci. Food Saf.* **2010**, *9*, 552–571.

6. Winkler, M.; Lacerda, T. M.; Mack, F.; Meier, M. A. R. Renewable Polymers from Itaconic Acid by Polycondensation and Ring-Opening-Metathesis Polymerization. *Macromolecules* **2015**, *48*, 1398–1403.

7. Wilbon, P. A.; Chu, F.; Tang, C. Progress in Renewable Polymers from Natural Terpenes, Terpenoids, and Rosin. *Macromol. Rapid Commun.* **2013**, *34*, 8–37.

8. Yu, L.; Dean, K.; Li, L. Polymer blends and composites from renewable resources. *Prog. Polym. Sci.* **2006**, *31*, 576–602.

9. Peltzer, M.; Pei, A.; Zhou, Q.; Berglund, L.; Jiménez, A. Surface modification of cellulose nanocrystals by grafting with poly(lactic acid). *Polym. Int.* **2014**, *63*, 1056–1062.

10. Yao, K.; Tang, C. Controlled Polymerization of Next-Generation Renewable Monomers and Beyond. *Macromolecules* **2013**, *46*, 1689–1712.

11. Kerton, F. M. Chapter 6:Renewable Solvents and Other "Green" VOCs. In *Chapter 6:Renewable Solvents and Other "Green" VOCs*; 2013; pp. 149–174.

12. Kim, Y. W.; Kim, M. J.; Chung, B. Y.; Bang, D. Y.; Lim, S. K.; Choi, S. M.; Lim,

D. S.; Cho, M. C.; Yoon, K.; Kim, H. S.; Kim, K. B.; Kim, Y. S.; Kwack, S. J.; Lee, B.-M. Safety Evaluation And Risk Assessment Of d-Limonene. *J. Toxicol. Environ. Health Part B* **2013**, *16*, 17–38.

13. Filipsson, A. F.; Aseda, J. B.; Karlsson, S. *Concise International Chemical Assessment Document 5: Limonene*; 1998th ed.; Genebra.

14. Bauer, K.; Garbe, D.; Surburg, H. *Common Fragrance and Flavor Materials: Preparation, Properties and Uses*; John Wiley & Sons, 2008.

15. Breitmaier, E. Terpenes: Importance, General Structure, and Biosynthesis. In *Terpenes*; Wiley-VCH Verlag GmbH & Co. KGaA, 2006; pp. 1–9.

16. Gu, Y.; Jérôme, F. Bio-based solvents: an emerging generation of fluids for the design of eco-efficient processes in catalysis and organic chemistry. *Chem. Soc. Rev.* **2013**, *42*, 9550.

17. Singh, A.; Kamal, M. Synthesis and characterization of polylimonene: Polymer of an optically active terpene. *J. Appl. Polym. Sci.* **2012**, *125*, 1456–1459.

18. Mathers, R. T.; McMahon, K. C.; Damodaran, K.; Retarides, C. J.; Kelley, D. J. Ring-Opening Metathesis Polymerizations in d-Limonene: A Renewable Polymerization Solvent and Chain Transfer Agent for the Synthesis of Alkene Macromonomers. *Macromolecules* **2006**, *39*, 8982–8986.

19. Mathers, R. T.; Damodaran, K. Renewable chain transfer agents for metallocene polymerizations: The effects of chiral monoterpenes on the polyolefin molecular weight and isotacticity. *J. Polym. Sci. Part Polym. Chem.* **2007**, *45*, 3150–3165.

20. Mathers, R. T.; Damodaran, K.; Rendos, M. G.; Lavrich, M. S. Functional Hyperbranched Polymers Using Ring-Opening Metathesis Polymerization of Dicyclopentadiene with Monoterpenes. *Macromolecules* **2009**, *42*, 1512–1518.

21. Delancey, J. M.; Cavazza, M. D.; Rendos, M. G.; Ulisse, C. J.; Palumbo, S. G.; Mathers, R. T. Controlling crosslinking in thermosets via chain transfer with monoterpenes. *J. Polym. Sci. Part Polym. Chem.* **2011**, *49*, 3719–3727.

22. Brum, F. J. B.; Laux, F. N.; Forte, M. M. C. Synthesis of hydrocarbon polymers by cationic polymerization and their thermal properties. *Des. Monomers Polym.* **2013**, *16*, 291–301.

23. Podzimek, S. Light Scattering. In *Light Scattering, Size Exclusion Chromatography and Asymmetric Flow Field Flow Fractionation*; John Wiley & Sons, Inc., 2011; p. p. 71.

24. Ren, S.; Trevino, E.; Dubé, M. A. Copolymerization of Limonene with n-Butyl Acrylate. *Macromol. React. Eng.* **2015**, *9*, 339–349.

25. Dubé, M. A.; Penlidis, A. A systematic approach to the study of multicomponent polymerization kinetics: the butyl acrylate/methyl methacrylate/vinyl acetate example, 2. Bulk (and solution) terpolymerization. *Macromol. Chem. Phys.* **1995**, *196*, 1101–1112.

26. Beauchemin, R.-C.; Dubé, M. A. Bulk Terpolymer Composition Prediction from Copolymer Reactivity Ratios. *Polym. React. Eng.* **1999**, *7*, 485–499.

27. Zhang, Y.; Dubé, M. A. Copolymerization of n-Butyl Methacrylate and

D-Limonene. *Macromol. React. Eng.* **2014**, *8*, 805–812.

28. Dubé, M. A.; Penlidis, A. A systematic approach to the study of multicomponent polymerization kinetics—the butyl acrylate/methyl methacrylate/vinyl acetate example: 1. Bulk copolymerization. *Polymer* **1995**, *36*, 587–598.

29. Scorah, M. J.; Hua, H.; Dubé, M. A. Bulk and solution copolymerization of methyl methacrylate and vinyl acetate. *J. Appl. Polym. Sci.* **2001**, *82*, 1238–1255.

30. Cameron, N. R.; Lagrille, O.; Lovell, P. A.; Thongnuanchan, B. Solution homopolymerizations of n-butyl acrylate and styrene mediated using 2,2,5-trimethyl-4-tert-butyl-3-azahexane-3-oxyl (TITNO). *Polymer* **2014**, *55*, 772–781.

31. Bizilj, S.; Kelly, D.; Serelis, A.; Solomon, D.; White, K. The Self-Reactions of 1-Methoxycarbonyl-1-methylethyl and Higher Ester Radicals: Combination vs Disproportionation and Oligomeric Products from Secondary Reactions. *Aust. J. Chem.* **1985**, *38*, 1657.

32. Moad, G.; Solomon, D. H. 5 - Termination. In *The Chemistry of Radical Polymerization (Second Edition)*; Elsevier Science Ltd: Amsterdam, 2005; pp. 233–278.

33. Tadlaoui, K.; Pietrasanta, Y.; Michel, A.; Verney, V. Influence of molecular weight on the glass transition temperature and the melt rheological behaviour of methyl methacrylate telomers. *Polymer* **1991**, *32*, 2234–2237.

34. Fox, T. G.; Loshaek, S. Influence of molecular weight and degree of crosslinking

on the specific volume and glass temperature of polymers. *J. Polym. Sci.* **1955**, *15*, 371–390.

Chapter 7. Adhesive Performance Modification in Core-Shell Latex Films Using *d*-Limonene as a Chain Transfer Agent

Int. J. Adhes. Adhes. Submitted Oct. 2016.

Adhesive Performance Modification in Core-Shell Latex Films Using d-Limonene as a Chain Transfer Agent

Shanshan Ren and Marc A. Dubé*

Department of Chemical and Biological Engineering, Centre for Catalysis Research and Innovation, University of Ottawa

Abstract

Core-shell latex-based pressure-sensitive adhesives comprising *n*-butyl acrylate, styrene and acrylic acid were prepared via two-stage seeded semi-batch emulsion polymerization. *d*-Limonene (Lim) was used as a renewable chain transfer agent. Adhesive performance was modified by manipulating the microstructure of both the latex particle cores and shells. In the first stage of the polymerization, the concentrations of Lim and divinylbenzene (DVB) crosslinker were varied to alter the core microstructure and thus, the cohesive strength of the adhesive films. The particle shell microstructure was modified in the second stage of the polymerization by varying only the amount of Lim. As a result, a variety of particle microstructures and morphologies were generated. Tack and peel strength decreased with increasing Lim concentration while shear strength showed a maximum at a moderate core Lim concentration of 2 phm. Empirical models were developed using stepwise regression to correlate tack, peel strength and shear strength to Lim concentration in the core/shell and DVB concentration in the core.

Keywords: water based, latex and dispersions, pressure-sensitive, *d*-Limonene

7.1 Introduction

Water-based pressure sensitive adhesives (PSAs) are in high demand for packaging applications because they have a high solids content and are devoid of hazardous solvents. Latex-based adhesives have found wide application as labels, food-contact packaging, medical tapes and many others. Acrylic adhesives demonstrate the advantage of colorlessness, excellent cohesive strength and necessary tack and peel strength, as well as good resistance to heat and aging[1,2].

In a typical latex-based acrylic adhesive formulation, one finds a combination of soft monomers, hard monomers and some functional monomers [3]. Soft monomers, thus named for their low glass transition temperature (T_g), such as *n*-butyl acrylate (BA, T_g = -54 ℃) and 2-ethylhexyl acrylate (T_g = -50 ℃), provide viscosity, flow and wetting abilities, which ultimately impart properties such as tack and peel strength to the PSA film. Hard monomers, so named for their high T_g, such as styrene (Sty, T_g = 100 ℃) and methyl methacrylate (T_g = 105 ℃), offer hardness and internal strength to the PSA. The addition of small amounts of functional monomers such as acrylic acid (AA) can impart polarity and balance the viscous-elastic properties, adhesion and internal strength of the PSA film[4–6]. In recent years, latexes with a

core-shell particle morphology have enabled outstanding control over the adhesive properties by combining polymers with different microstructures in the same particle [7–10].

Crosslinker and chain transfer agent (CTA) are two common modifiers used to tailor polymer microstructure and properties. In general, the addition of a CTA would increase the flexibility and mobility of adhesive polymers by reducing the molecular weight and the gel content level [11]. An increase in crosslinker concentration would result in an increase in gel content, which improves the rigidity and the internal strength of the PSA[12,13]. Manipulating both CTA and crosslinker concentrations simultaneously allows for a broad range of polymer microstructure and adhesive performance [14–17]. Thiol compounds such as tert-butanethiol and n-dodecanethiol, are the most commonly used CTAs in emulsion polymerization due to their water solubility and high efficiency [18–20]. However, thiols exhibit an unpleasant odor and are considered as a VOC which is counter to sustainable practice.

Terpene is one of the largest naturally occurring chemical feedstocks, and is a constituent of essential oils found in many conifer and citrus plants. *d*-Limonene (Lim) is a cyclic monoterpene with two unconjugated double bonds in its backbone (see Figure 7.1). Previous studies have reported that the allylic hydrogen is very active and leads to a degradative chain transfer during the polymerization with acrylic monomers [21–23]. Lim has been used as a CTA and solvent in ring-opening polymerizations and metallocene polymerizations of olefins [24,25].

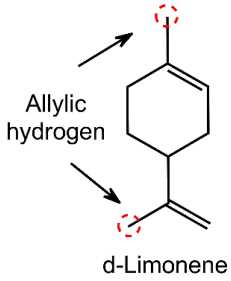

Figure 7.1 *d*-Limonene and allylic hydrogen.

In this work, a core-shell latex-based PSA was prepared using Lim as a renewable CTA. The shell polymer was designed to achieve a lower T_g and viscosity than the core polymer, in order to offer better flow ability, substrate wettability and thus, better adhesion, and increase energy dissipation during the debonding process. To balance the viscoelasticity behaviour of the PSA, the core was designed with higher T_g and higher crosslinking density to ensure adequate cohesive strength of the PSA film. By simultaneously manipulating the crosslinker and Lim concentrations, the gel content and molecular weight were modified, and their influence on the adhesive performance (i.e., tack, peel strength and shear strength) was investigated.

7.2 Experimental

7.2.1 Material

The monomers styrene (Sty, Sigma-Aldrich, 99%), *n*-butyl acrylate (BA, Sigma-Aldrich, 99%), and acrylic acid (AA, Acros, 99.5%), and the solvent, tetrahydrofuran (THF, Fisher, 99.9%) were used as received without further purification. *d*-Limonene (Lim, Fisher, 96%) was distilled under vacuum at 65-70^{o}C before use to

remove tocopherol inhibitor. A biodegradable anionic surfactant, EF-800 (49-51 wt% aqueous solution), was donated by Cytec (USA) and used as received. Potassium persulfate (KPS, Sigma-Aldrich, 99%) initiator, sodium bicarbonate buffer, and divinylbenzene (DVB, Sigma Aldrich, 80%) crosslinker, were all used as received. Distilled deionized (DDI) water was used throughout the experiment. Poly(vinylidene fluoride) (PVDF) porous membranes (47 mm diameter, 5 μm pore size, Cole-Parmer) were used in gel content measurements.

7.2.2 Latex preparation

Polymerizations were carried out at 80 ℃ in a 1 L Mettler-Toledo LabMax® jacketed glass reactor equipped with an anchor stirring blade, reflux condenser, and inlets for nitrogen, monomer, and initiator semi-batch feeds. The latexes were prepared using a two-stage seeded semi-batch polymerization process (Table 7.1).

Core-stage

A mixture of surfactant, buffer, and DDI water was initially charged into the reactor. Nitrogen purging was started and the temperature of the reaction was gradually increased to 80^{o}C within 30 min, while stirring (220 rpm). To start the polymerization, 42 g of monomer mixture and the 15.4 g KPS aqueous solution were charged into the reactor. After a 30 min seed production stage, a sample was taken to measure latex particle size and monomer conversion. The core monomer mixture and the remaining initiator solution were then fed to the reactor over 3 and 3.5 h, respectively. After completing the feed, the system was then allowed to react for an

additional 40 min to increase the conversion. The latex was then cooled to 30^{o}C.

Shell-stage

Buffer, DDI water and core latex were weighed and charged into the 1 L reactor. The reactor temperature was increased to 80^{o}C within 30 min under nitrogen atmosphere. The stirring speed was maintained at 280 rpm throughout the polymerization. A 15 g KPS solution was then charged into the reactor. After 5 min, a mixture of monomers and Lim, and the remaining initiator solution were fed into the reactor over 3.5 and 4 h, respectively. At completion of the feed procedure, reaction was continued for 40 min and then cooled to 30^{o}C. Samples were taken to monitor particle growth and monomer conversion. The particle diameter of the final latex was in the range of 110-120 nm for all cases. The final latex was stored at room temperature for further characterization.

7.2.3 Characterization

Solids content was measured gravimetrically. Latex particle size and polydispersity index (PDI) were measured using a Malvern NanoS Zetasizer Dynamic Light Scattering (DLS) instrument at room temperature. One drop of latex was diluted with 4 mL DDI water, and then pipetted into the test vial. The PDI of all the latexes were less than 0.05, which is considered as a narrow particle size distribution. There was no evidence of secondary particle nucleation.

The T_g of the dry polymer was determined using differential scanning calorimetry (DSC, TA Instruments, Model Q1000). Dry polymer (~10 mg) was

scanned twice from -80 to 130ºC at a heating/cooling rate of 10ºC/min to eliminate the thermal history of the sample. The T_g was determined as the inflection point on the second heat flow curve.

Table 7.1 Latex formulation by seeded semi-batch emulsion polymerization at 80 ℃.

Latexes	**Stages**	**Component**	**Amount (g)**
Core-stage polymerization	Initial charge	Water	313
		EF-800[a]	24
		Sodium bicarbonate	0.4
		BA	33
		Sty	9
		2.5 wt.% KPS solution	15.4
	Semi-batch feeding	BA	197.8
		Sty	40.2
		AA	9.5
		Lim	4.8
		DVB	0.48
		2.5 wt.% KPS solution	82.1
Shell-stage polymerization	Initial charge	core latex	287
		Water	56.6
		Sodium bicarbonate	0.16
		2.2 wt.% KPS solution	15.4
	Semi-batch feeding	BA	189.7
		Sty	17.1
		AA	8.3
		Lim	6.2
		2.2 wt.% KPS solution	86.9

Gel content was determined using the membrane partitioning method [26]. A dried polymer sample (~0.03 g) was sealed in a PVDF porous membranes pouch (pore size = 5 μm; diameter = 47 mm). The pouch was immersed in 25 mL THF in a 100 mL glass jar and gently shaken for 6 h. The swollen pouch was then placed in a fume hood and air-dried until a constant weight was achieved. Gel content was calculated by dividing the weight of the sample after the soluble polymer extraction by its original weight. The reported values are an average of three measurements. The THF solution containing sol polymer was concentrated by evaporation and then characterized for average molecular weight via gel permeation chromatography (GPC). The GPC system (Agilent technology) was equipped with two columns (MZ-Gel SD plus 10^5 Angstroms 300 x 8.00 mm, particle size 5 μm, MZ-Gel SD plus 10^4 Angstroms 300 x 8.00 mm, particle size 5 μm) and three detectors: a multi-angle laser light scattering detector (Wyatt Dawn Heleos II, λ = 633 nm), a differential refractive index detector (Wyatt Optilab T-rEX) and a differential viscometer (Wyatt ViscoStar ll). THF was used as eluent at a flow rate of 1 mL/min. Samples were filtered through a 0.45 μm syringe filter prior to injection to the GPC. The refractive index increment (dn/dc) used to calculate the molecular weight was estimated based on the dn/dc values for the homopolymers weighted by each terpolymer composition. For poly(BA), poly(Sty), poly (AA) the dn/dc (THF, 25^{o}C) values were taken to be 0.064 mL g^{-1}, 0.185 mL g^{-1} and 0.0738 mL g^{-1}, respectively [27,28]; for poly(Lim), a dn/dc value of 0.133 mL g^{-1} for poly(Lim) resin (donated by Pinova Inc.) was

measured and used. Data analysis was performed using Wyatt Astra software.

Latexes were cast onto a 60 μm thick poly(ethylene terephthalate) film with a #50 Meyer rod. Latex coagulum was removed with a sieve (#30 mesh) before casting. Prior to testing, the PSA films were dried for 4 days at 23±2°C, 50±5 % R.H and achieved a final thickness of ~40 μm. For each latex, 5 or 6 specimens were prepared for the evaluation of loop tack, 180° peel strength and shear strength measurement, respectively. The reported value in this work was the average of the 5 or 6 specimens. PSA performance was measured according to the Pressure Sensitive Tape Council standards (PSTC). Tack was measured using the PSTC-16 standard. Both loop tack and peel strength were tested with an Instron E3000 Universal Tester (Instron, Inc.). A sample strip of 25.4 mm x 177.8 mm (1" x 7") was formed into a teardrop loop. The loop end was covering with a 25.4 mm wide masking tape and inserted into the upper grip of the tester. The crosshead was moved downward to allow the loop to cover an area of 25.4 mm x 25.4 mm on a stainless steel panel (25.4 mm x 76.2 mm). The maximum force per unit length (25.4 mm) needed to remove the loop specimen from the panel at a speed of 300/min was reported as tack. The 180° peel test was measured using the PSTC-101 standard. A specimen of 25.4 mm x 304.8 mm (1" x 12") was applied to a stainless steel panel (50.8 mm x 152.4 mm) with a 2045 g hand roller at a rate of 10 mm/s (back and forth). The panel was clamped onto the jaw of the test. The end of sample strip was covered with masking tape and placed in the upper grip of the tester. The average force per unit length (25.4 mm) required to peel the specimen at an angle of 180°

with a speed of 300 mm/min was recorded. For shear strength evaluation, the PSTC-107 standard was used. A 12.7 mm x 152.4 mm (0.5" x 6") sample strip was used. One end of the specimen (an area of 12.7 mm x 12.7 mm) was applied to a stainless steel panel (50.8 mm x 76.2 mm) with a 2045 g hand roller at a rate of 10 mm/s (back and forth). A clamp was placed vertically at the free end of the specimen. By placing the panel onto a test stand, a 500 g weight was applied on the clamp. The time elapse until the sample completely separated (weight fell down) from the panel was recorded using Labview™ software (National Instruments).

7.3 Results and Discussion

A series of core-shell latexes were prepared by varying the concentration of Lim (0/2/5 phm) and crosslinker divinylbenzene (0.2/0.3 phm) in the core, and the concentration of Lim (0/3 phm) in the shell-stage polymerization. For all cases, BA and Sty were used as monomers with a BA/Sty composition of 80/20 mol/mol (core) and 90/10 (shell). To maintain consistency in core properties, each batch of core latex was split and used separately with a different shell formulation. The experimental design and latex properties for 6 core latexes and 11 core-shell latexes are given in Table 7.2. All latexes were colloidally stable for over one year and no coagulum was observed during polymerization. A final conversion beyond 96 wt.% was achieved for all runs. The solids contents for the core and final latexes were 42.5±0.5 % and 51.0±1 %, respectively. The average particle diameters were between 71 and 73 nm

for the core latex, and between 107 and 115 nm for the final latexes. The core-shell mass ratio was designed to be 1:1.75. This ratio would ensure complete coverage of all core particles.

Table 7.2 Lim and crosslinker concentration and latex properties. The core-shell latex ID identifies the core used (i.e., A – F) and the amount of Lim in the shell stage (i.e., 0 or 3 phm). For example, PSA-C3 is the core-shell latex using core C with 3 phm Lim added at the shell stage.

Core Latex (BA/Sty 80/20, mole fraction)					Shell Latex (BA/Sty 90/10, mole fraction)			
Latex ID	Lim (phm)	DVB (phm)	Particle Size (nm)	PDI	Latex ID	Lim (phm)	Particle Size (nm)	PDI
Core A	0	0.2	71	0.03	PSA-A0	0	108	0.03
					PSA-A3	3	107	0.02
Core B	2	0.2	72	0.02	PSA-B0	0	110	0.02
					PSA-B3	3	110	0.03
Core C	5	0.2	73	0.04	PSA-C0	0	114	0.05
					PSA-C3	3	111	0.03
Core D	0	0.3	73	0.03	PSA-D0	0	110	0.02
					PSA-D3	3	110	0.04
Core E	2	0.3	73	0.04	PSA-E0	0	115	0.05
					PSA-E3	3	113	0.03
Core F	5	0.3	73	0.02	PSA-F3	3	108	0.02

*phm means parts per hundred monomer

7.3.1 Influence of Lim and crosslinker on gel content and molecular weight

Figure 7.2 presents the gel content for the core and core-shell latexes. Crosslinker (i.e., DVB) was added to the core latex in order to provide better cohesive

strength for the PSA. In all cases, core latexes exhibited a higher gel content compare to the final core-shell latexes (no crosslinker was added at the shell stage). In addition and as expected, the gel content was consistently higher with increasing DVB concentration. It is known that the polymerization of BA yields high gel content polymers resulting from intermolecular chain transfer and the termination by combination of branched tertiary radicals (resulting from intramolecular chain transfer of BA) [16,29–33]. Thus, the presence of BA with or without crosslinker would still yield significant gel content. This explains why the difference in gel content of the core (with crosslinker) and core-shell polymer (without crosslinker added to the shell) was not large. In other words, the absence of crosslinker in the shell feed was somewhat compensated by additional BA.

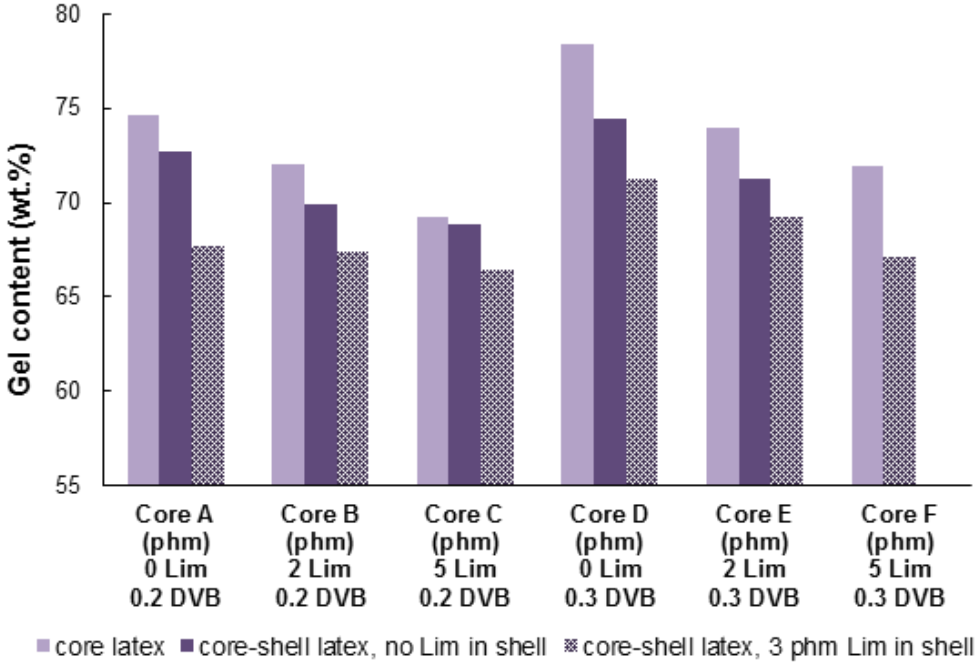

Figure 7.2 Effect of crosslinker and Lim concentration on gel content.

The number- and weight-average molecular weights and polydispersity index (PDI) of the soluble fractions of the core and core-shell latexes are given in Table 7.3. The addition of Lim (3 phm) during the shell stage resulted in a lower gel content and a lower sol M_w compare to latex with no Lim added in the shell (Figure 7.2 and Table 7.3). This trend in molecular weight is consistent with our previous results showing that Lim plays a role of chain transfer agent due to its active allylic hydrogen [21,22,34]. Similarly, higher Lim concentrations in the core latexes resulted in a decrease in gel content (Figure 7.2). At the same crosslinker level but with increasing Lim content from 0 to 2 to 5 phm, the sol M_w of the core latex decreased and then increased (compare core A, B, and C; Core D, E and F in Table 7.3); similar effects were reported by Qie [16]. Without Lim, the average polymer chain length was larger. Most of these long chain polymers underwent further branching and crosslinking and formed gel polymer while a small amount of short chain polymers remained as sol polymer. At an increased Lim concentration (2 phm), the average polymer chain length was decreased. These shorter polymers required more growth to form gel. As a consequence, the gel content decreased. When Lim concentration was increased to 5 phm, the increased number of short chain polymer formed highly branched polymers, and not all of them could grow to a sufficient size and become gel polymer. Thus, in the latter case less gel formed but the highly branched polymer remains as a sol polymer with a higher average molecular weight.

Table 7.3 Average molecular weight results of the synthesized latexes. Note that M_w is weight-average molecular weight, M_n is number-average molecular weight. (For explanation of Latex ID, and Lim and DVB concentrations, see Table 7.2)

Core Latex (BA/Sty 80/20, mole fraction)				Shell Latex (BA/Sty 90/10, mole fraction)			
Latex ID	Mn (kDa)	Mw (kDa)	PDI	Latex ID	Mn (kDa)	Mw (kDa)	PDI
Core A	95.3	191.4	2.01	PSA-A0	73.7	191.9	2.60
				PSA-A3	67.7	174.9	2.58
Core B	64.4	139.6	2.17	PSA-B0	62.8	158.6	2.53
				PSA-B3	48.8	114.8	2.35
Core C	80.3	189.2	2.36	PSA-C0	64.2	152.4	2.37
				PSA-C3	65.5	132.6	2.03
Core D	82.8	192.3	2.32	PSA-D0	69.9	187.5	2.68
				PSA-D3	56.5	125.2	2.22
Core E	70.9	145.0	2.05	PSA-E0	64.9	165.3	2.55
				PSA-E3	55.5	129.6	2.34
Core F	88.8	212.4	2.40	PSA-F3	81.6	179.7	2.20

7.3.2 Influence of Lim and crosslinker on T_g

Typical DSC curves for the core and core-shell latexes are shown in Figure 7.3. The T_g of the core latex was at -20^{o}C while that of the core-shell latex was roughly 10^{o}C less. It was noted in Figure 7.2 that there was a difference of 5 wt% in gel content between the core and core-shell latexes. Thus, on the basis of gel content alone, one would not expect such a large difference in T_g. On the other hand, the difference in monomer composition between the core and shell was 80 vs. 90 mol% BA. Thus, the difference in T_g values between the core and core-shell latexes is consistent with these composition differences. At the same time, if the core and shell

of each particle were physically distinct, one would expect to see two separate transitions on the DSC curves. However, only one T_g was detected. This implies that during the shell stage, it is quite possible that the monomer penetrated the core, leaving no distinct boundary between core and shell. Thus, one cannot refer to this as a true core-shell latex but there is still likely a composition gradient within each particle.

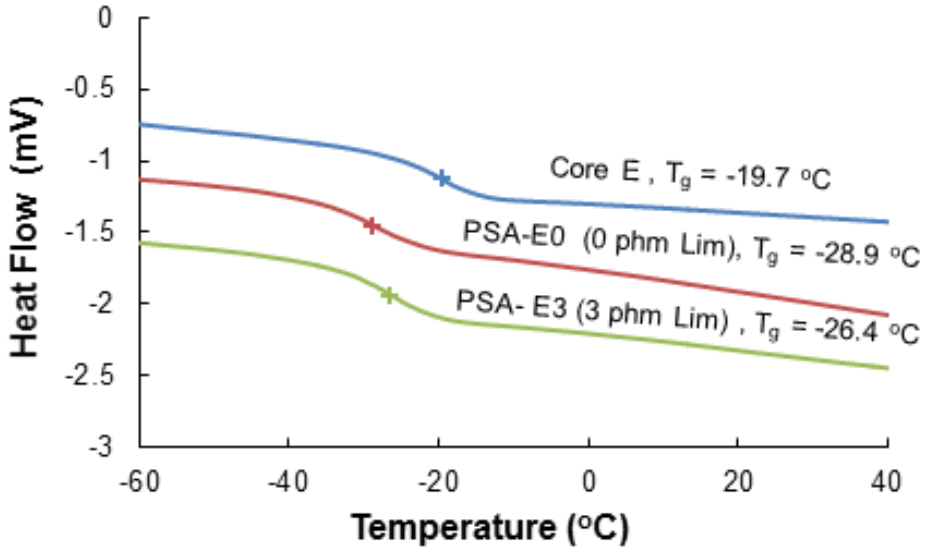

Figure 7.3 DSC curves of core latex sample (Core E) and core-shell latex sample (PSA-E0 and E3)

The T_g for core latexes ranged from -18.6°C to -23.3°C, and for core-shell latexes ranged from -25.8°C to -30.0°C (Figure 7.4). As noted from Figure 7.3, the core polymer exhibited a higher T_g than the core-shell polymer due to the higher Sty fraction in the core. Previously, we showed that increasing the Lim fraction in a

BA-based polymer results in an increase in polymer T_g[21,22]. The rigid Lim structure imparts a high T_g of 116°C to its homopolymer[35]. A T_g of 78°C was measured for Lim oligomer[21]. This is consistent with the observation that the T_g of both the core latex and core-shell latex increased with increasing Lim concentration (Figure 7.4).

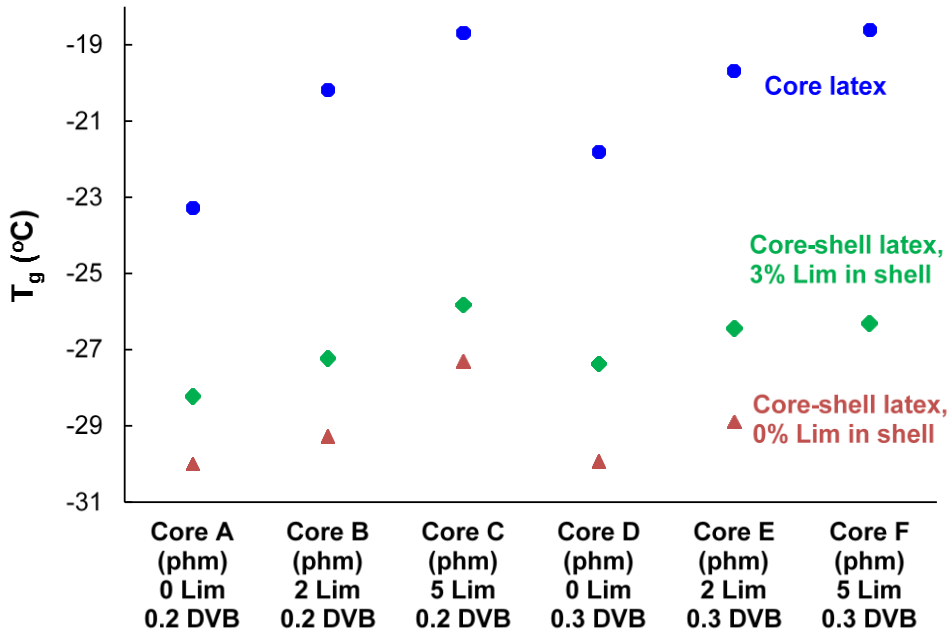

Figure 7.4 Effect of crosslinker and Lim concentration on T_g.

7.3.3 PSA performance

For the design of experiments, three variables (i.e., DVB concentration in the core, Lim concentration in the core, Lim concentration in the shell) were manipulated in these runs. Because these variables were changed simultaneously, graphical interpretation of results is made more difficult. However, fitting empirical models to

the data is possible and greatly simplifies interpretation of the results.

Three separate empirical models were developed to correlate tack, peel strength and shear strength to Lim concentration in the core (LC), Lim concentration in the shell (LS) and DVB concentration in the core (DVB) using Minitab™ software. A backward stepwise regression method was used due to the correlation present in the experimental design matrix[36]. Higher-order terms were added to the models to improve the fit. The reduced models were evaluated using residual plots and significance testing. Reduction of the number of fitted parameters was performed by removing terms with p-values >0.05 from the model. Each reduced model explained a significant amount of variability in the data. The reduced models are:

$$\text{tack} = 24.93 - 2.29\,LC - 17.90\,DVB - 0.63\,LS + 4.05\,LC{*}DVB \quad \text{(Eq. 7.1)}$$

$$\text{peel strength} = 12.39 - 1.35\,LC - 0.36\,LS + 0.19\,LC^2 - 1.34\,LC{*}DVB \quad \text{(Eq. 7.2)}$$

$$\text{shear strength} = 29.49 - 27.72\,LC + 5.51\,LC^2 + 148.10\,LC{*}DVB + 4.31\,LS{*}DVB - 30.14\,LC^2{*}DVB \quad \text{(Eq. 7.3)}$$

As would be expected from these types of empirical models, excellent predictions of the data were achieved (Figure 7.5). The changes in microstructure in both the core and shell of the latex particles had an influence on PSA performance; i.e., tack, peel strength and shear strength (Figure 7.5). Due to the high gel content (66 to 75%) of all the PSA latexes, no cohesive failure was observed for these tests.

a) DVB = 0.2 phm Lim in shell = 0 phm

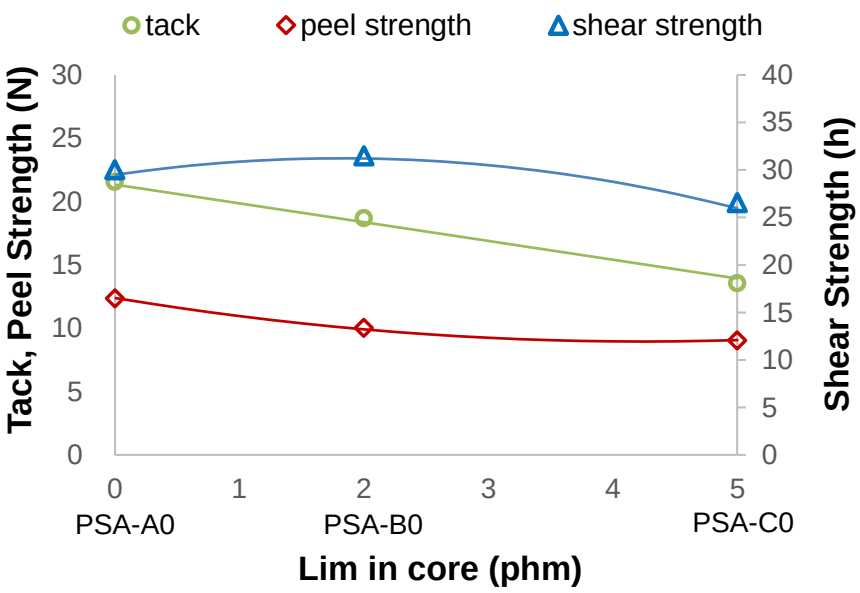

b) DVB = 0.2 phm Lim in shell = 3 phm

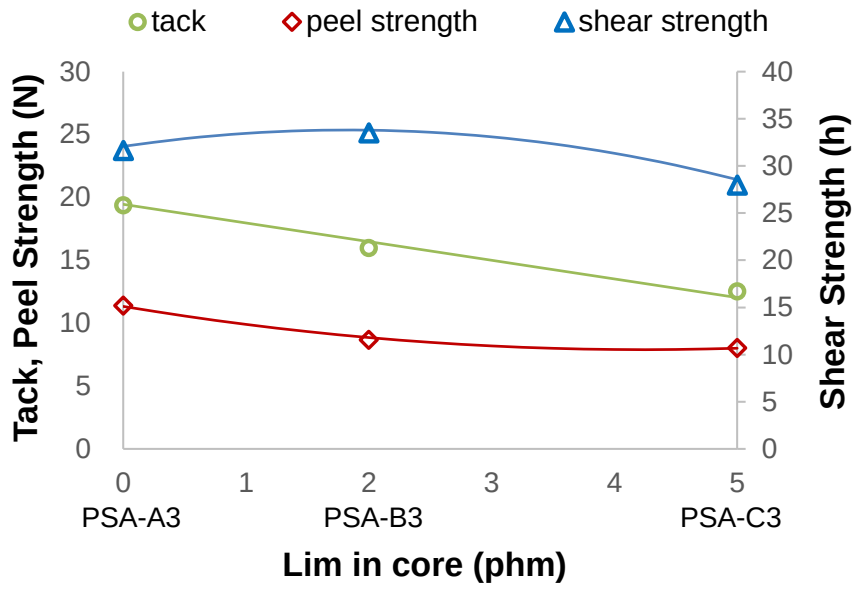

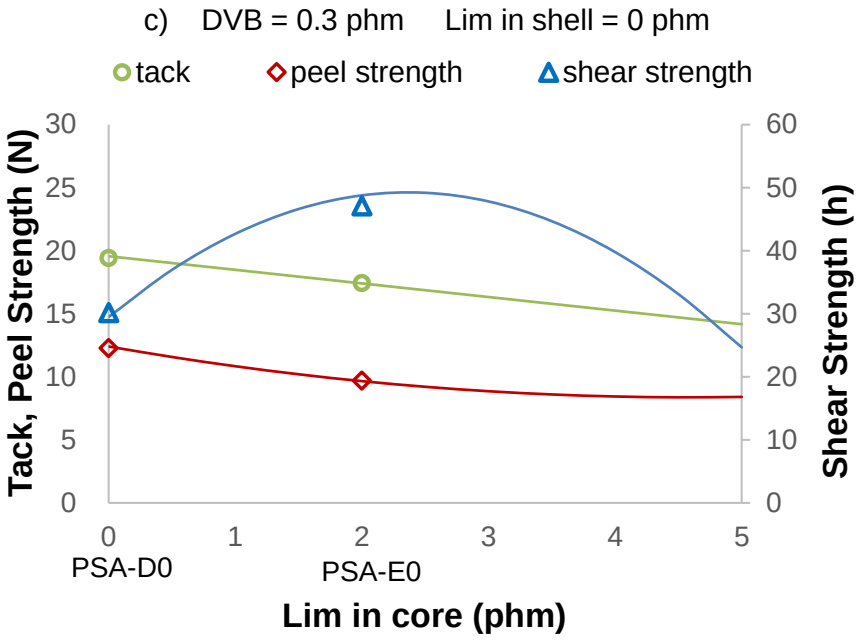

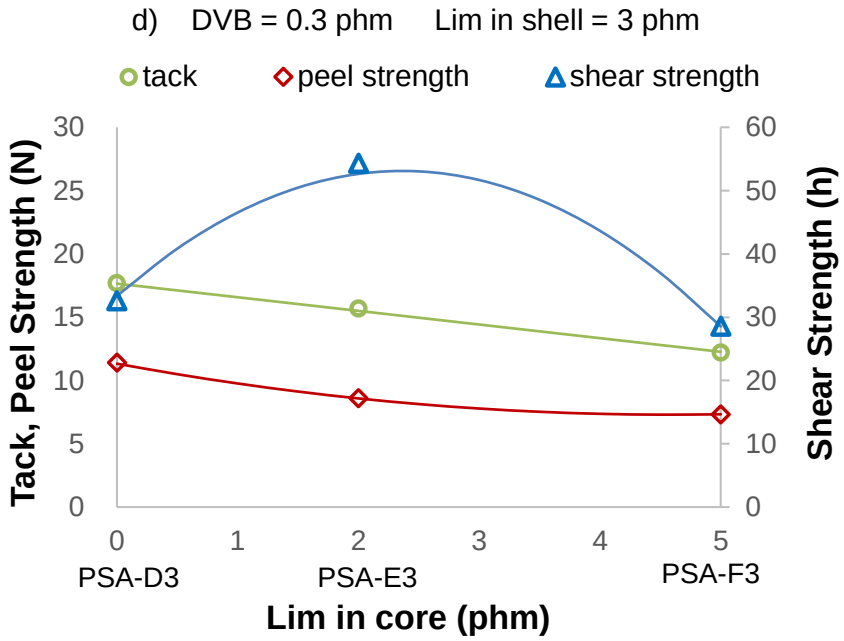

Figure 7.5 PSA test results (solid lines are empirical model predictions).

When examining the empirical models, it is important to note the signs and relative magnitudes of the model parameters. According to the tack model (Equation

7.1), the DVB concentration had a strong negative effect on tack, as would be expected[12,16]. This is not strongly evident from Figure 7.5 and one should recall that the DVB concentration was changed only by 0.1 phm. Addition of Lim to both the core and the shell caused a small reduction in tack, which is related to the increase in T_g by addition of the stiffer Lim molecules to the polymer matrix. Peel strength exhibited similar trends to tack performance (Figure 7.5). However, there was comparatively less influence of the DVB concentration on peel strength (compare Equation 7.1 and 7.2).

As shown earlier in Figure 7.2, increasing DVB concentration in the core resulted in higher gel content latexes. Thus, as would be expected, the higher gel content PSA films exhibited higher shear strength. From the empirical model (Equation 7.3), the interaction effect between Lim in the core and DVB dominate the shear strength predictions. Interestingly, shear strength measurements went through a maximum (Figure 7.5). At Lim concentrations of 2 phm in the core, PSA films (i.e., PSA-B0, -B3 and PSA-E0, -E3) exhibited higher shear strength compare to those with no Lim added (i.e., PSA-A0, -A3 and PSA-D0, -D3). This reflects the increase in T_g by addition of Lim to the polymer matrix and compensates for the lowered gel content. However, when the Lim concentration was further increased to 5 phm, the shear strength dramatically decreased (PSA-C0, -C3 and PSA-F3). This is because at higher Lim concentrations in the cores, a greater number of short chain sol polymers were produced. Physical entanglements of the polymer chains were therefore reduced. In

addition, this led to the formation of highly branched polymer chains and polymer networks with looser crosslinks and more defects. These incomplete crosslinking networks could not provide enough inherent strength to the PSA, and resulted in reduced shear strength.

7.4 Conclusion

In this study, Lim was used as a renewable chain transfer agent along with DVB crosslinker to modify the microstructure and PSA performance of core-shell PSA latex films. The PSA latex particles were designed to produce hard cores and soft shells, though there was some evidence that distinct cores and shells were unlikely. Rather, a gradient of hard material at the particle cores and softer material in the shells was the more likely morphology. Nonetheless, by simultaneously manipulating the CTA and cross-linker concentrations, a range of microstructures was achieved, yielding different PSA properties.

The use of an empirical modeling approach provided a means, with fewer experiments, to elucidate the effects of Lim and DVB on PSA properties. These models illustrate the complex interplay between the various factors: Lim concentration in the cores, Lim concentration in the shells and DVB concentration in the cores. Competing effects of T_g, gel content, sol molecular weight and looseness and/or amount of defects in the gel network are all testament to this complexity.

It can be argued that Lim is not as effective a CTA compared to thiols.

However, the renewability and essentially non-toxic nature of Lim make it a good candidate to replace more toxic, fossil-based compounds. Considering its rigid structure, Lim can be used in coating and adhesive formulations at moderate concentrations to adjust molecular weight and improve the stiffness and the inherent strength of the product.

7.5 Acknowledgements

The authors acknowledge the support of the China Scholarship Commission for the support of Ms. Shanshan Ren. Furthermore, financial support for this project by Intellectual Ventures and the Natural Sciences and Engineering Research Council (NSERC) of Canada is greatly appreciated. We also thank Dr. Esther Trevino (CIQA, Mexico) for the discussion and advices with the polymerization procedure.

7.6 References

1. Paul B. Foreman Acrylic Adhesives. In *Technology of Pressure-Sensitive Adhesives and Products*; Handbook of Pressure-Sensitive Adhesives and Products; CRC Press, 2008; p. p. 5_2.

2. Ebnesajjad, S.; Landrock, A. H. Chapter 5 - Characteristics of Adhesive Materials. In *Adhesives Technology Handbook (Third Edition)*; William Andrew Publishing: Boston, 2015; pp. p. 84–159.

3. Jovanović, R.; Dubé, M. A. Emulsion‐Based Pressure‐Sensitive Adhesives: A

Review. *J. Macromol. Sci. Part C* **2004**, *44*, 1–51.

4. Ulrich, E. W. Pressure-sensitive adhesive sheet material 1960.

5. Aubrey, D. W.; Ginosatis, S. Peel Adhesion Behaviour of Carboxylic Elastomers. *J. Adhes.* **1981**, *12*, 189–198.

6. Benedek, I.; Feldstein, M. M. *Technology of pressure-sensitive adhesives and products*; Handbook of pressure-sensitive adhesives and products; CRC Press: Boca Raton, FL, 2008.

7. Liu, X.; Fan, X.-D.; Tang, M.-F.; Nie, Y. Synthesis and Characterization of Core-Shell Acrylate Based Latex and Study of Its Reactive Blends. *Int. J. Mol. Sci.* **2008**, *9*, 342–354.

8. Borthakur, L. J.; Jana, T.; Dolui, S. K. Preparation of core–shell latex particles by emulsion co-polymerization of styrene and butyl acrylate, and evaluation of their pigment properties in emulsion paints. *J. Coat. Technol. Res.* **2010**, *7*, 765–772.

9. Ma, J.; Liu, Y.; Bao, Y.; Liu, J.; Zhang, J. Research advances in polymer emulsion based on "core–shell" structure particle design. *Adv. Colloid Interface Sci.* **2013**, *197-198*, 118–131.

10. Tan, C.; Tirri, T.; Wilen, C.-E. The effect of core–shell particle morphology on adhesive properties of poly(styrene-co-butyl acrylate). *Int. J. Adhes. Adhes.* **2016**, *66*, 104–113.

11. Plessis, C.; Arzamendi, G.; Leiza, J. R.; Alberdi, J. M.; Schoonbrood, H. A. S.; Charmot, D.; Asua, J. M. Seeded semibatch emulsion polymerization of butyl acrylate:

Effect of the chain-transfer agent on the kinetics and structural properties. *J. Polym. Sci. Part Polym. Chem.* **2001**, *39*, 1106–1119.

12. Zosel, A. The effect of fibrilation on the tack of pressure sensitive adhesives. *Int. J. Adhes. Adhes.* **1998**, *18*, 265–271.

13. Bouvier-Fontes, L.; Pirri, R.; Asua, J. M.; Leiza, J. R. Seeded Semicontinuous Emulsion Copolymerization of Butyl Acrylate with Cross-Linkers. *Macromolecules* **2005**, *38*, 1164–1171.

14. Chauvet, J.; Asua, J. M.; Leiza, J. R. Independent control of sol molar mass and gel content in acrylate polymer/latexes. *Polymer* **2005**, *46*, 9555–9561.

15. Kajtna, J.; Golob, J.; Krajnc, M. The effect of polymer molecular weight and crosslinking reactions on the adhesion properties of microsphere water-based acrylic pressure-sensitive adhesives. *Int. J. Adhes. Adhes.* **2009**, *29*, 186–194.

16. Qie, L.; Dubé, M. A. Manipulation of chain transfer agent and cross-linker concentration to modify latex micro-structure for pressure-sensitive adhesives. *Eur. Polym. J.* **2010**, *46*, 1225–1236.

17. Qie, L.; Dubé, M. A. Manipulating Latex Polymer Microstructure Using Chain Transfer Agent and Cross-Linker to Modify PSA Performance and Viscoelasticity. *Macromol. React. Eng.* **2011**, *5*, 117–128.

18. Dietrich, B. K.; Pryor, W. A.; Wu, S. J. Chain transfer constants of mercaptans in the emulsion polymerization of styrene. *J. Appl. Polym. Sci.* **1988**, *36*, 1129–1141.

19. Barudio, I.; Guillot, J.; Fevotte, G. Efficiency of mercaptan chain transfer agents

in emulsion copolymerizations. I. Influence on kinetics and microstructure. Modeling of radical desorption. *J. Polym. Sci. Part Polym. Chem.* **1998**, *36*, 157–168.

20. Gugliotta, L. M.; Salazar, A.; Vega, J. R.; Meira, G. R. Emulsion polymerization of styrene. Use of n-nonyl mercaptan for molecular weight control. *Polymer* **2001**, *42*, 2719–2726.

21. Ren, S.; Trevino, E.; Dubé, M. A. Copolymerization of Limonene with n-Butyl Acrylate. *Macromol. React. Eng.* **2015**, *9*, 339–349.

22. Ren, S.; Zhang, L.; Dubé, M. A. Free-radical terpolymerization of n-butyl acrylate/butyl methacrylate/d-limonene. *J. Appl. Polym. Sci.* **2015**, *132*, n/a–n/a.

23. Ren, S.; Vivaldo-Lima, E.; Dubé, M. A. Modeling of the Copolymerization Kinetics of n-Butyl Acrylate and d-Limonene Using PREDICI ®. *Processes* **2015**, *4*, 1.

24. Mathers, R. T.; McMahon, K. C.; Damodaran, K.; Retarides, C. J.; Kelley, D. J. Ring-Opening Metathesis Polymerizations in d-Limonene: A Renewable Polymerization Solvent and Chain Transfer Agent for the Synthesis of Alkene Macromonomers. *Macromolecules* **2006**, *39*, 8982–8986.

25. Mathers, R. T.; Damodaran, K. Renewable chain transfer agents for metallocene polymerizations: The effects of chiral monoterpenes on the polyolefin molecular weight and isotacticity. *J. Polym. Sci. Part Polym. Chem.* **2007**, *45*, 3150–3165.

26. Tobing, S. D.; Klein, A. Molecular parameters and their relation to the adhesive performance of acrylic pressure-sensitive adhesives. *J. Appl. Polym. Sci.* **2001**, *79*,

2230–2244.

27. Podzimek, S. Light Scattering. In *Light Scattering, Size Exclusion Chromatography and Asymmetric Flow Field Flow Fractionation*; John Wiley & Sons, Inc., 2011; p. p. 71.

28. American Polymer Standards Corporation Home http://www.ampolymer.com/dn-dcValues.html.

29. Plessis, C.; Arzamendi, G.; Leiza, J. R.; Schoonbrood, H. A. S.; Charmot, D.; Asua, J. M. Seeded Semibatch Emulsion Polymerization of n-Butyl Acrylate. Kinetics and Structural Properties. *Macromolecules* **2000**, *33*, 5041–5047.

30. Plessis, C.; Arzamendi, G.; Leiza, J. R.; Schoonbrood, H. A. S.; Charmot, D.; Asua, J. M. Modeling of Seeded Semibatch Emulsion Polymerization of n-BA. *Ind. Eng. Chem. Res.* **2001**, *40*, 3883–3894.

31. Elizalde, O.; Arzamendi, G.; Leiza, J. R.; Asua, J. M. Seeded Semibatch Emulsion Copolymerization of n-Butyl Acrylate and Methyl Methacrylate. *Ind. Eng. Chem. Res.* **2004**, *43*, 7401–7409.

32. Asua, J. M. Emulsion polymerization: From fundamental mechanisms to process developments. *J. Polym. Sci. Part Polym. Chem.* **2004**, *42*, 1025–1041.

33. González, I.; Leiza, J. R.; Asua, J. M. Exploring the Limits of Branching and Gel Content in the Emulsion Polymerization of n-BA. *Macromolecules* **2006**, *39*, 5015–5020.

34. Zhang, Y.; Dubé, M. A. Copolymerization of n-Butyl Methacrylate and

D-Limonene. *Macromol. React. Eng.* **2014**, *8*, 805–812.

35. Singh, A.; Kamal, M. Synthesis and characterization of polylimonene: Polymer of an optically active terpene. *J. Appl. Polym. Sci.* **2012**, *125*, 1456–1459.

36. Roberge, S.; Dubé, M. A. Emulsion-based pressure sensitive adhesives from conjugated linoleic acid/styrene/butyl acrylate terpolymers. *Int. J. Adhes. Adhes.* **2016**, *70*, 17–25.

Chapter 8. General Discussion and Conclusion

Nowadays, nearly all synthetic materials are derived from fossil-based resources. To reduce our dependence on fossil fuels and decrease carbon emissions, we need to develop alternatives based on renewable resources as a means towards a more sustainable future. This work evaluated the use of *d*-limonene (Lim), an important renewable terpene monomer, in polymer formulations, especially in latex-based PSA formulations. Bulk copolymerization of BA with Lim was firstly performed to estimate reactivity ratios and evaluate Lim's influence on polymer properties; high conversion experiments were also performed to study the molecular weight development of the polymers and to validate the prediction of polymer composition. As far as we know, there is no report on the free-radical polymerization of Lim up to high conversions. An existing kinetic model was further developed to include a degradative chain transfer mechanism for Lim and an intramolecular chain transfer mechanism for BA. The model parameters were refined and the model was validated using high conversion experimental data. Lim's behaviour was also studied in a multi-component polymerization formulation. The terpolymerizations of BA/BMA/Lim were performed at seven different compositions. At the same time, due to the lack of reported reactivity ratios for the BA/BMA system, a series of free-radical copolymerizations of BA/BMA were performed to estimate these important paramters. The behaviour of BA/BMA/Lim terpolymerization confirmed

our previous findings and further validated the reactivity ratios estimated for BA/Lim and the BA/BMA systems. Finally, Lim was used as a renewable CTA in latex-based PSA formulation. To our knowledge, this is the first report of using Lim as a CTA in emulsion polymerization and in an adhesive recipe. Core-shell latexes with various microstructures were synthesized by varying the Lim concentration in core/shell and crosslinker concentrations in the core. Lim's influence on gel content, molecular weight, T_g and PSA performances was examined.

8.1 Main Contributions and Findings

8.1.1 Copolymerization of Limonene with *n*-Butyl Acrylate

Reactivity ratios for the free radical copolymerization of BA and Lim were estimated as $r_{BA} = 6.07$, $r_{Lim} = 0.0067$, which indicates that the copolymer composition was dominated by BA. From the analysis of copolymer ^{1}H-NMR spectra, two types of Lim units were detected: Lim units with only the internal double bonds, and Lim' units with both internal and external doubled bonds (Figure 8.1). Two possible routes for the inclusion of Lim in the copolymer were proposed: (1) normal propagation via addition reaction on the external double bonds and (2) as the end-unit of the polymer chain due to a degradative chain transfer mechanism caused by the active allylic hydrogens next to the double bonds. The latter mechanism competes remarkably well with regular chain propagation and leads to fairly low incorporation of Lim into the copolymers.

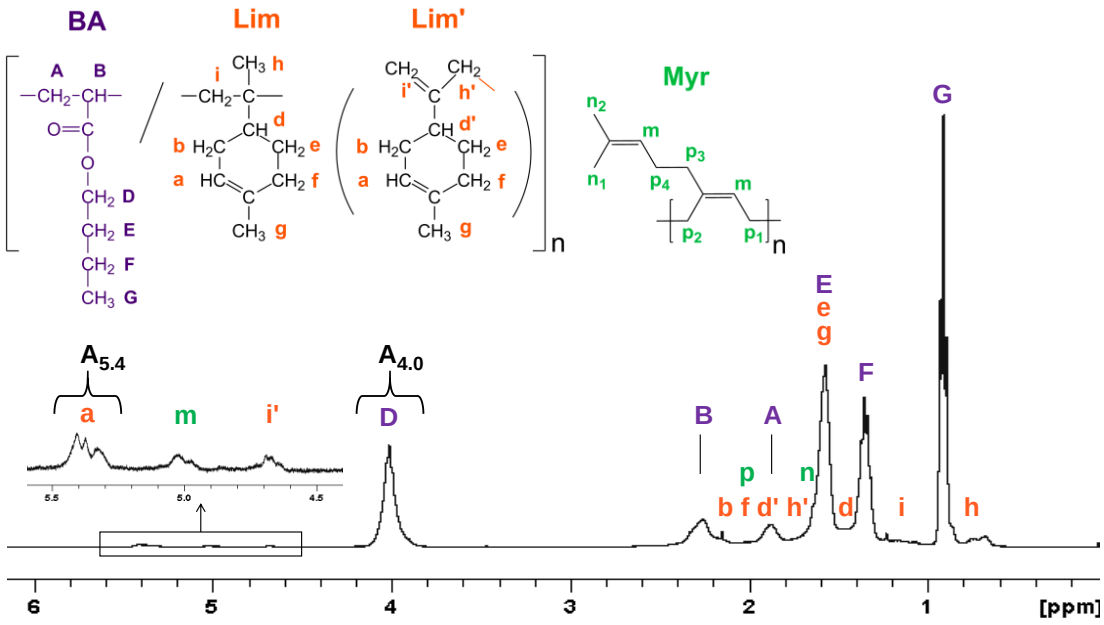

Figure 8.1 ^{1}H-NMR spectrum of BA/Lim copolymer.

High conversion BA/Lim copolymerizations were performed at nine different feed compositions. A limiting conversion was observed for each feed, which indicated that Lim is incapable of undergoing homopolymerization after BA was consumed. Composition development showed a small drift with increasing conversion. The composition model predictions using the estimated reactivity ratios in the Mayo-Lewis equation exhibited good fit to the experimental data (Figure 8.2). With increasing Lim concentration, the average-molecular weight and PDI decreased, indicating more frequent degradative chain transfer reactions. The incorporation of the rigid Lim molecules resulted in an increase in T_g. The T_g of BA/Lim copolymer was much higher than that of poly-BA (-54^{o}C); and increased with Lim concentration (Figure 8.3).

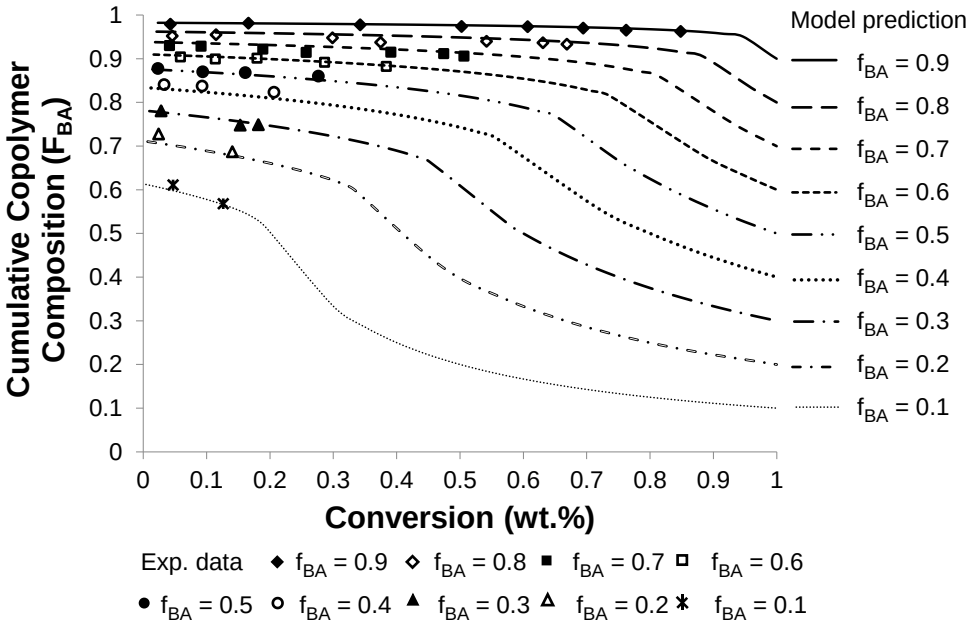

Figure 8.2 Cumulative copolymer composition vs. conversion for BA/Lim bulk copolymerization at various f_{BA}. 80°C, BPO = 1 wt%. Lines are integrated Mayo-Lewis model predictions.

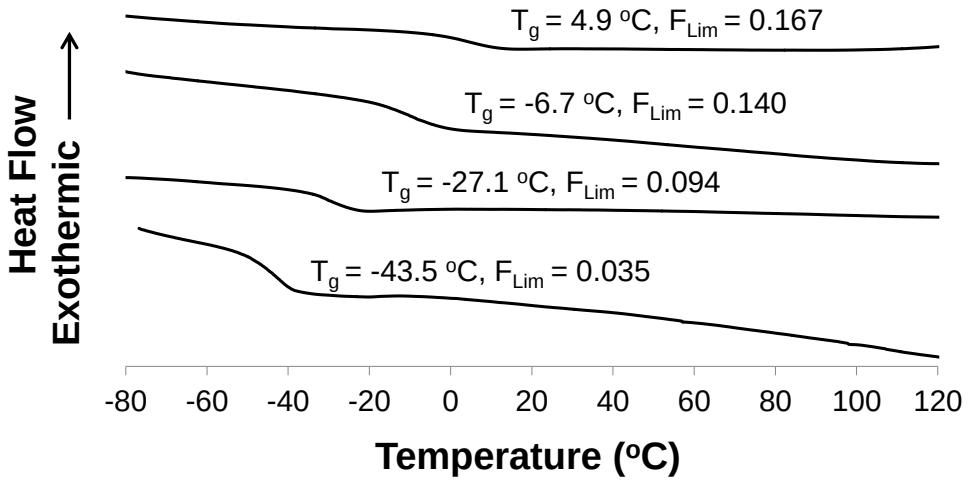

Figure 8.3 DSC curves of poly(n-BA) and BA/Lim copolymers of various composition.

8.1.2 Modeling of the Copolymerization Kinetics of *n*-Butyl acrylate and d-Limonene using PREDICI

A kinetic model was developed using PREDICI for the free-radical polymerization of BA/Lim. The simulation mechanism was based on conventional free-radical copolymerization kinetics, which includes initiation, propagation, chain transfer and termination. The chain transfer constants of Lim were estimated as Cs = 4.9×10^{-3} based on previous experimental results using the Mayo equation. By fitting the reactivity ratios and other Lim-related rate constants, good predictions on conversion, copolymer composition and molecular weight were achieved. The model supports the presence of a significant degradative chain transfer to Lim as well as the intramolecular chain transfer of BA. Also, from the propagation and chain transfer rate constants fitted for the Lim molecules, it was found that Lim acts more like a chain transfer agent than a co-monomer.

8.1.3 Bulk Free-Radical Copolymerization of *n*-Butyl Acrylate and *n*-Butyl Methacrylate: Reactivity Ratio Estimation

The reactivity ratios for free-radical polymerization of BA/BMA were estimated as r_{BMA} = 2.01 and r_{BA} = 0.46. High conversion experiments were then performed at three feed compositions (f_{BMA} = 0.2, 0.5, and 0.8) to examine the development of composition, molecular weight, and gel content with conversion. Autoacceleration occurred earlier at high BA concentrations (f_{BMA} = 0.2) due to the more frequent intra- and intermolecular chain transfer of BA. The good fit between

the composition data and model predictions derived from the Mayo-Lewis equation further validated the reactivity ratio estimates (Figure 8.4). The presence of BMA interfered with the intra- and intermolecular chain transfer of BA as there was no gel formed at moderate and high BMA concentrations. Also, a significant increase in molecular weight was observed at high BA concentrations (f_{BMA} = 0.2), while a relatively flat molecular weight profile was observed for high BMA concentrations (f_{BMA} = 0.8) (Figure 8.5). This is consistent with the autoacceleration effect.

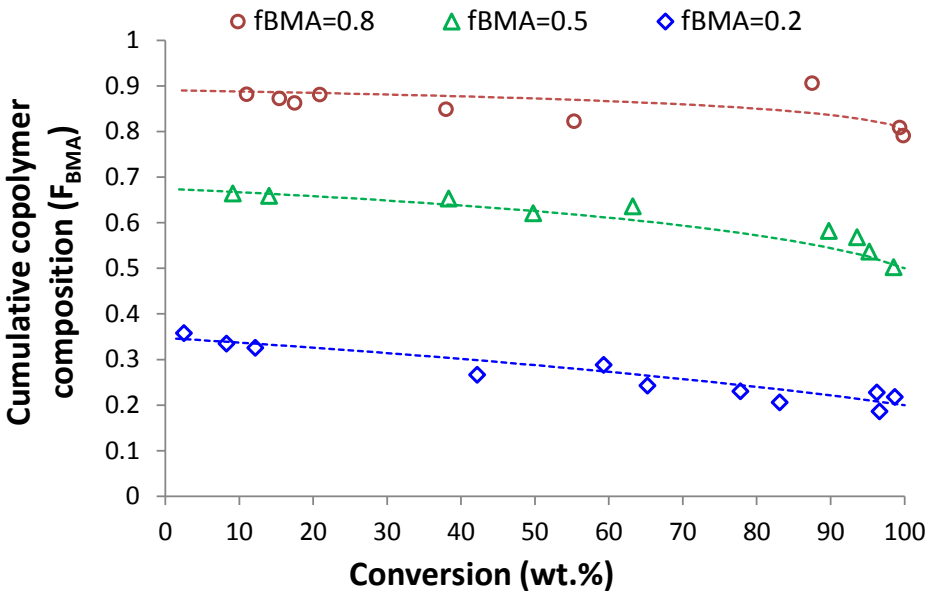

Figure 8.4 Cumulative copolymer composition vs. conversion for BA/BMA bulk copolymerization at various f_{BMA}. Dashed lines are integrated Mayo-Lewis model predictions.

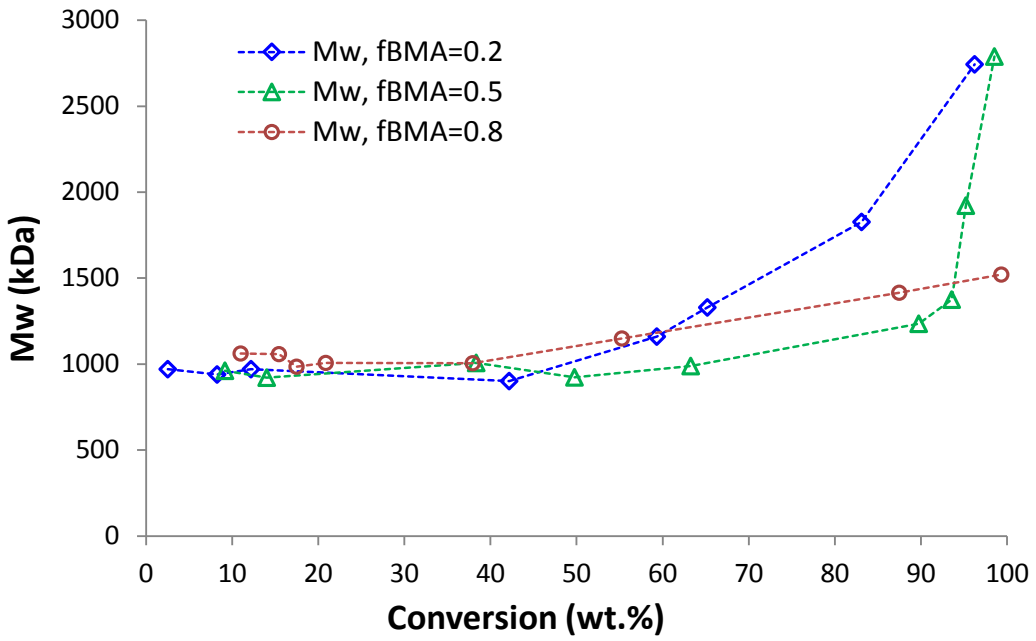

Figure 8.5 Molecular weight vs. conversion results at various BA/BMA monomer feed ratios. (Dashed lines are not model predictions but are provided to make the plot more readable).

8.1.4 Free-radical Terpolymerization of *n*-Butyl Acrylate/ Butyl Methacrylate/*d*-Limonene

Lim's behaviour in a multi-component polymerization system was shown to be similar to that of the copolymerization of BA/Lim. With an increase in Lim concentration from 10 to 40 mol%, the polymerization rate and final conversion were reduced due to the more frequent degradative chain transfer reactions caused by Lim. The terpolymer composition development was successfully predicted by using three pairs of reactivity ratios (i.e., BA/Lim, BMA/Lim and BA/BMA systems) in the Mayo-Lewis equation. Similar to the BA/Lim copolymerization, both the average-molecular weight and PDI decreased with increasing Lim concentration. The

BA/BMA ratio had no significant impact on number-average molecular weight, but its strong influence on PDI was due to the different termination modes of the BA vs. BMA monomers. Terpolymer T_g was increased with increased BMA and Lim fraction in the terpolymer.

8.1.5 Adhesive Performance Modification in Core-Shell Latex Films Using *d*-Limonene as a Chain Transfer Agent

Lim was used as a renewable CTA in core-shell latex based PSA formulations. PSA latexes with various microstructures were prepared with varying Lim concentration in the core (0/2/5 phm) and in the shell (0/3 phm), and DVB crosslinker concentration in the core (0.2/0.3 phm). The increase in DVB concentration resulted in an increase in gel content and slight increase in T_g; while the increase of Lim concentration resulted in a decrease in gel content and an increase in T_g. The core Lim concentration increase from 0 to 2 to 5 phm initially resulted in a sol molecular weight decrease due to the degradative chain transfer of Lim but then increased due to the formation of branched polymers. Higher DVB concentrations caused a higher gel content and a slightly higher T_g. As a result, the tack and peel strength of PSAs were reduced with increasing Lim and DVB concentrations while shear strength showed a maximum at a moderate core Lim concentration (2 phm) and a higher DVB concentration (0.3 phm). Empirical models developed using a stepwise regression confirmed the effects of Lim and DVB on PSA performance.

8.1.6 Publications

This thesis contains six manuscripts published or submitted for publication:

1. Ren S, Trevino E, Dubé MA. Copolymerization of Limonene with *n*-Butyl Acrylate. Macromol React Eng. 2015 Aug 1;9(4):339–49.

2. Ren S, Vivaldo-Lima E, Dubé MA. Modeling of the Copolymerization Kinetics of *n*-Butyl Acrylate and d-Limonene Using PREDICI ®. Processes. 2015 Dec 24;4(1):1.

3. Ren S, Dubé MA. Bulk Free-Radical Copolymerization of *n*-Butyl Acrylate and *n*-Butyl Methacrylate: Reactivity Ratio Estimation. Macromol React Eng. **Submitted September 2016.**

4. Ren S, Zhang L, Dubé MA. Free-radical terpolymerization of *n*-butyl acrylate /butyl methacrylate/d-limonene. J Appl Polym Sci. 2015 Dec 15;132(47)

5. Ren S, Dubé MA. Adhesive Performance Modification in Core-Shell Latex Films Using d-Limonene as a Chain Transfer Agent. Int. J. Adhes. Adhes., **Submitted October 2016.**

6. Ren S, Dubé MA. Nitroxide-Mediated Polymerization of *n*-Butyl Acrylate and

D-Limonene. Macromol Symp. 2016 Feb 1;360(1):152–9.

8.2 Recommendations for future work

This thesis provides one of the first comprehensive studies on limonene polymerization. The work on this system does not end here. We therefore recommend the following research pathways for future consideration:

a) The biodegradability of Lim-containing polymers has not been investigated. This study has shown that the incorporation of Lim into polymer resulted in two types of Lim units, one with the internal double bond remaining intact and the other with both double bonds intact. These remaining double bonds may provide a possible site for degradation under aerobic conditions.

b) As discussed in the background section of the thesis, adhesion of PSA films is often improved by the addition of a tackifier. The adhesion of Lim-containing PSAs can therefore be further improved by adding a suitable, and perhaps renewable, tackifier. In fact, we noted the use of terpene resins, which are oligomers of pinene or Lim, as possible tackifiers.

c) The addition of Lim showed an obvious effect on polymer T_g; it served to increase the T_g. The target T_g range for coatings is higher than that for PSAs, and thus the use of Lim as a renewable chain transfer agent in coating formulations could be devised. This could possibly have an improvement on the hardness and scratch resistance of these coatings.

d) The allylic structure of Lim makes its free radical polymerization difficult, if not impossible. A modification of Lim molecules could possibly help reduce or eliminate the effects of the allylic hydrogens. One can ask why methyl methacrylate, which also possesses allylic hydrogens, polymerizes so readily while the vast majority of other allylic monomers do not. Perhaps the addition of polar functional groups, such as carboxylic groups, amino groups or hydroxyl groups on the double bonds could affect this deleterious mechanism. Solving this issue would open up enormous possibilities for new polymer products.

8.3 Conclusion

The objective of this thesis was to evaluate the use of Lim as a renewable component in free-radical polymerization. While our preferred, initial intent was it use as a monomer, it can be argued that it may be used more effectively as a chain transfer agent. However, its use in relatively low amounts as a monomer is still possible. Its distinct impact on polymer properties is evident and its use as a monomer can be explored further. Aside from the potential chemical modification of Lim, as noted above, there are still many engineering process design approaches that could be investigated to improve Lim incorporation into a polymer matrix.

The estimated reactivity ratios and model development for the BA/Lim copolymerization demonstrate the effect of Lim on polymerization kinetics, polymer microstructure and polymer performance properties. Our use of Lim in a latex-based

PSA formulation reveals the need for further optimization may be necessary but the thesis objective has been achieved.

Lim has been used in fragrances, food additives and medications. It is renewable, non-toxic and has a pleasant odour. It can be obtained in almost pure form (purity >95%) as a by-product of the juicing industry. Such a product presents great potential for use in a more sustainable polymer industry. Unfortunately, the degradative chain transfer mechanism, poses limitations on the amount of Lim that can be incorporated into a polymer. Many renewable monomers possess a similar allylic structure and we should strive to overcome this mechanism either via chemical modification of these monomers or find other mechanistic pathways for their polymerization.

Appendix A. Nitroxide-Mediated Polymerization of n-Butyl Acrylate and d-Limonene

Published in Macromol. Symp., 360: 152–159.

Nitroxide-Mediated Polymerization of n-Butyl Acrylate and *d*-Limonene

Shanshan Ren, Marc A. Dubé*

Department of Chemical and Biological Engineering, Centre for Catalysis Research and Innovation, University of Ottawa

Abstract

n-Butyl acrylate and *d*-limonene (Lim) were copolymerized in bulk via nitroxide-mediated polymerization (NMP) at 115°C using SG1-BlocBuilder. Compared to the free-radical initiation system, the NMP approach resulted in a moderate enhancement to final conversion and slightly higher incorporation of Lim into the copolymer microstructure. The copolymer composition using the NMP approach did not differ significantly from that of the free-radical method. A mechanism for the NMP of BA/Lim is proposed which includes a degradative chain transfer reaction due to the allylic hydrogen of Lim.

Keywords: renewable resources, *d*-limonene, chain transfer, controlled/living radical polymerization, SG1

A1. Introduction

Controlled/living radical polymerization (CLRP) has become a well-accepted technique to synthesize polymers because of its control over molecular weight, polydispersity and copolymer sequencing. This technique is based on a reversible-deactivation equilibrium of the propagating chain and the persistent radical. Among various CLRP techniques, nitroxide-mediated polymerization (NMP) is preferable because of its simplicity. In most NMP systems, a nitroxide-based agent (sometimes extra nitroxide is added) can simply initiate the living reaction. Considerable effort has been devoted to the improved controlled polymerization of a variety of monomers using NMP, in terms of molecular weight and architectural control, and block copolymer design[1]. For instance, TEMPO (2,2,6,6-tetramethylpiperidine 1-oxyl) and radical initiator were used for the synthesis of polystyrene with a narrow molecular weight distribution[2]. The use of TIPNO (2,2,5-trimethyl-4-phenyl-3-azahexane-3-oxy) was reported to be capable of controlling the polymerization of butadiene or isoprene related monomers[3].

Recently, SG1 nitroxide (N-tertbutyl-N-[1-diethylphosphono-(2,2-dimethylpropyl)] nitroxide) was developed and exhibited a much faster polymerization rate compared to TEMPO-based initiator at a relatively low temperature ($90^{o}C$)[4,5]. SG1 can also be used in aqueous media or in emulsion polymerization, which allows block copolymer to be synthesized in latex particles[6,7]. An SG1-mediated system has been used to control the polymerization of styrene[8,9] and acrylate monomers, such as n-butyl acrylate (BA) [8,9], acrylic

acid[10], and the copolymerization of styrene/methyl methacrylate[11,12]. Acrylate monomers are commonly used for coating and adhesive applications. However, it was reported the termination side reactions during the SG1-mediated polymerization of acrylic monomers occur frequently, and the addition of excess SG1 could reduce the frequency of termination side reactions by encouraging the recombination of polymer radicals with the stable radical and thus, controlled polymerization of acrylate monomers can be achieved[4,13].

d-Limonene (Lim) is a renewable di-substituted monoterpene typically extracted from citrus fruit peels with a worldwide production of over 70 million kg/year[14]. Lim is an ideal "green" monomer because it is renewable, possesses additional functionality and is non-toxic. In a previous study, the copolymerization of BA/Lim was performed via free-radical methods, and the reactivity ratios of the co-monomers were estimated as r_{BA} = 6.07, r_{Lim} = 0.0067[15]. In that work, however, significant degradative chain transfer due to the presence of allylic hydrogen in the Lim was observed. This mechanism was shown to compete remarkably well with chain propagation. The increased Lim in the reaction formulation resulted in significant decreases in polymerization rate, final conversion and molecular weight. Thus, the incorporation of Lim in the final product was less than desired.

The present study examines the copolymerization of BA/Lim via NMP methods using a SG1-based alkoxyamine initiator BlocBuilder MA (3,7-dioxa-4-aza-6-phosphanonanoic acid, 4,5-bis(1,1-dimethylethyl)-6-ethoxy-2,2-

dimethyl-,6-oxide. A goal of the study was to evaluate whether the activation-deactivation between the dormant and active species (the NMP mechanism) competes with the degradative chain transfer caused by Lim.

A2. Experimental

A2.1 Materials

Lim was obtained from Fisher Scientific (96% purity) and was distilled under vacuum before use. BA (≥99% purity) and benzoyl peroxide (BPO) were purchased from Sigma Aldrich. BA was purified of monomethyl ether hydroquinone inhibitor using an inhibitor removal column (Sigma Aldrich). BPO was recrystallized twice with acetone and deionized water, dried under vacuum at room temperature, and then stored in a refrigerator at 4^{o}C before use. BlocBuilder MA was donated by Arkema. SG1 was kindly donated by Prof. B. Lessard (synthesized according to the literature procedure[16]). All other solvents used for sample workup and characterization were used as received.

A2.2 Polymerization

The nitroxide-mediated polymerization of BA/Lim was carried out in glass ampoules (10 mm diameter and 200 mm in length). For each reaction condition chosen, a total of seven to nine ampoules was prepared. In a typical experiment, a mixture of BA (4.472 g, 0.035 mol), Lim (0.528 g, 3.9 mmol), BlocBuilder MA (0.05

g, 0.13 mmol), and SG1 (3.58 mg, 0.013 mmol) were pipet into each glass ampoule. Each ampoule was degassed using a pump-freeze-thaw procedure (typically, three cycles), flame-sealed. The ampoules were then immersed in a constant temperature oil bath at 115 ℃ for pre-determined time intervals, after which they were immediately placed into an ice bath to quench the reaction. The polymeric products were precipitated in a 10-fold excess of methanol and refrigerated (4 ℃) for 4 h. Then, the excess liquid was decanted and the polymer samples were dried in a vacuum oven until a constant weight was achieved. The presence of any oligomeric materials in the decanted liquid was verified and accounted for in the calculation of conversion and composition.

A2.3 Characterization

The overall monomer conversion was determined gravimetrically based on the mass of dried polymer. A ^{1}H-NMR spectrometer (Bruker, 400MHz, $CDCl_3$) was used to measure the copolymer composition at room temperature. A GPC system (Agilent) was used to determine the molecular weight and polydispersity of the copolymers. The GPC system equipped with two columns in series (MZ-Gel SD plus 10^5 Angstroms 300 x 8.00 mm, particle size 5 μm, MZ-Gel SD plus 10^4 Angstroms 300 x 8.00 mm, particle size 5 μm). Tetrahydrofuran (THF) was used as the eluant with a flow rate of 1 mL min^{-1}. The detection system consisted of a multi-angle laser light scattering detector (Wyatt Dawn Heleos II, λ=633 nm), a differential refractive index detector (Wyatt Optilab T-rEX) and a differential viscometer (Wyatt ViscoStar ll).

Samples diluted in THF were filtered through a 0.45 μm syringe filter prior to injection into the GPC. The refractive index increment (dn/dc) of BA/Lim copolymer (BA mol. % = 0.90) was measured (in THF at 25^{o}C) as 0.140 mL g^{-1} with the Wyatt Optilab T-rEX refractometer (l.633 nm). This value was applied to all copolymer samples for molecular weight calculation. Data analysis was performed using Wyatt Astra software. Further details on the composition and molecular weight analyses are given elsewhere[15].

A3. Results and discussion

A3.1 Monomer conversion

A series of screening runs was used to compare the performance of a free-radical initiator, benzoyl peroxide (BPO), with the alkoxyamine initiator, BlocBuilder. These were examined at 80 and 115^{o}C, respectively. A summary of the reaction conditions for screening run is shown in Table A.1. Note that NMP requires an elevated temperature because of the slow polymerization kinetics. The proper reaction temperature for BlocBuilder is suggested to be between 90 and 120^{o}C. Final conversion levels attained at various feed compositions (f_{BA}) are shown in Figure A.1. For each feed composition (f_{BA} = 0.6 - 0.9), the NMP runs exhibited higher final monomer conversions compared to the free radical runs, with increasing differences with greater amounts of Lim in the reaction formulation. For instance, at the feed composition of f_{BA} = 0.8, a final conversion of 67 wt.% was attained with 1 wt.%

BPO after 17 h (note: BPO has a half-life of ~4.6h at 80^{o}C; after 17h, the initiator was almost completely depleted and the final conversion had reached a plateau), whereas the reaction using BlocBuilder reached a final conversion of 82 wt.% after 66.5 h. The observed improvement in final conversion relates to the reversible-deactivation feature of NMP, wherein the equilibrium between the dormant and active species ensures continued propagation of the polymer chain (see Figure A.2).

In the copolymerization of BA/Lim, the chain transfer reaction to Lim is very competitive to the chain propagation (see Figure A.3). The Lim radicals resulting from the chain transfer reaction are highly likely to react with a propagating radical and terminate the polymer chain. In the presence of SG1 radicals, both the propagating radicals and Lim radicals can be capped by SG1 before they react with each other, and thus extend the lifetime of the growing chains. From the discussion above, it is believed that the persistent radical effect of NMP plays an important role in the enhancement of the polymerization rate and final conversion in the BA/Lim system.

Table A.1 Experimental conditions for BA/Lim bulk copolymerizations.

Initiator type	Initiator concentration	T (°C)	Feed composition f_{BA} (mol%)	Reaction time (h)
BPO	1 wt.%	80	60	17.0
			70	17.0
			80	17.0
			90	17.0
BlocBuilder	1 wt.%	115	60	66.5
			70	66.5
			80	66.5
			90	66.5
BlocBuilder + extra SG1	1 wt.% BlocBuilder 10 mol.% [SG1]/[BlocBuilder]	115	90	17.0

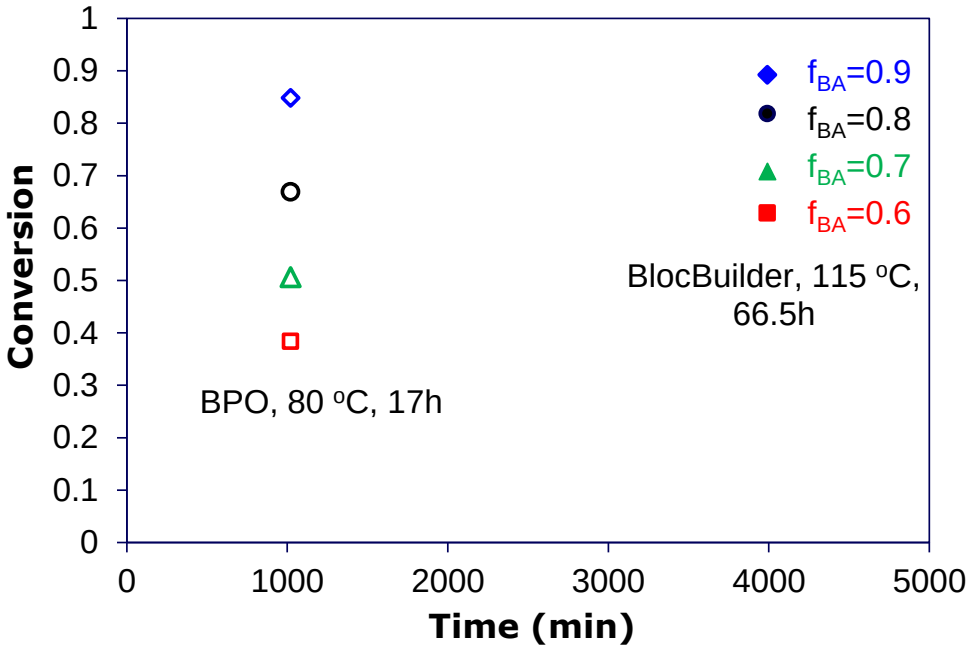

Figure A.1 Conversion vs. time of BA/Lim copolymerized at various f_{BA} via free-radical polymerization (open symbols; 1 wt.% BPO, 80°C, 17 h) and NMP (closed symbols; 1 wt.% BlocBuilder, 115°C, 66.5 h).

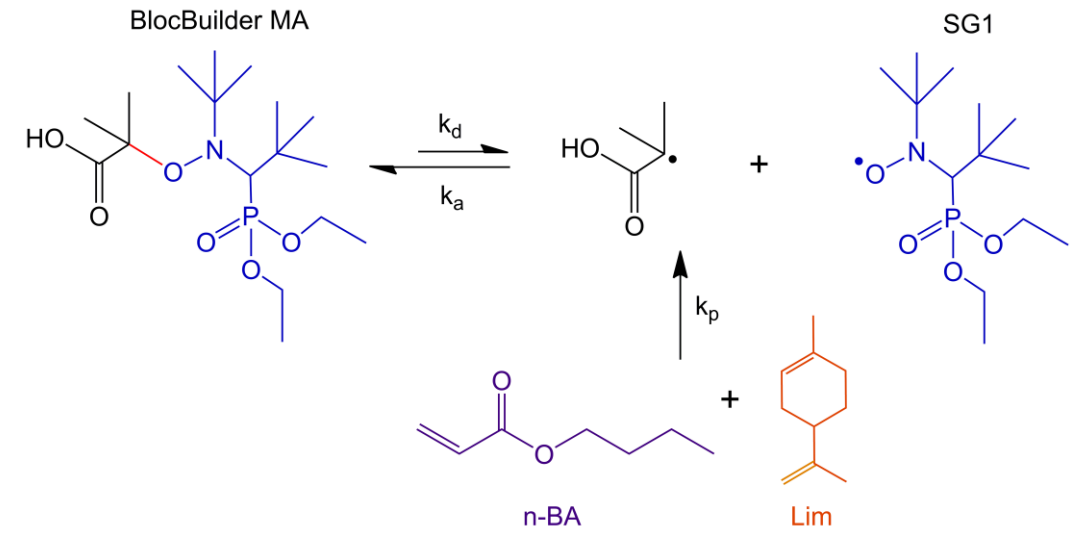

Figure A.2 BlocBuilder initiated NMP for BA/Lim copolymerization.

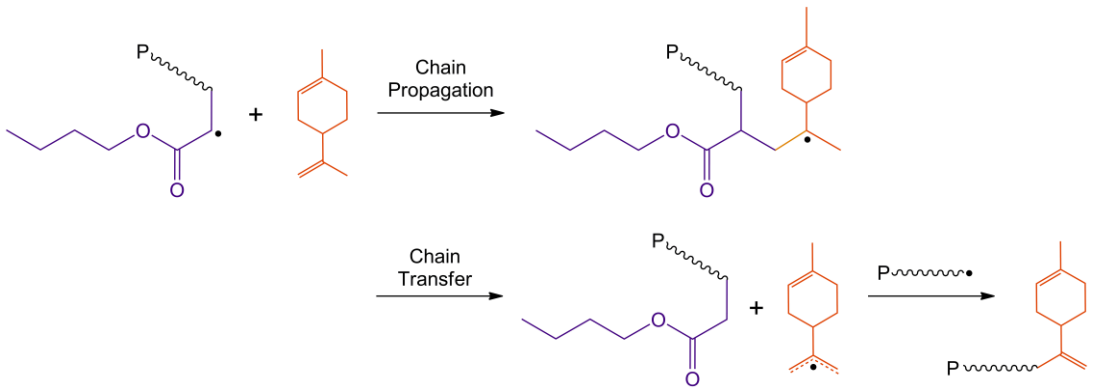

Figure A.3 Propagation and chain transfer in BA/Lim copolymerization.

Three sets of full conversion experiments were performed: two using BPO at 80 and 115°C, and another using BlocBuilder with 10 mol% extra SG1 free nitroxide relative to the BlocBuilder at 115°C (the reaction conditions for these runs are shown in Table A.1). In the presence of extra SG1, a conversion of 92 wt.% was reached, while the polymerization rate was much higher compared to the runs using 1 wt.% BPO at 80°C (see Figure A.4). A conversion of 69 wt.% was achieved after 180 min in the presence of BPO at 80°C and after only 98 min for the BlocBuilder case using

extra SG1 at 115ºC. A conversion of 64 wt.% was attained after 318 min in the presence of BlocBuilder alone. On the other hand, even though a much faster reaction rate (a conversion of 50% was achieved in 10 min) was observed when using BPO at 115ºC, a dead-end polymerization (near complete depletion of initiator) was observed. The addition of extra SG1 free nitroxide could drive the equilibrium towards the dormant species: both the propagating chains and the Lim radicals had a higher possibility of being capped by SG1 radicals instead of undergoing termination, and therefore higher polymerization rates were observed in the presence of extra SG1. Furthermore, a linear first order kinetic plot of ln(1/(1-X)) vs. time plot up to 57% conversion was observed (see Figure A.5). However, as the polymerization proceeded, the SG1 may also have been consumed by the growing number of Lim radicals; the termination between growing chains became more frequent, which lowered the polymerization rate and eventually, the "livingness" of the polymerization in the final stages of the reaction was lost.

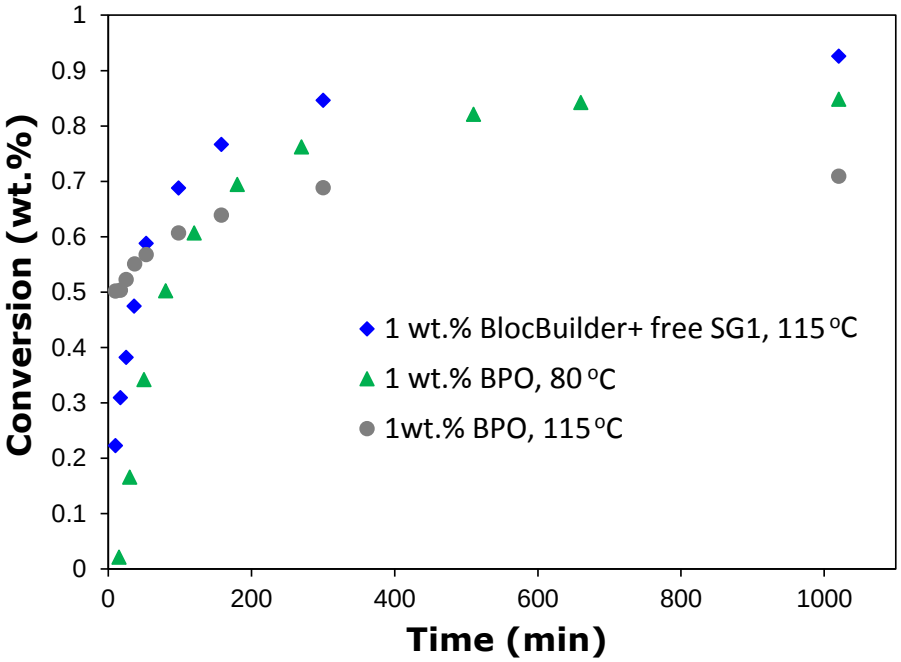

Figure A.4 Conversion vs. time plot of BA/Lim (f_{BA} = 0.9) polymerized via free-radical polymerization (1 wt.% BPO, 80°C) and NMP (1 wt.% BlocBuilder/1 wt.% BlocBuilder and 10 mol% free SG1 relative to BlocBuilder, 115°C).

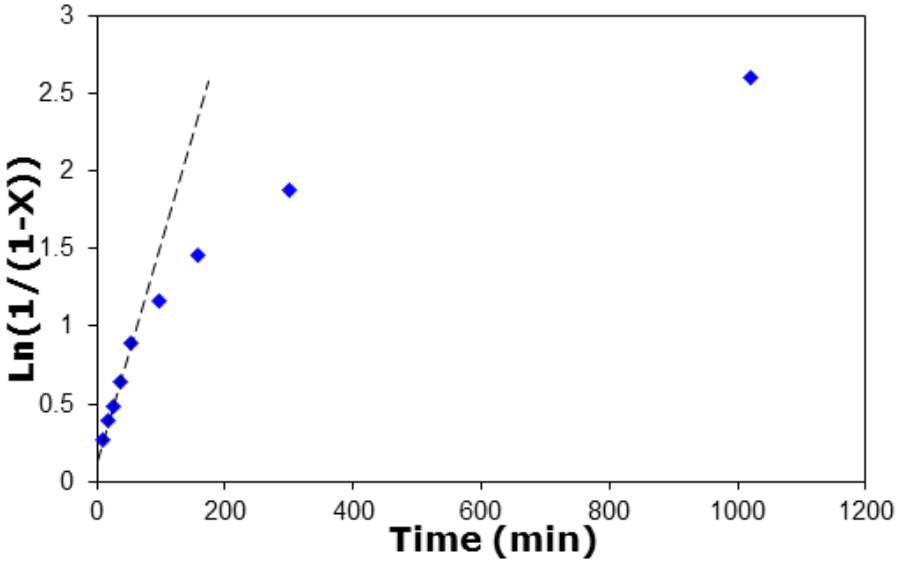

Figure A.5 First order kinetic plot of ln(1/(1-X)) vs. time for BA/Lim (f_{BA} = 0.9) polymerized at 115°C in bulk with 1 wt.% BlocBuilder and 10 mol% free SG1 relative to BlocBuilder.

A3.2 Copolymer composition

Trends observed for copolymer composition vs. overall monomer conversion for various BA/Lim feed ratios are plotted in Figure A.6. Model predictions were obtained using an integrated Mayo-Lewis equation with the co-monomer reactivity ratios of r_{BA} = 6.07 and r_{Lim} = 0.0067, estimated from low conversion bulk copolymerizations of BA/Lim at 80 ℃ using BPO as the initiator[15]. The copolymer composition data for both conventional free-radical polymerization and nitroxide-mediated polymerization are well predicted by the model developed from the free-radical system. This indicates that the comonomer reactivity was not significantly affected by the use of the BlocBuilder initiator. Nonetheless, the incorporation of Lim was slightly increased while higher conversion was reached; e.g., for the feed in which f_{BA} = 0.7, the fraction of Lim in the copolymer was about 0.09 at a conversion of 51 wt.% when using BPO, whereas it was 0.09 and 0.113 at a conversion of 43 wt.% and 71 wt.% in the presence of BlocBuilder.

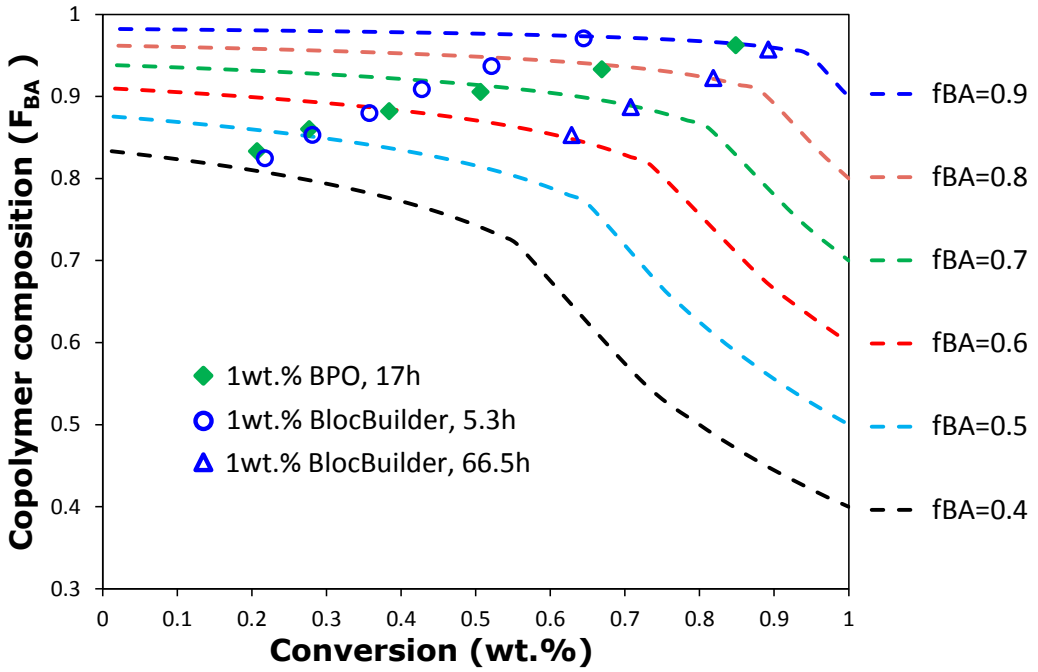

Figure A.6 Copolymer composition vs. conversion plot of BA/Lim polymerized at various f_{BA} via free-radical polymerization (1 wt.% BPO, 80°C) and NMP (1 wt.% BlocBuilder, 115°C). Dashed lines are the integrated Mayo-Lewis model predictions.

Similar effects were observed for the runs with extra SG1 free nitroxide (see Figure A.7). Comparing with the free-radical polymerization data at f_{BA} = 0.9, the trend of copolymer compositions vs. composition was not significantly affected by the use of the additional SG1 free nitroxide. The nitroxide-mediated polymerization of BA/Lim appeared to follow the same trajectory as in free-radical polymerization.

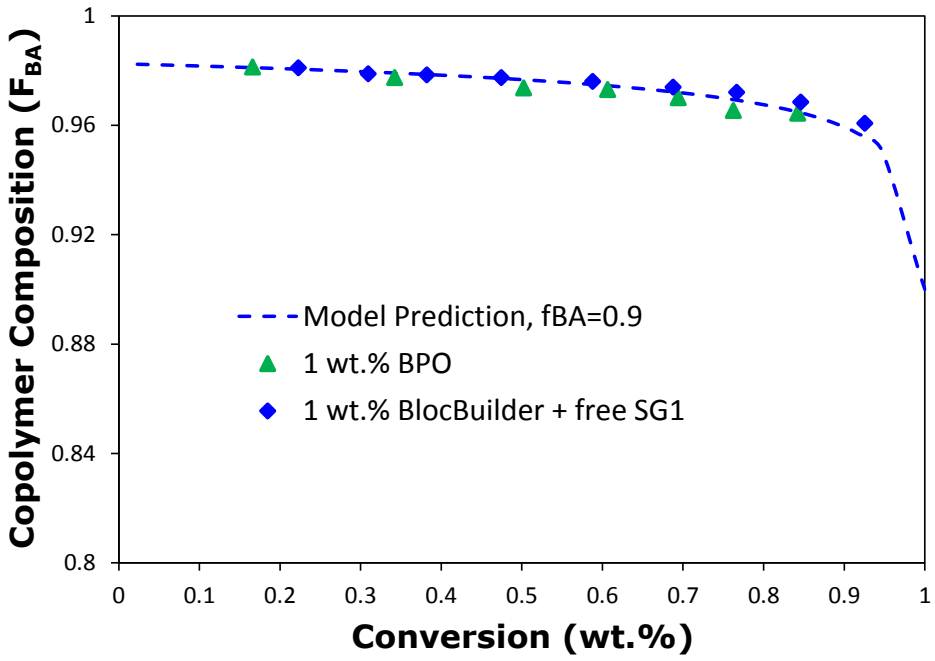

Figure A.7 Copolymer composition vs. conversion plot of BA/Lim (f_{BA} = 0.9) polymerized via free-radical polymerization (1 wt.% BPO, 80°C) and via NMP (1 wt.% BlocBuilder and 10 mol% free SG1 relative to BlocBuilder, 115°C).

A3.3 Molecular weight and polydispersity

Molecular weight results for the copolymerization of BA/Lim (f_{BA} = 0.9) are shown in Figure A.8. A much narrower molecular weight distribution (M_w/M_n = 1.2 – 2.3) was observed in the presence of BlocBuilder and extra SG1 compared to the BPO-initiated runs (M_w/M_n = 1.5 – 3.0). One should note that the low polydispersities encountered are consistent with termination being almost exclusively due to combination along with low degrees of branching. The trends in number-average molecular weight (M_n) vs. conversion deviated from the linear theoretical evolution expected for controlled living polymerization. Still, the M_w/M_n value increased

significantly in the final stages of the reaction, which is a clear departure from living control of the polymerization. As discussed earlier, while the Lim radicals resulting from the degradative chain transfer reaction kept consuming the SG1 radicals, the growing radicals were likely to terminate, which would result in a decrease in polymerization rate and an increase in polydispersity.

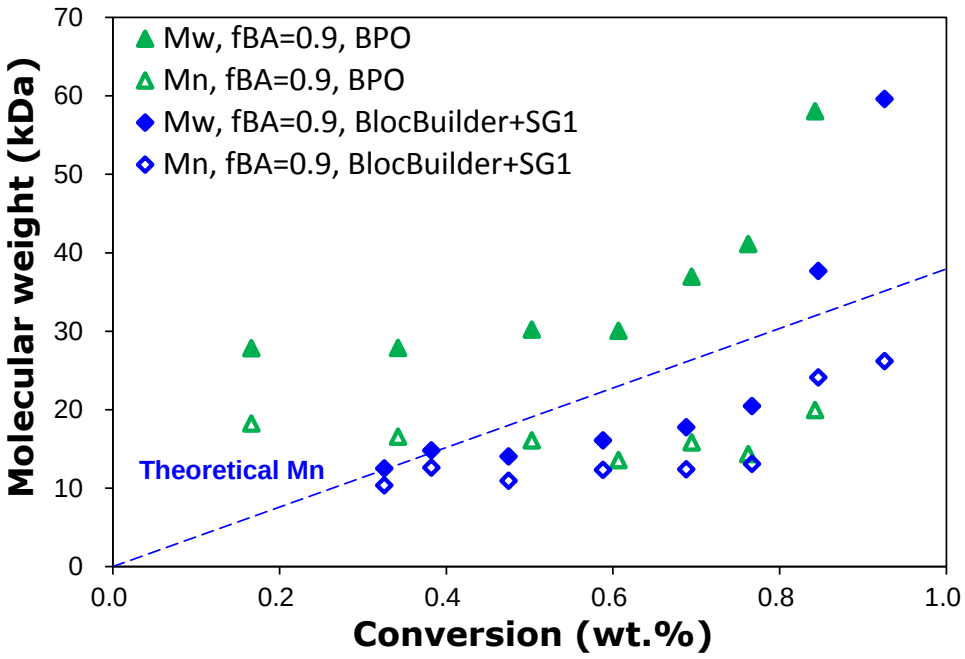

Figure A.8 Molecular weight vs. conversion plot of BA/Lim (f_{BA} = 0.9) polymerized in free-radical polymerization (1 wt.% BPO, 80°C) and in nitroxide-mediated polymerization (1 wt.% BlocBuilder and 10 mol.% free SG1 relative to BlocBuilder, 115°C).

A4. Conclusion

In this study, the NMP of BA/Lim was studied in bulk at 115°C using

BlocBuilder and extra SG1 nitroxide as the initiators. Comparing to the free-radical polymerization of BA/Lim, higher final conversions and greater incorporation of Lim were attained in the presence of BlocBuilder, whereas the trend of copolymer composition with respect to conversion still followed the integrated Mayo-Lewis model developed from the free-radical system. In the presence of additional SG1 free nitroxide, the polymerization rate was significantly increased and a monomer conversion of 92 wt.% was attained (f_{BA} = 0.9). Moreover, a much narrower PDI was observed compared to that for the free-radical system.

Our objective to increase the incorporation of Lim in the copolymer using an NMP approach yielded only modest improvements. The Lim radical resulted from degradative chain transfer was capped by SG1 nitroxide; less termination between the propagating chain and Lim radical happened, and thus reaction rate and conversion increased. A Higher conversion and faster polymerization rate could be expected by the addition of more extra SG1 nitroxide. However, there were indications that the NMP mechanism competed somewhat with that of degradative chain transfer. With the proceeding of the polymerization, the Lim radical kept consuming SG1 nitroxide, and more frequent termination occurred. This eventually resulted in a loss of livingness in the final stage.

A5. Acknowledgements

The authors acknowledge scholarship support of the China Scholarship

Commission for Ms. Shanshan Ren. We also thank Prof. Benoît Lessard for donating the SG1 mediator used in this work. Furthermore, financial support for this project by Intellectual Ventures and the Natural Sciences and Engineering Research Council (NSERC) of Canada is greatly appreciated.

A6. References

1. Grubbs, R. B. Nitroxide-Mediated Radical Polymerization: Limitations and Versatility. *Polym. Rev.* **2011**, *51*, 104–137.

2. Georges, M. K.; Veregin, R. P. N.; Kazmaier, P. M.; Hamer, G. K. Narrow molecular weight resins by a free-radical polymerization process. *Macromolecules* **1993**, *26*, 2987–2988.

3. Benoit, D.; Harth, E.; Fox, P.; Waymouth, R. M.; Hawker, C. J. Accurate Structural Control and Block Formation in the Living Polymerization of 1,3-Dienes by Nitroxide-Mediated Procedures. *Macromolecules* **2000**, *33*, 363–370.

4. Lessard, B.; Graffe, A.; Marić, M. Styrene/tert-Butyl Acrylate Random Copolymers Synthesized by Nitroxide-Mediated Polymerization: Effect of Free Nitroxide on Kinetics and Copolymer Composition. *Macromolecules* **2007**, *40*, 9284–9292.

5. Grimaldi, S.; Finet, J.-P.; Le Moigne, F.; Zeghdaoui, A.; Tordo, P.; Benoit, D.; Fontanille, M.; Gnanou, Y. Acyclic β-Phosphonylated Nitroxides: A New Series of Counter-Radicals for "Living"/Controlled Free Radical Polymerization. *Macromolecules* **2000**, *33*, 1141–1147.

6. Charleux, B.; Nicolas, J. Water-soluble SG1-based alkoxyamines: A breakthrough in controlled/living free-radical polymerization in aqueous dispersed media. *Polymer* **2007**, *48*, 5813–5833.

7. Darabi, A.; Shirin-Abadi, A. R.; Jessop, P. G.; Cunningham, M. F. Nitroxide-Mediated Polymerization of 2-(Diethylamino)ethyl Methacrylate (DEAEMA) in Water. *Macromolecules* **2015**, *48*, 72–80.

8. Benoit, D.; Grimaldi, S.; Robin, S.; Finet, J.-P.; Tordo, P.; Gnanou, Y. Kinetics and Mechanism of Controlled Free-Radical Polymerization of Styrene and n-Butyl Acrylate in the Presence of an Acyclic β-Phosphonylated Nitroxide. *J. Am. Chem. Soc.* **2000**, *122*, 5929–5939.

9. Chauvin, F.; Dufils, P.-E.; Gigmes, D.; Guillaneuf, Y.; Marque, S. R. A.; Tordo, P.; Bertin, D. Nitroxide-Mediated Polymerization: The Pivotal Role of the kd Value of the Initiating Alkoxyamine and the Importance of the Experimental Conditions. *Macromolecules* **2006**, *39*, 5238–5250.

10. Couvreur, L.; Lefay, C.; Belleney, J.; Charleux, B.; Guerret, O.; Magnet, S. First Nitroxide-Mediated Controlled Free-Radical Polymerization of Acrylic Acid. *Macromolecules* **2003**, *36*, 8260–8267.

11. Darabi, A.; Shirin-Abadi, A. R.; Pinaud, J.; Jessop, P. G.; Cunningham, M. F. Nitroxide-mediated surfactant-free emulsion copolymerization of methyl methacrylate and styrene using poly(2-(diethyl)aminoethyl methacrylate-co-styrene) as a stimuli-responsive macroalkoxyamine. *Polym. Chem.* **2014**, *5*, 6163–6170.

12. Nicolas, J.; Dire, C.; Mueller, L.; Belleney, J.; Charleux, B.; Marque, S. R. A.; Bertin, D.; Magnet, S.; Couvreur, L. Living Character of Polymer Chains Prepared via Nitroxide-Mediated Controlled Free-Radical Polymerization of Methyl Methacrylate in the Presence of a Small Amount of Styrene at Low Temperature. *Macromolecules* **2006**, *39*, 8274–8282.

13. Lessard, B.; Schmidt, S. C.; Marić, M. Styrene/Acrylic Acid Random Copolymers Synthesized by Nitroxide-Mediated Polymerization: Effect of Free Nitroxide on Kinetics and Copolymer Composition. *Macromolecules* **2008**, *41*, 3446–3454.

14. Kerton, F. M. Chapter 6:Renewable Solvents and Other "Green" VOCs. In *Chapter 6:Renewable Solvents and Other "Green" VOCs*; 2013; pp. 149–174.

15. Ren, S.; Trevino, E.; Dubé, M. A. Copolymerization of Limonene with n-Butyl Acrylate. *Macromol. React. Eng.* **2015**, *9*, 339–349.

16. Hlalele, L.; Klumperman, B. In Situ NMR and Modeling Studies of Nitroxide Mediated Copolymerization of Styrene and n-Butyl Acrylate. *Macromolecules* **2011**, *44*, 6683–6690.

Appendix B. Sample Calculation and Extra Figures

B1. Composition calculation from ^{1}H-NMR spectrum

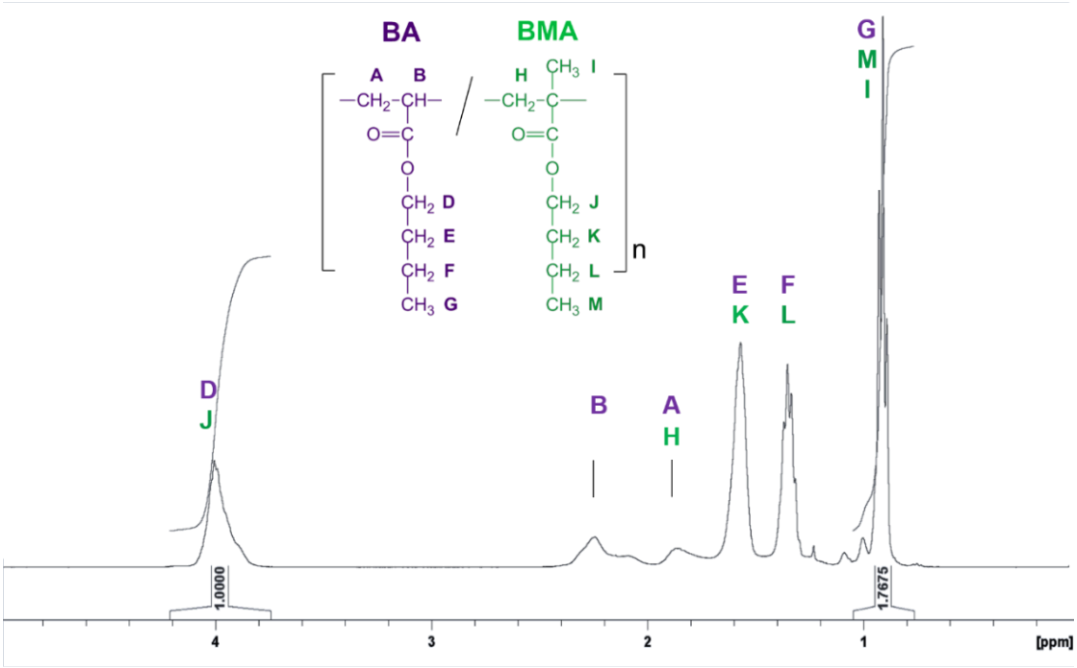

Figure B.1 ^{1}H-NMR spectrum of BA/BMA copolymer (F_{BMA} = 0.178, F_{BA} = 0.822).

BA = x, BMA = y

$2x + 2y = A_{4.0}$ ($A_{4.0}$ refers to the peak area at ~4.0 ppm, 3.8 to 4.2 ppm)

$3x + 6y = A_{1.0}$ ($A_{1.0}$ refers to the peak area at ~1.0 ppm, 0.7 to 1.1 ppm)

$x = (6A_{4.0} - 2A_{1.0})/6$

$y = (2A_{1.0} - 3A_{4.0})/6$

$$F_{BMA}(\text{mol fraction}) = \frac{BMA}{BA + BMA} = \frac{2A_{1.0}}{3A_{4.0}} - 1 = \frac{2 \times 1.7675}{3 \times 1.000} - 1 = 0.178$$

B2. Extra Figures

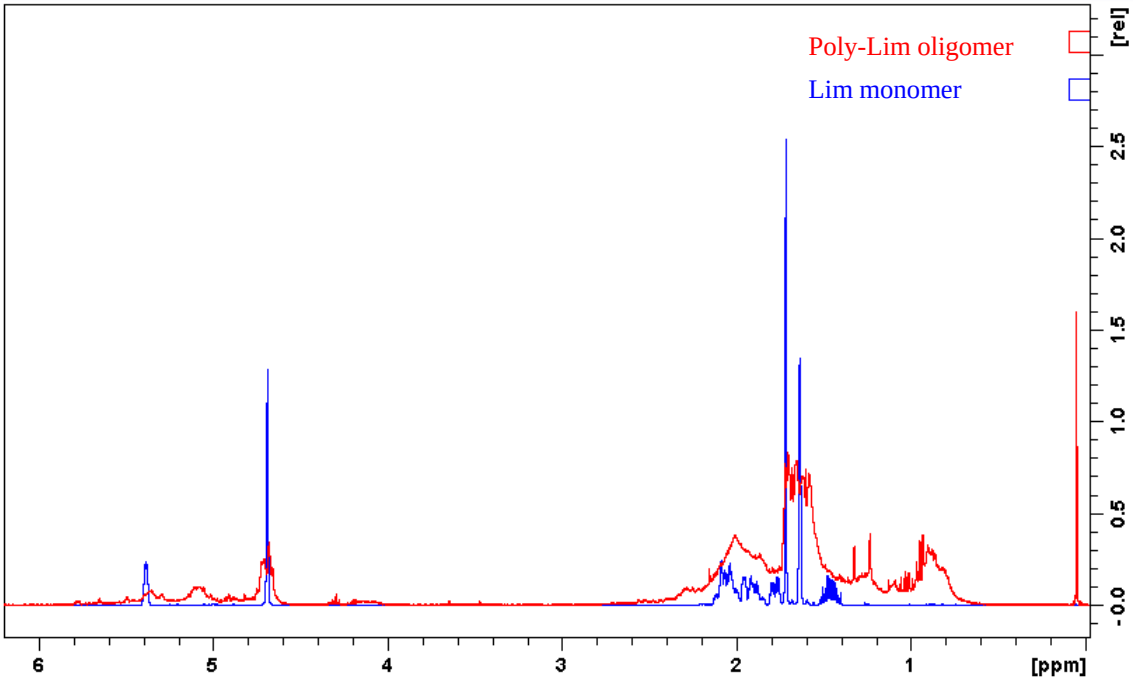

Figure B. 2 HNMR spectrum of Lim monomer and poly-Lim oligomer (80°C, [BPO] = 3 wt.%, monomer conversion = 2.3 wt.%)

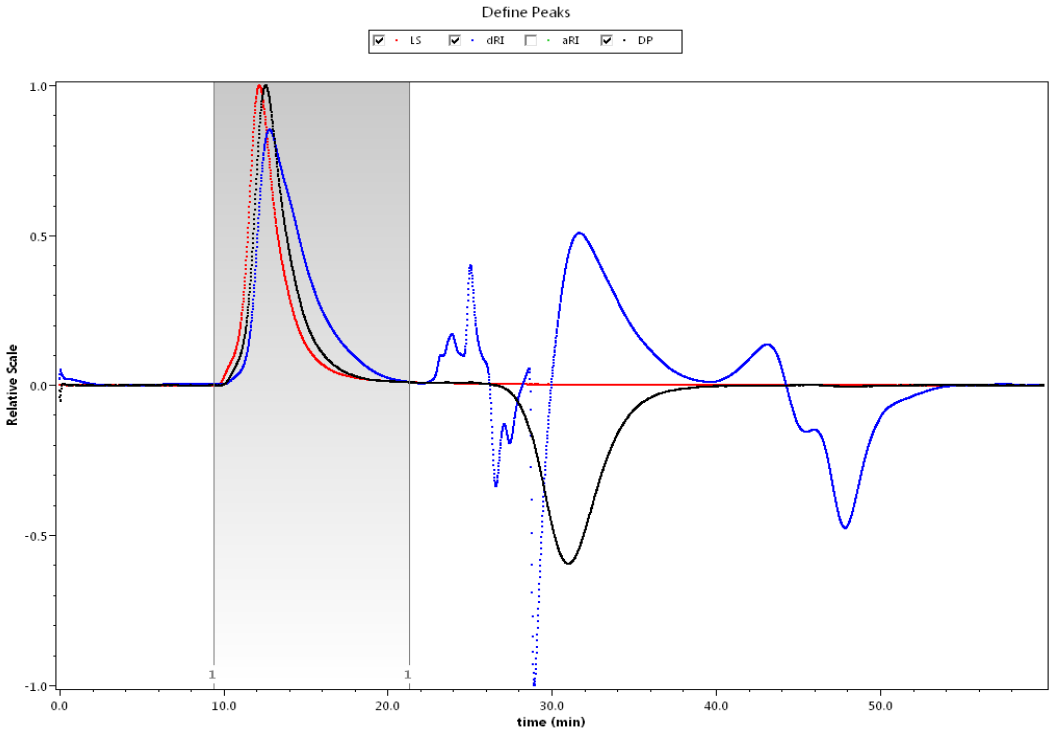

Figure B.3 GPC results for BA/BMA copolymer (f_{BMA}=0.5, conv.% =95.2 wt.%, average M_w = 1922 kDa) using Wyatt Astra software.

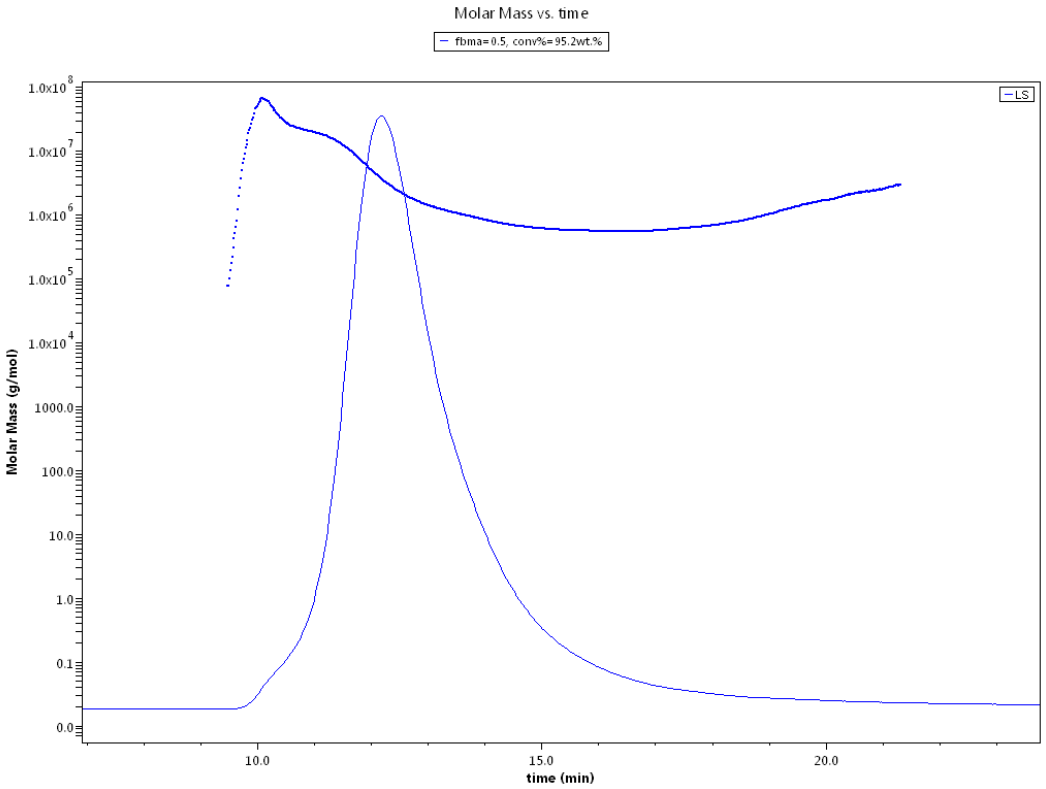

Figure B.4 Molar Mass results for BA/BMA copolymer (f_{BMA}=0.5, conv.% =95.2 wt.%, average M_w = 1922 kDa) using Wyatt Astra software.

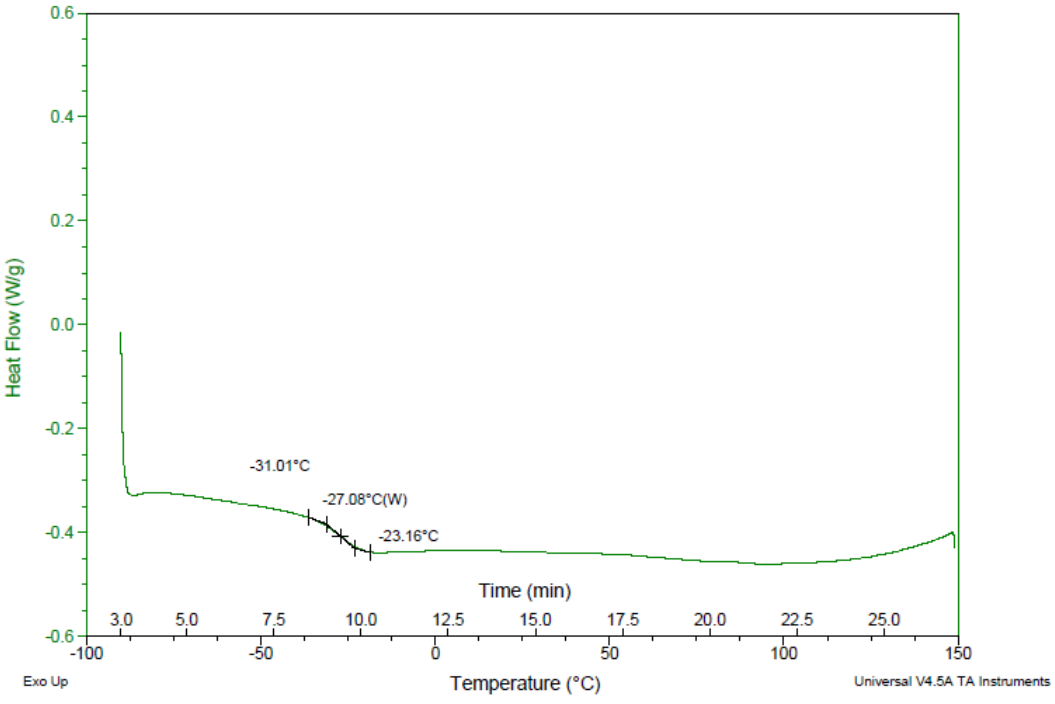

Figure B.5 DSC curve of BA/Lim copolymer (F_{Lim} = 0.094).

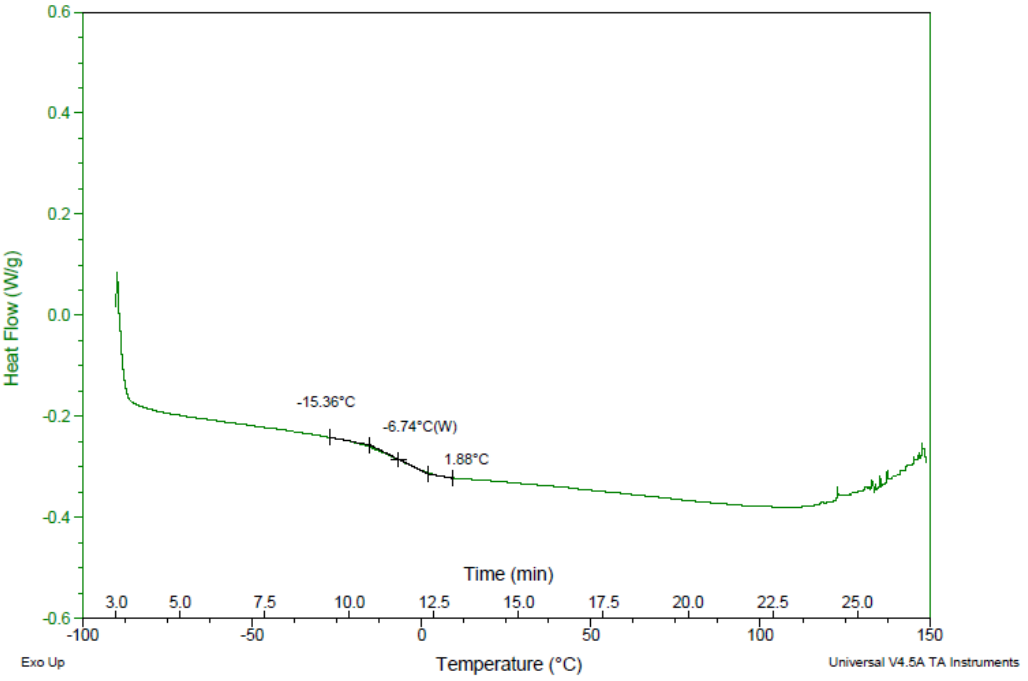

Figure B.6 DSC curve of BA/Lim copolymer (F_{Lim} = 0.140).

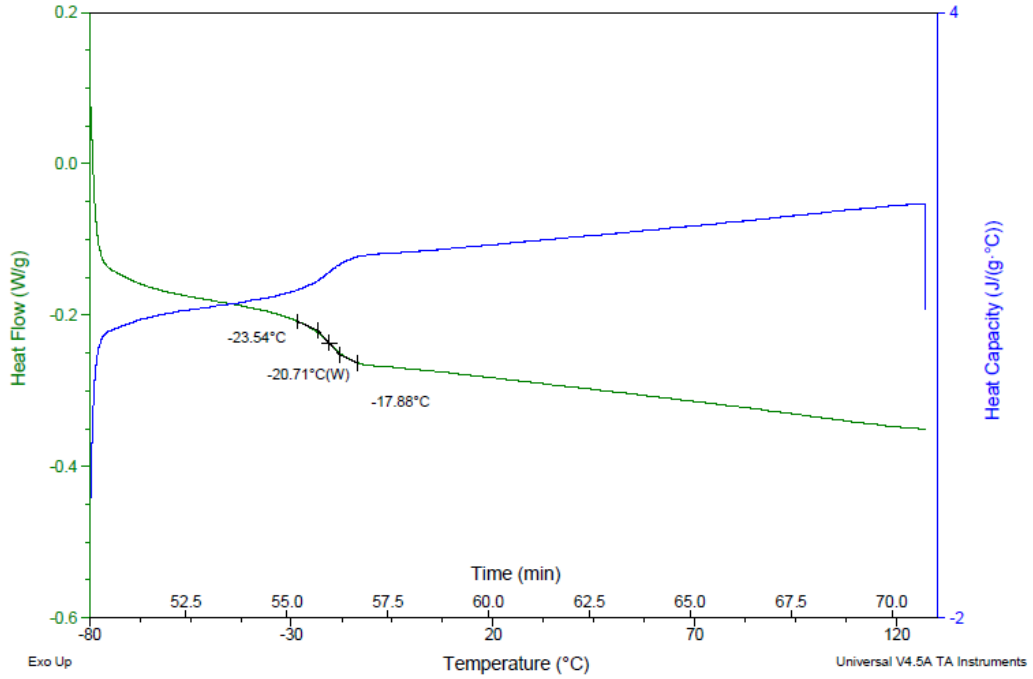

Figure B.7 DSC curve of core latex (core B, [Lim] = 2 phm, [DVB] = 0.2 phm).

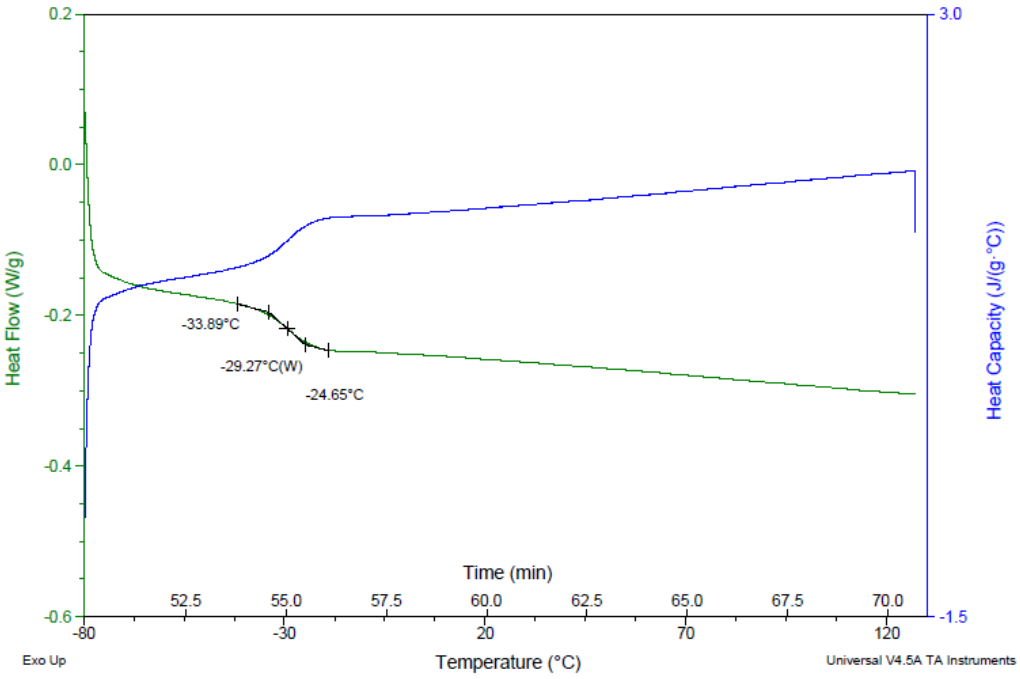

Figure B.8 DSC curve of core-shell latex (PSA- B3, core: [Lim] = 2 phm, [DVB] = 0.2 phm; shell: [Lim] = 3 phm).